SLAC-PUB-12273
January 2007

Improved Distances to Type Ia Supernovae with Multicolor Light Curve Shapes: MLCS2k2

Saurabh Jha[1,2], Adam G. Riess[3], and Robert P. Kirshner[4]

saurabh@slac.stanford.edu

ABSTRACT

We present an updated version of the Multicolor Light Curve Shape method to measure distances to type Ia supernovae (SN Ia), incorporating new procedures for K-correction and extinction corrections. We also develop a simple model to disentangle intrinsic color variations and reddening by dust, and expand the method to incorporate U-band light curves and to more easily accommodate prior constraints on any of the model parameters. We apply this method to 133 nearby SN Ia, including 95 objects in the Hubble flow ($cz \geq 2500$ km s^{-1}), which give an intrinsic dispersion of less than 7% in distance. The Hubble flow sample, which is of critical importance to all cosmological uses of SN Ia, is the largest ever presented with homogeneous distances. We find the Hubble flow supernovae with $H_0 d_{\rm SN} \geq 7400$ km s^{-1} yield an expansion rate that is 6.5 ± 1.8% lower than the rate determined from supernovae within that distance, and this can have a large effect on measurements of the dark energy equation of state with SN Ia. Peculiar velocities of SN Ia host galaxies in the rest frame of the Local Group are consistent with the dipole measured in the Cosmic Microwave Background. Direct fits of SN Ia that are significantly reddened by dust in their host galaxies suggest their mean extinction law may be described by $R_V \simeq 2.7$, but optical colors alone provide weak constraints on R_V.

Subject headings: cosmology: observations — distance scale — galaxies: distances and redshifts — supernovae: general

---

[1]Miller Institute and Department of Astronomy, 601 Campbell Hall, University of California, Berkeley, CA 94720

[2]present address: Kavli Institute for Particle Astrophysics and Cosmology, Stanford Linear Accelerator Center, 2575 Sand Hill Road MS 29, Menlo Park, CA 94025

[3]Space Telescope Science Institute, 3700 San Martin Drive, Baltimore, MD 21218

[4]Harvard-Smithsonian Center for Astrophysics, 60 Garden Street, Cambridge, MA 02138

Submitted to Astrophysical Journal

Work supported in part by the US Department of Energy contract DE-AC02-76SF00515

1. Introduction

The cosmological applications of type Ia supernovae (SN Ia) result from precise distances to these calibrated candles. It has been well established that the intrinsic luminosity of SN Ia is correlated with the shape of their optical light curves (Phillips 1993; Hamuy et al. 1995; Riess, Press, & Kirshner 1995a; Hamuy et al. 1996a; Riess, Press, & Kirshner 1996a). Determining a precise distance requires well-observed SN Ia light curves in multiple passbands, to constrain the intrinsic luminosity and extinction by dust along the line of sight to each SN Ia.

A number of methods have been developed to measure calibrated distances from SN Ia multi-color light curves, with each enjoying a similar level of success. The first of these was introduced by Phillips (1993), who noted that the parameter $\Delta m_{15}(B)$, the amount by which a SN Ia declined in the *B*-band during the first fifteen days after maximum light, was well correlated with SN Ia intrinsic luminosity. The Δm_{15} method was transformed by Hamuy et al. (1996a), in which Δm_{15} became a parameter in a multi-dimensional fit to six template *BVI* light curves spanning a wide range in $\Delta m_{15}(B)$ as it was originally defined. Phillips et al. (1999) present the current version of this method, which incorporates measurement of the extinction via late-time $B-V$ color measurements (roughly independent of Δm_{15}) and $B-V$ and $V-I$ measurements at maximum light (for the measured Δm_{15}, determined in an iterative fashion). Updates to this technique are given by Germany et al. (2004) and Prieto, Rest, & Suntzeff (2006), the latter developing a technique to describe a continuous family of light curves parameterized by Δm_{15}.

Tripp & Branch (1999) present a two-parameter method, empirically correlating SN Ia luminosity to Δm_{15} and maximum light $B-V$ color, but without regard to the source of the color variation (i.e., extinction or intrinsic variation). Parodi et al. (2000) and Reindl et al. (2005) present similar studies, with empirical correlations between SN Ia maximum light magnitudes in *BVI* , Δm_{15} and color.

Other methods include the stretch correction of Perlmutter et al. (1997), in which the SN Ia intrinsic luminosity is correlated with a simple stretching of the time axis of a fiducial light curve. This method has been presented in detail for the *B* band (Goldhaber et al. 2001), and can be extended straightforwardly to *U* and *V* (with *R* and *I* posing more difficulty; Nugent, Kim, & Perlmutter 2002; Knop et al. 2003; Nobili et al. 2005; Jha et al. 2006). Guy et al. (2005) use an innovative approach to constrain the spectral energy distribution of SN Ia, parameterized continuously as a function of color and stretch, and allows for the generation of light curve templates in arbitrary passbands. These methods all determine distances by correlating a distance-dependent parameter (such as peak magnitude in a particular passband, or an average magnitude difference between the observations and templates) and one or more distance-independent parameters (such as color, stretch, or Δm_{15}).

Wang et al. (2003) describe a novel technique which derives distances based on “light curves”

as a function of color rather than time, which may have interesting implications for the physics behind the observed correlations. Finally, Tonry et al. (2003) follow a non-parametric approach, by directly fitting an observed multicolor light curve to a library of nearby SN Ia, and deriving an average distance weighted by the goodness of fit to each object in the library.

Here we describe an updated version of the Multicolor Light Curve Shape method, denoted here as MLCS2k2. Riess, Press, & Kirshner (1995a) presented the first incarnation of this method (called LCS as it was based only on *V* band data), in which a continuum of template light curves was created based on a "training set" of SN Ia with known relative distances and the parameter Δ, a particular SN's under- or over-luminosity relative to some fiducial value. The luminosity correction, Δ, was used as a parameter in a least-squares fit, resulting in a best-fit distance for each SN, along with a quantitative estimate of the uncertainty. The MLCS method, presented by Riess, Press, & Kirshner (1996a) gave the details of the model, as well as incorporating *BVRI* light curves and providing an estimate of extinction by dust. Riess et al. (1998a) updated the training set, using reliable distances measured by the Hubble Law in favor of other methods, added a quadratic (Δ^2) term to create the template light curves, and included the effects of covariance in the model. The application of this version of MLCS to nearby SN Ia and the Hubble Constant is given by Jha et al. (1999a).

The MLCS approach has some advantages: by using a relatively large training set to define a continuum of templates, the method becomes less sensitive to peculiarities of individual objects. During the training process, the variance and covariance in the residuals determine the uncertainty in the model, and this is then used to determine statistically reliable estimates of goodness-of-fit and parameter uncertainties when the model is applied to other objects. The model also attempts a physically motivated separation of extinction by dust from intrinsic color variations (rather than empirical correlations with color), and uses all of the light curves (at all epochs) to constrain the extinction. Finally the model is easily extended, for example, with the inclusion of a quadratic term in Δ, or the incorporation of the *U*-band presented here. The major disadvantage is that the method requires accurate estimates of luminosity and extinction for the training set sample in order to construct reliable templates.

We have compiled modern multicolor photoelectric and CCD Johnson/Cousins *UBVRI* data from a variety of sources. The precision of SN Ia distances demands high quality photometry, and we have relied most heavily on large, homogeneous data sets, such as the observations presented by Hamuy et al. (1996b) from the Calán/Tololo survey (29 SN Ia), as well as those of Riess et al. (1999) and Jha et al. (2006), consisting of 22 and 44 SN Ia, respectively, from the CfA monitoring campaign. The complete sample we analyze consists of 133 SN Ia described in Table 1. For a number of objects we have combined data sets from different sources (see Jha et al. 2006 for some comparisons); in some cases we had to make subjective assessments of the relative quality of inconsistent data.

The basic framework for MLCS2k2 was laid out by Jha (2002)[1] and it has already been applied to SN Ia cosmology, including the silver and gold samples of Riess et al. (2004). This work showed that the Universe underwent a transition from an epoch of deceleration due to dark matter to current acceleration driven by dark energy, whose inferred properties are consistent with the cosmological constant. In addition, Riess et al. (2005) use MLCS2k2 distances to show various estimates of H_0 from SN Ia can be reconciled through the use of modern Cepheid and supernova data, deriving $H_0 = 73 \pm 4$ (statistical) $\pm$ 5 (systematic) km s^{-1} Mpc^{-1}. In this paper, we focus only on relative distances to nearby SN, independent of the zeropoint derived from external measurements (e.g., Cepheid distances to SN Ia hosts; Freedman et al. 2001; Sandage et al. 2006).

[1]Because the basic algorithms were designed in 2002, we continue to refer to this SN distance fitter as MLCS2k2, even though its implementation, applicability, and robustness have evolved substantially since then. Details of the model presented here, as well as recent updates, can be found at http://astro.berkeley.edu/~saurabh/mlcs2k2/

Table 1. Supernova and Host Galaxy Data

SN Ia	ℓ[a] deg	b[a] deg	$cz_\odot$[b] km s^{-1}	cz_{LG}[b] km s^{-1}	cz_{CMB}[b] km s^{-1}	Morph[c]	SN Offsets[d] ″N	″E	t_1[e] days	Filters	$E(B-V)$[f] mag	References
1972E	314.84	+30.08	404	190	678	Sd/Irr	−100.0	−38.0	+8.7	UBV	0.056	1
1980N	240.16	−56.63	1760	1633	1653	S0	−20.0	+220.0	−1.0	UBVRI	0.021	2
1981B	292.97	+64.74	1808	1662	2151	Sbc	+42.0	+39.0	−0.2	UBVR	0.018	3,4
1981D	240.21	−56.69	1760	1633	1653	S0	−100.0	−20.0	−5.3	UBV	0.021	2
1986G	309.54	+19.40	547	301	803	S0	−60.0	+120.0	−5.7	UBVRI	0.115	5
1989B	241.92	+64.42	703	567	1051	Sb	+50.0	−15.0	−2.5	UBVRI	0.032	6
1990N	294.36	+75.98	978	885	1298	Sbc	−1.0	+65.0	−10.4	UBVRI	0.026	7
1990O	37.65	+28.35	9193	9340	9175	Sa	−3.9	+21.8	+0.6	BVRI	0.093	8
1990T	341.50	−31.53	12112	12025	12013	Sa	−1.9	+24.8	+14.9	BVRI	0.053	8
1990Y	232.64	−53.85	11721	11597	11622	E	−5.0	+1.0	+16.2	BVRI	0.008	8
1990af	330.81	−42.20	15169	15059	15056	S0	+7.4	−8.0	−3.1	BV	0.035	8
1991M	30.36	+45.90	2180	2265	2277	Sc	+60.0	+36.0	+1.8	VRI	0.038	9
1991S	214.06	+57.43	16369	16263	16688	Sb	+17.3	+4.4	+10.8	BVRI	0.026	8,10
1991T	292.60	+65.19	1736	1591	2078	Sbc	+44.0	+26.0	−11.1	UBVRI	0.022	7,10
1991U	311.82	+36.20	9503	9292	9801	Sbc	+5.8	−2.2	+10.4	BVRI	0.062	8
1991ag	342.56	−31.60	4264	4182	4161	Sb	+22.1	−4.4	+5.6	BVRI	0.062	8
1991bg	278.23	+74.46	1060	955	1391	E	−57.0	+2.0	+0.9	BVRI	0.041	11,12,13
1992A	235.90	−54.06	1877	1747	1781	S0	+62.0	−3.0	−7.0	UBVRI	0.018	10,14
1992G	184.62	+59.84	1565	1541	1827	Sc	−10.0	+27.0	+3.0	VRI	0.020	9
1992J	263.55	+23.50	13371	13077	13708	E/S0	+12.0	−11.9	+14.6	BVI	0.057	8
1992K	306.28	+16.30	3087	2828	3340	Sb	−15.4	−1.9	+13.6	BVI	0.101	8
1992P	295.62	+73.10	7555	7449	7881	Sa	+9.8	−4.3	−0.5	BVI	0.021	8
1992ae	332.70	−41.90	22544	22440	22426	E	+4.0	+2.1	+2.5	BV	0.036	8
1992ag	312.48	+38.30	7465	7260	7765	Sa	0.0	−3.0	−0.4	BVI	0.097	8
1992al	347.33	−38.40	4377	4324	4228	Sb	−12.0	+19.0	−4.9	BVRI	0.034	8
1992aq	1.78	−65.30	30519	30536	30254	Sa	−7.1	+2.4	+2.2	BVI	0.012	8
1992au	319.11	−65.80	18407	18338	18213	E	+8.9	+21.2	+12.6	BVI	0.017	8
1992bc	245.70	−59.60	6056	5933	5936	Sab	−2.0	+16.1	−10.1	BVRI	0.022	8
1992bg	274.61	−18.30	10553	10261	10697	Sa	+5.8	−3.4	+4.3	BVI	0.185	8
1992bh	267.85	−37.30	13490	13254	13518	Sbc	−3.6	+1.9	−0.6	BVI	0.022	8
1992bk	265.01	−48.90	17418	17229	17372	E	+21.1	+11.9	+8.6	BVI	0.015	8
1992bl	344.12	−63.90	13101	13076	12871	S0/Sa	−21.8	+15.3	+3.1	BVI	0.011	8
1992bo	261.88	−80.30	5666	5636	5435	E/S0	−54.7	−47.3	−7.5	BVRI	0.027	8
1992bp	208.83	−51.00	23773	23704	23646	E/S0	−1.4	−5.4	−1.6	BVI	0.069	8
1992br	288.01	−59.40	26442	26306	26319	E	−6.3	+3.6	+1.8	BV	0.026	8
1992bs	240.02	−55.33	19097	18965	18998	Sb	+3.6	−9.0	+2.5	BV	0.011	8
1993B	273.32	+20.46	20866	20563	21191	Sb	+5.4	+0.9	+3.6	BVI	0.079	8
1993H	318.22	+30.33	7165	6962	7430	Sb	+12.3	+1.0	−1.1	BVRI	0.060	8,10
1993L	5.95	−64.37	1858	1885	1587	Sc	+1.4	−25.0	+17.3	BVRI	0.014	10
1993O	312.41	+28.92	15289	15065	15567	E/S0	+8.4	−14.1	−6.3	BVI	0.053	8
1993ac	149.70	+17.21	14800	14959	14784	E	+31.0	−5.3	+7.0	BVRI	0.163	15
1993ae	144.62	−63.22	5712	5820	5410	E	+22.7	+16.1	+13.8	BVRI	0.038	15
1993ag	268.43	+15.92	14690	14382	15003	E/S0	−6.1	−5.0	−1.7	BVI	0.112	8
1993ah	25.88	−76.77	8842	8892	8543	S0	+8.1	−0.9	+11.8	BVI	0.020	8
1994D	290.15	+70.14	592	469	928	S0	+7.8	−9.0	−13.5	UBVRI	0.022	10,16,17,18
1994M	291.68	+63.03	6943	6788	7289	E	−28.2	+3.4	+3.1	BVRI	0.023	15

Table 1—Continued

SN Ia	ℓ[a] deg	b[a] deg	$cz_\odot$[b] km s^{-1}	cz_{LG}[b] km s^{-1}	cz_{CMB}[b] km s^{-1}	Morph[c]	SN Offsets[d] ″N	″E	t_1[e] days	Filters	$E(B-V)$[f] mag	References
1994Q	64.38	+39.67	8672	8871	8670	S0	−3.7	−0.1	+10.8	BVRI	0.017	15
1994S	187.37	+85.14	4525	4501	4806	Sab	−6.9	−14.0	−4.5	BVRI	0.021	15
1994T	318.01	+59.83	10396	10265	10709	Sa	−12.0	+3.8	+0.2	BVRI	0.029	15
1994ae	225.34	+59.66	1301	1175	1637	Sc	+6.1	−29.7	−11.6	UBVRI	0.030	10,19
1995D	230.02	+39.65	1966	1774	2300	S0	−87.8	+11.8	−6.5	BVRI	0.058	10,15
1995E	141.99	+30.26	3470	3638	3496	Sb	−20.8	+7.6	−1.9	BVRI	0.027	15
1995ac	58.69	−55.04	14990	15157	14635	Sa	−1.4	−0.9	−5.1	BVRI	0.042	10,15
1995ak	169.65	−48.98	6811	6875	6589	Sbc	+0.8	−7.1	+3.6	BVRI	0.038	15
1995al	192.17	+50.83	1514	1465	1777	Sbc	−3.1	−14.7	−3.9	UBVRI	0.014	15
1995bd	187.11	−21.66	4377	4364	4326	Sa	−1.0	+22.9	−8.4	BVRI	0.498	15
1996C	99.59	+65.00	8094	8206	8244	Sa	+13.2	−1.8	+2.4	BVRI	0.013	15
1996X	310.23	+35.64	2032	1815	2333	E	−31.7	−51.4	−3.0	UBVRI	0.069	15,20
1996Z	253.60	+22.55	2254	1971	2584	Sb	−69.9	+2.0	+6.1	BVR	0.064	15
1996ab	43.15	+56.93	37109	37201	37239	Sa	+0.6	+2.0	+1.0	BV	0.032	15
1996ai	101.58	+79.24	873	910	1101	Scd	+2.9	+23.3	−1.1	UBVRI	0.014	15
1996bk	111.25	+54.88	1985	2139	2085	S0	−9.7	−18.1	+3.0	BVRI	0.018	15
1996bl	116.99	−51.30	10793	10990	10447	Sc	+5.6	−3.2	−2.4	BVRI	0.092	15
1996bo	144.46	−48.95	5182	5328	4893	Sc	−2.1	+6.7	−6.2	BVRI	0.077	10,15
1996bv	157.33	+17.97	4996	5119	5013	Sa	+2.0	−2.0	+5.1	BVRI	0.105	15
1997E	140.20	+25.81	4001	4184	3997	S0	+57.0	−32.0	−2.6	UBVRI	0.124	21
1997Y	124.77	+62.37	4806	4911	4964	Sb	+2.0	−8.0	+2.2	UBVRI	0.017	21
1997bp	301.15	+51.21	2492	2301	2831	Sd/Irr	−20.0	−15.0	−2.1	UBVRI	0.044	10,21
1997bq	136.29	+39.48	2780	2943	2839	Sbc	−60.0	+50.0	−10.3	UBVRI	0.024	21
1997br	311.84	+40.32	2085	1884	2391	Sd/Irr	+52.0	−21.0	−8.7	UBVRI	0.113	10,21,22
1997cn	9.14	+69.51	4855	4846	5092	E	−12.0	+7.0	+5.4	UBVRI	0.027	21,23
1997cw	113.09	−49.48	5133	5342	4782	Sab	+4.0	+8.0	+12.0	UBVRI	0.073	21
1997dg	103.61	−33.98	9238	9507	8890	···	0.0	+2.0	+0.8	UBVRI	0.078	21
1997do	171.00	+25.26	3034	3084	3140	Sbc	−4.0	−3.0	−6.1	UBVRI	0.063	21
1997dt	87.56	−39.12	2194	2451	1828	Sbc	+1.0	−9.0	−7.9	UBVRI	0.057	21
1998D	63.78	+72.91	3765	3825	3962	Sa	−7.0	−26.0	+32.4	UBVRI	0.015	21
1998V	43.94	+13.34	5268	5464	5148	Sb	+21.0	−21.0	+2.7	UBVRI	0.196	21
1998ab	124.86	+75.19	8134	8181	8354	Sc	+12.0	+2.0	−7.4	UBVRI	0.017	21
1998aq	138.83	+60.26	1184	1274	1354	Sb	+7.0	−18.0	−10.1	UBVRI	0.014	19
1998bp	43.64	+20.48	3127	3312	3048	E	+13.0	−1.0	−1.5	UBVRI	0.076	21
1998bu	234.41	+57.01	855	702	1204	Sab	+55.0	+4.0	−7.7	UBVRI	0.025	24,25
1998co	41.52	−44.94	5418	5573	5094	S0	+5.0	+2.0	+3.0	UBVRI	0.043	21
1998de	122.03	−35.24	4990	5228	4671	S0	+3.0	+72.0	−8.6	UBVRI	0.057	21,26
1998dh	82.82	−50.64	2678	2892	2307	Sbc	+10.0	−54.0	−7.8	UBVRI	0.068	21
1998dk	102.85	−62.16	3963	4128	3609	Sc	+3.0	+5.0	+18.9	UBVRI	0.044	21
1998dm	145.97	−67.40	1968	2061	1668	Sc	−37.0	−14.0	+9.9	UBVRI	0.044	21
1998dx	77.67	+26.67	16197	16459	16102	Sb	−12.0	+21.0	+1.2	UBVRI	0.041	21
1998ec	166.29	+20.71	5966	6043	6032	Sb	−20.0	−9.0	+13.3	UBVRI	0.085	21
1998ef	125.88	−30.56	5319	5558	5020	Sa	−2.0	+6.0	−7.3	UBVRI	0.073	21
1998eg	76.46	−42.06	7423	7662	7056	Sc	−25.0	−26.0	−0.1	UBVRI	0.123	21
1998es	143.18	−55.18	3168	3301	2868	S0/Sa	+11.0	0.0	−11.0	UBVRI	0.032	21,27
1999X	186.58	+39.59	7503	7474	7720	···	+6.0	+4.0	+14.0	UBVRI	0.032	21

Table 1—Continued

SN Ia	ℓ[a] deg	b[a] deg	$cz_\odot$[b] km s^{-1}	cz_{LG}[b] km s^{-1}	cz_{CMB}[b] km s^{-1}	Morph[c]	SN Offsets[d] ″N	″E	t_1[e] days	Filters	$E(B-V)$[f] mag	References
1999aa	202.72	+30.31	4330	4227	4572	Sc	+28.0	+1.0	−10.1	UBVRI	0.040	10,21,27,28
1999ac	19.88	+39.94	2848	2904	2943	Scd	−30.0	+24.0	−14.4	UBVRI	0.046	21,27
1999aw	260.24	+47.45	11392	11168	11763	···	0.0	0.0	−8.2	BVRI	0.032	29
1999by	166.91	+44.11	657	704	827	Sb	+91.0	−96.0	−10.9	UBVRI	0.016	27,30
1999cc	59.66	+48.74	9392	9549	9452	Sc	+2.0	+17.0	−2.7	UBVRI	0.023	21,31
1999cl	282.26	+76.50	2281	2187	2605	Sb	+23.0	−46.0	−6.5	UBVRI	0.038	21,31
1999cp	334.85	+52.71	2845	2737	3115	Scd	+23.0	−52.0	−7.4	BVRI	0.024	28
1999cw	101.77	−67.91	3725	3863	3380	Sab	−2.0	+21.0	+24.0	UBVRI	0.036	21
1999da	89.73	+32.64	3806	4059	3748	E	+1.0	−71.0	−8.7	BVRI	0.056	27,32
1999dk	137.35	−47.46	4485	4654	4181	Sc	+26.0	+4.0	−0.9	UBVRI	0.054	10,32
1999dq	152.83	−35.87	4295	4436	4060	Sc	−6.0	−4.0	−10.6	UBVRI	0.110	21,27
1999ee	6.50	−55.93	3422	3451	3163	Sbc	−10.0	+10.0	−9.5	UBVRI	0.020	33
1999ef	125.72	−50.09	11733	11920	11402	Scd	−10.0	+20.0	+6.8	UBVRI	0.087	21
1999ej	130.44	−28.95	4114	4344	3831	S0/Sa	−20.0	+18.0	+5.3	UBVRI	0.071	21
1999ek	189.40	−8.23	5253	5221	5278	Sbc	−12.0	−12.0	−2.8	UBVRI	0.561	21,34
1999gd	198.83	+33.98	5535	5451	5775	···	+17.0	+7.0	+3.5	UBVRI	0.041	21
1999gh	255.04	+23.73	2302	2019	2637	E	+16.0	+52.0	+7.4	UBVRI	0.058	21
1999gp	143.25	−19.50	8018	8215	7806	Sb	+10.0	−11.0	−13.0	UBVRI	0.056	21,27,32
2000B	166.35	+22.79	5901	5976	5977	E	+19.0	−14.0	+15.7	UBVRI	0.068	21
2000E	100.89	+14.84	1415	1711	1257	Sbc	−26.7	−6.3	−15.5	UBVRI	0.364	35
2000bh	293.74	+40.33	6905	6666	7248	···	−11.0	−8.0	+5.4	BVRI	0.048	36
2000bk	295.29	+55.23	7628	7444	7976	S0	−10.0	+61.0	+12.3	BVRI	0.025	32
2000ca	313.20	+27.83	7080	6857	7352	Sbc	+4.7	+0.6	−2.3	UBVRI	0.067	36
2000ce	149.10	+32.00	4888	5025	4946	Sb	+17.0	+15.0	+7.0	UBVRI	0.057	21,32
2000cf	99.88	+42.16	10920	11137	10930	···	+4.0	+3.0	+3.2	UBVRI	0.032	21,31
2000cn	53.44	+23.31	7043	7257	6958	Scd	−7.0	−7.0	−7.8	UBVRI	0.057	21
2000cx	136.50	−52.48	2379	2536	2068	S0	−109.0	−23.0	−8.4	UBVRI	0.082	10,21,37,38
2000dk	126.83	−30.34	5228	5465	4931	E	+9.0	−5.0	−4.5	UBVRI	0.070	21
2000fa	194.17	+15.48	6378	6313	6533	Sd/Irr	+4.0	+7.0	−10.1	UBVRI	0.069	21
2001V	218.92	+77.73	4539	4478	4846	Sb	+28.0	+52.0	−12.9	UBVRI	0.020	39
2001ay	35.98	+68.83	9067	9108	9266	Sb	+9.0	−10.0	−3.0	UBVRI	0.019	40
2001ba	285.39	+28.03	8819	8537	9152	Sb	−22.0	+19.0	−3.5	BVI	0.064	36
2001bt	337.32	−25.87	4388	4275	4332	Sb	+17.1	−14.1	−8.0	BVRI	0.065	34
2001cn	329.65	−24.05	4647	4498	4628	Sc	−17.9	−2.6	+4.7	UBVRI	0.059	34
2001cz	302.11	+23.29	4612	4350	4900	Sbc	−31.4	−0.6	−6.3	BVRI	0.092	34
2001el	251.52	−51.40	1168	1002	1102	Scd	+19.0	−22.0	−10.7	UBVRI	0.014	41
2002bf	156.46	+50.08	7254	7327	7418	Sb	+4.0	+0.6	−9.9	BVRI	0.011	42
2002bo	213.04	+54.85	1293	1184	1609	Sa	−14.2	+11.6	−13.4	UBVRI	0.025	34,43,44
2002cx	318.71	+69.14	7184	7085	7494	···	−18.0	+11.0	−5.3	BVRI	0.032	45
2002er	28.67	+25.83	2568	2681	2563	Sc	+4.7	−12.3	−7.5	UBVRI	0.157	46
2003du	101.18	+53.21	1912	2081	1992	Sd/Irr	−13.5	−8.8	−4.7	BVRI	0.010	42

[a]Host-galaxy galactic longitude and latitude, from the NASA/IPAC Extragalactic Database (NED); http://nedwww.ipac.caltech.edu.

[b]Host-galaxy heliocentric radial velocities are taken from NED; they are transformed to the Local Group and CMB rest frames using the formulas also provided by NED; http://nedwww.ipac.caltech.edu/help/velc_help.html#notes.

[c]NED host-galaxy morphological type.

[d]Positional offset relative to host-galaxy nucleus, from the IAU List of Supernovae; http://cfa-www.harvard.edu/iau/lists/Supernovae.html.

[e]Epoch of the first photometric observation, relative to *B* maximum light, in the SN rest frame.

[f]Milky Way dust reddening, from Schlegel, Finkbeiner, & Davis (1998).

References. — (1) Leibundgut et al. 1991; (2) Hamuy et al. 1991; (3) Buta & Turner 1983; (4) Tsvetkov 1982; (5) Phillips et al. 1987; (6) Wells et al. 1994; (7) Lira et al. 1998; (8) Hamuy et al. 1996b; (9) Ford et al. 1993; (10) Altavilla et al. 2004; (11) Filippenko et al. 1992; (12) Leibundgut et al. 1993; (13) Turatto et al. 1996 (14) N. Suntzeff, personal communication; (15) Riess et al. 1999; (16) Richmond et al. 1995; (17) Patat et al. 1996; (18) Meikle et al. 1996; (19) Riess et al. 2005; (20) Salvo et al. 2001; (21) Jha et al. 2006; (22) Li et al. 1999; (23) Turatto et al. 1998; (24) Suntzeff et al. 1999; (25) Jha et al. 1999a; (26) Modjaz et al. 2001; (27) W. Li, personal communication; (28) Krisciunas et al. 2000; (29) Strolger et al. 2002; (30) Garnavich et al. 2004; (31) Krisciunas et al. 2006; (32) Krisciunas et al. 2001; (33) Stritzinger et al. 2002; (34) Krisciunas et al. 2004b; (35) Valentini et al. 2003; (36) Krisciunas et al. 2004a; (37) Li et al. 2001; (38) Candia et al. 2003; (39) K. Mandel et al. 2007, in preparation; (40) K. Krisciunas, personal communication; (41) Krisciunas et al. 2003; (42) Leonard et al. 2005; (43) Szabó et al. 2003; (44) Benetti et al. 2004; (45) Li et al. 2003; (46) Pignata et al. 2004

2. Groundwork

Comparison of light curves from many SN Ia requires understanding and correction for a number of effects to put the photometry on a common basis. These include corrections from the observational photometric system to standard passbands, correction for Galactic extinction, correction for time dilation and the *K*-correction. We have updated a number of these foundations in our development of MLCS2k2.

2.1. *K*-correction

The stretching and shifting of spectra due to the cosmological expansion leads to changes in measured flux observed through a fixed detector passband as a function of redshift. *K*-corrections for SN Ia in *B* and *V* have been presented by Hamuy et al. (1993), based on spectra of three objects. Kim, Goobar, & Perlmutter (1996) provide additional *K*-corrections in *R*, as well as developing a method of "cross-filter" *K*-corrections used at high redshift. These methods use a fixed set of spectra to define the *K*-correction for all objects, and do not include spectral energy distribution (SED) variations arising from intrinsic differences among supernovae (either in the detailed spectral features or in the continuum shape) or changes in in the SED due to extinction.

Nugent, Kim, & Perlmutter (2002) developed a method that accounts for these variations with a simple, yet effective, "trick" in which both the intrinsic and extinction-related SED variations are effected by adjusting the SED by the $R_V = 3.1$ extinction law of Cardelli, Clayton & Mathis (1989; hereinafter CCM89) to match the color of the SN as observed.[2] This procedure is reasonably well motivated; at early times, SN Ia are in the photospheric phase and the SED is continuum dominated, so that adjustment of the SED by a relatively slowly varying function of wavelength, like the CCM89 extinction law, to match the observed color will do a good job of mimicking the true SED. At late times, much of the color variation is due, in fact, to extinction and so the adjustment is appropriate. Furthermore, the adjustment is done using a color "local" to the spectral region being adjusted, minimizing any adverse effects. The difference in the *K*-correction accounting for these color variations and assuming a constant color for all objects is typically small (generally $\lesssim 0.1$ mag), but systematic. Nugent et al. (2002) show the efficacy of this color-based procedure.

Our concern in this paper is for accurate *K*-corrections at low redshift ($z \lesssim 0.1$), so we restrict our attention to *K*-corrections within each passband, not the cross-filter *K*-correction. We have implemented the Nugent et al. (2002) procedure using a sample of 91 SN Ia spectra covering phases from −14 to +92 days past maximum light, compiled from a number of sources, including archival IUE and HST data, Keck and Lick Observatory SN Ia spectra from UC Berkeley (Filippenko

[2]Here we use the extinction law to adjust the SED redder *or bluer*, to match the observed SN color.

1997), and unpublished spectra from the CfA SN Ia follow-up program (Matheson et al. 2007, in preparation). Of these, 57 spectra extend far enough to the red to cover the *I* passband, while 32 spectra cover the *U* passband in the blue. The number of spectra that cover the *U*-band decreases quickly as the spectra are artificially redshifted to calculate the *K*-correction; however, of the 133 SN Ia described here, the maximum redshift for which there are *U* observations is only $z \simeq 0.06$, meaning that is the extent to which we need to calculate K_{UU}.

To derive the *K*-corrections, the basic procedure is as follows. For each of *UBVRI* (we adopt the standard Bessell 1990 passbands), we choose standard colors including that passband (specifically, for *U*: $U-B$; *B*: $U-B$ and $B-V$; *V*: $B-V$, $V-R$, and $V-I$; *R*: $V-R$ and $R-I$; *I*: $V-I$ and $R-I$). Then for a particular combination of passband and color, we calculate *K*-corrections in that passband, such that the spectra are forced to take on a range of observed colors, using the CCM89 extinction law to adjust the spectra to any particular color. Thus, we tabulate the *K*-correction as a function of three parameters: epoch (i.e., days after maximum light), redshift and color. We measure the colors in the observer frame, so that for example, to determine the *K*-correction in the *V*-band for a supernova at maximum light at redshift $z = 0.05$ with an observed $B-V = 0.0$ mag, we have taken our maximum light spectra, redshifted them to $z = 0.05$, adjusted them using the CCM89 extinction law to have $B-V = 0.0$ as measured with synthetic photometry, and calculated the *K*-correction for that adjusted spectrum. In this example, the answer is $K_{VV} = -0.04 \pm 0.02$ mag, where the uncertainty is measured from the scatter among the individual spectra about a smooth curve. If the observed color had been redder, e.g., $B-V = 0.5$ mag, then $K_{VV} = 0.06 \pm 0.01$ mag.

The advantage of calculating the *K*-correction as a function of observer-frame color (as opposed to the SN rest-frame color) is that no iteration is then required: the measured color directly determines the SN SED in the observer frame. However, in other applications, for example, if one wants to transform rest-frame templates (with known rest-frame colors) to the observer-frame, it is more convenient to tabulate the *K*-correction as a function of rest-frame color. For the present sample, all SN have well-measured (to better than ~0.1 mag) observer-frame colors, so we can apply the *K*-corrections to the data directly, and expediently fit the SN in the rest frame. Though not used here, we are also developing an implementation of MLCS2k2 to take rest-frame model light curves, convert them into the observer frame, and then fit the observed data directly. That approach is more appropriate, e.g., for high-redshift observations where observer-frame color information is of lower quality and *K*-corrections based on the model light-curve colors should be used.

In Figure 1 we show the derived *K*-corrections in the *U*-band. It is interesting to note that the *K*-corrections in *U* at maximum light are quite significant (~0.1 mag), even for very modest redshifts. Ignoring the *K*-correction would lead to spurious correlations of supernova parameters (including those that are nominally distance-independent, such as decline rate or color) with redshift and distance.

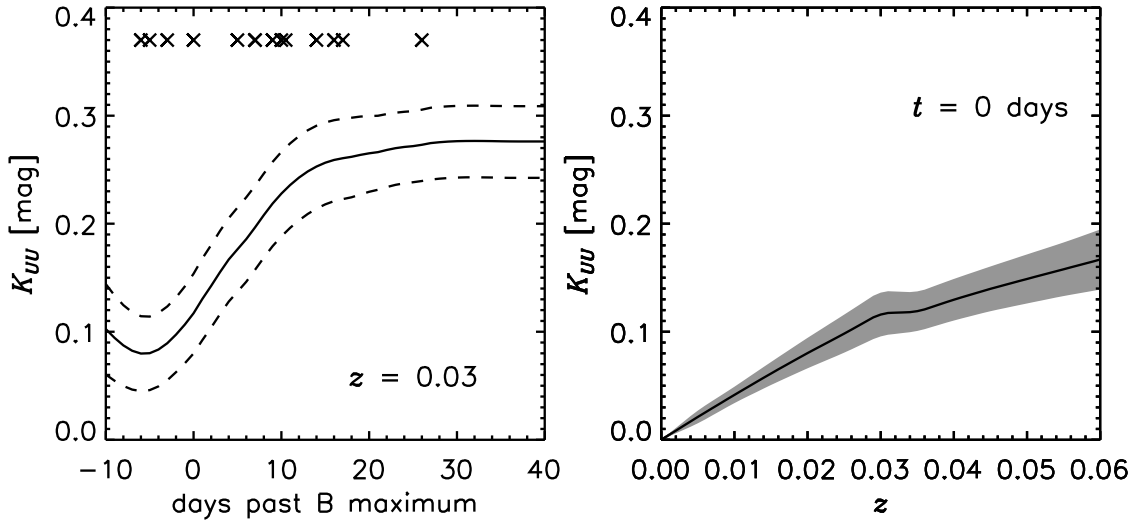

Fig. 1.— *K*-corrections in the *U*-band. The left panel shows K_{UU} as a function of supernova age at a redshift of $z = 0.03$. The solid line corresponds to an observed maximum-light $U-B = -0.35$ (corresponding to a SN rest-frame color at maximum light $U-B = -0.50$). The dashed lines above and below the solid line correspond to SN Ia that are 0.2 mag redder and bluer, respectively, in $U-B$ at all epochs. The crosses indicate the phases of the spectra used in the calculation. The right panel shows K_{UU} at maximum light as a function of redshift, assuming a rest-frame color of $U-B = -0.50$. The shaded region indicates the *K*-correction uncertainty. The "kinks" in the right panel occur when individual spectra (out of 32 total) drop out of the *K*-correction calculation as their wavelength coverage ceases to encompass the entire *U*-band.

Nugent et al. (2002) caution against using the CCM89 extinction law adjustment procedure applied to normal SN Ia spectra in determining *K*-corrections for SN 1991bg-like objects, whose strong Ti II spectral features dominate the photometric colors (particularly in *B*), even at early times. We have calculated *K*-corrections independently for this class of SN Ia, a small minority of the entire sample, using a separate spectral sample consisting of only 1991bg-like objects. The affected objects are SN 1986G, 1991bg, 1992K, 1992bo, 1993H, 1997cn, 1998bp, 1998de, 1999by, 1999da, and 1999gh.

2.2. Extinction

Extinction by dust along the line of sight to a SN Ia is recognized by its reddening effect on the SN colors. As discussed by Phillips et al. (1999) and Nugent et al. (2002), the evolution of the SN Ia SED over time leads to variations in the observed extinction in any given passband. Furthermore the extinction itself alters the SED such that the reddening is a nonlinear function of the total extinction. These effects are small (typically at the level of a few hundredths of a magnitude), but systematically affect the observed light curves in a way that can impact the luminosity/light-curve shape relationship and derived distances. In this section we describe in some detail the methods we have used to account for host-galaxy extinction in MLCS2k2.

The dust extinction along a particular line of sight is typically parameterized by the extinction in a given band X, A_X and by the amount of reddening, given by the color excess, typically $E(B-V)$. Following Phillips et al. (1999) and Nugent et al. (2002), we distinguish between the "true" reddening $E(B-V)_{\rm true}$ which depends only on the dust itself (and is calculated from the effects of that dust on idealized stellar spectra; CCM89), and the "observed" reddening $E(B-V)_{\rm obs} \equiv A_B - A_V$, which varies with time as the supernova spectrum evolves. From these, we can construct the ratio $R_X^{\rm true} \equiv A_X/E(B-V)_{\rm true}$, which varies in time as the numerator varies, and $R_X^{\rm obs} \equiv A_X/E(B-V)_{\rm obs}$, for which both the numerator and denominator vary in time. We have calculated both of these ratios similarly to Phillips et al. (1999) and Nugent et al. (2002), by simulating the effects of extinction on the sample of 91 spectra described in §2.1, using the $R_V = 3.1$ extinction law of CCM89,[3] as modified by O'Donnell (1994), and synthetic photometry through the Bessell (1990) standard passbands.[4]

We present our calculations of $R_X^{\rm true}$ and $R_X^{\rm obs}$ in Figures 2 and 3, respectively. We find a good match in general to the results of Nugent et al. (2002) and Phillips et al. (1999), which is not

[3]We have also explored using the extinction law presented by Fitzpatrick (1999), with similar results.

[4]Previous incarnations of MLCS used extinction coefficients tabulated for the Johnson *R* and *I* passbands, rather than the Kron/Cousins passbands. We have rectified this here.

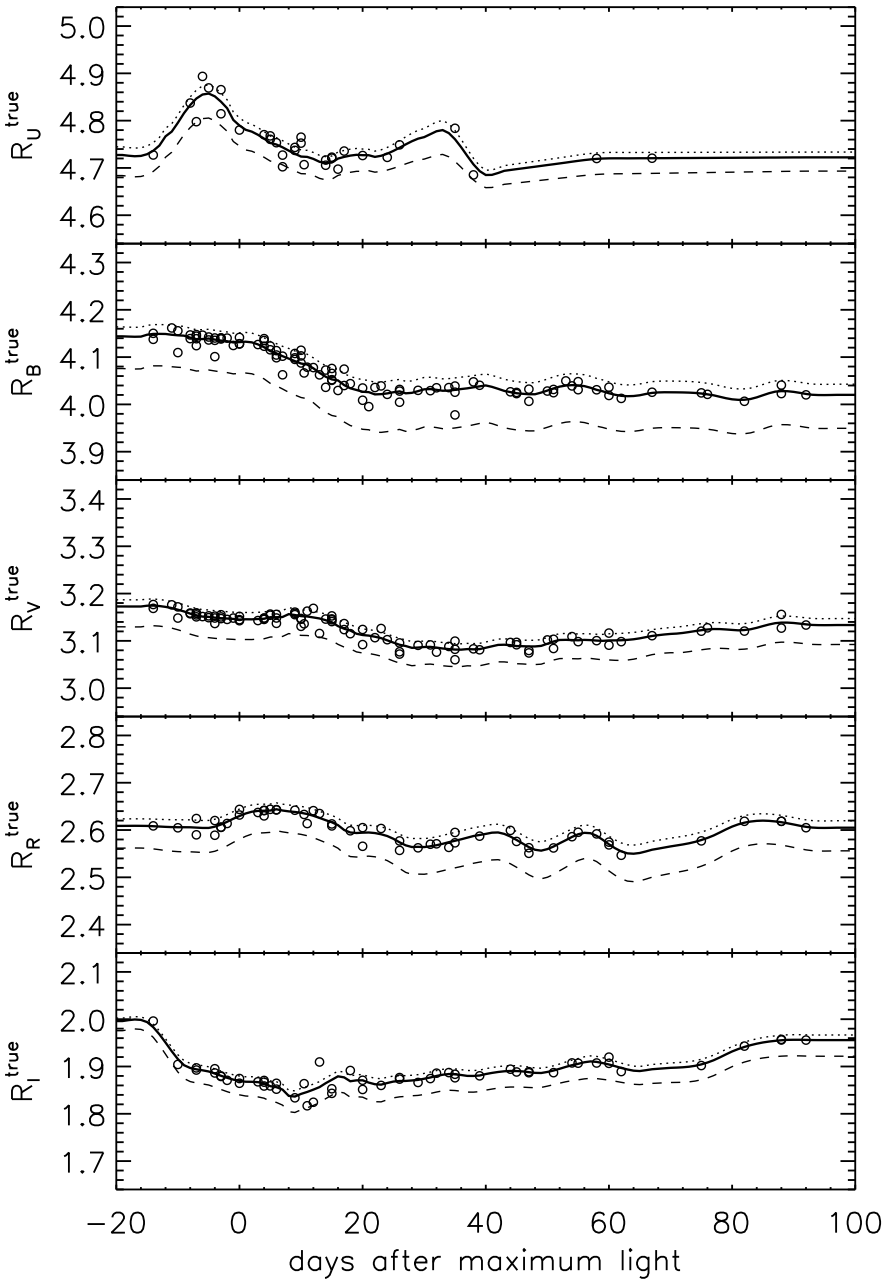

Fig. 2.— Variation of $R_X^{\rm true} \equiv A_X/E(B-V)_{\rm true}$ in *UBVRI* as a function of supernova phase. The open circles represent the measurement from the individual spectra and the heavy solid line is the smoothed representation. The dotted and dashed lines show the variation of $R_X^{\rm true}$ with the total extinction (cf. Phillips et al. 1999, their Figure 2). The dashed line corresponds to $E(B-V)_{\rm true} = +1.0$ mag relative to the solid line (which was calculated for $E(B-V)_{\rm true}$ approaching zero). The dotted line corresponds to $E(B-V)_{\rm true} = -0.5$ mag relative to the solid line (for illustration only, as it would be unphysical unless the extinction zeropoint for the solid line was significantly underestimated).

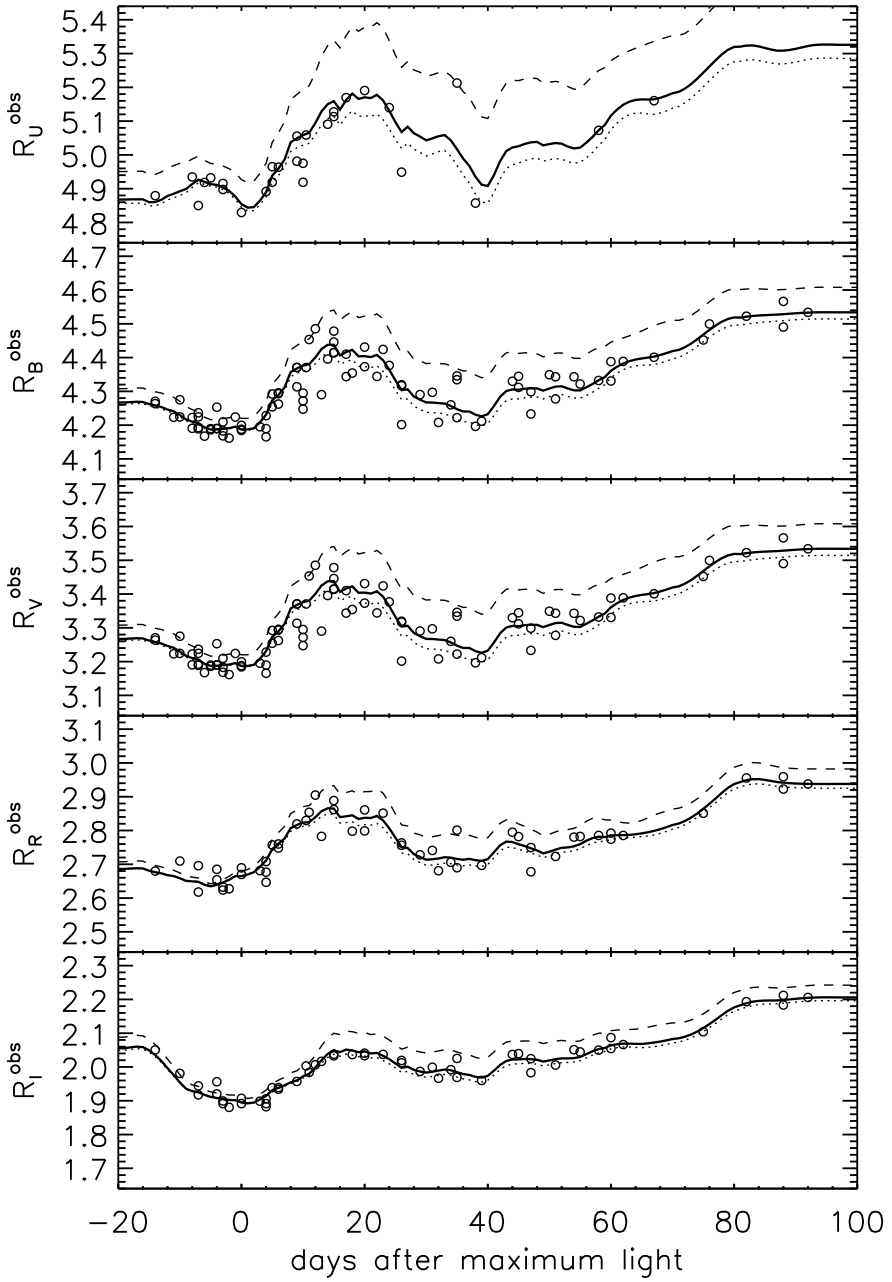

Fig. 3.— Same as Figure 2, except showing the variation of $R_X^{\rm obs} \equiv A_X/E(B-V)_{\rm obs}$. Note that the y-axis ranges have been increased in this figure, to encompass the larger variations in $R_X^{\rm obs}$, and that $R_B^{\rm obs} = R_V^{\rm obs} + 1$ by definition.

surprising, as we have many of the input spectra in common. The figures show the time variation of these two ratios as well as its variation over two magnitudes in $E(B-V)_{\rm true}$. Both of these ratios have their uses, depending on whether one knows the extinction *a priori* (for instance, using a Galactic reddening map) or is measuring it from the observed SN colors. Because we have used the SED of SN Ia themselves to calculate these quantities (and their time variation), it is preferable to use these results rather than those from standard filter tables (e.g., Table 6 of Schlegel, Finkbeiner & Davis 1998).

So far we have restricted ourselves to the standard $R_V = 3.1$ extinction law of CCM89, but we would like our distance measuring technique to allow for variations in the properties of the dust. CCM89 have shown that in the optical passbands, dust in our Galaxy follow extinction laws that can be expressed in terms R_V.[5] Clearly, using extinction laws with different values of R_V will lead directly to variations in $R_X^{\rm true}$ and $R_X^{\rm obs}$. The variation with the total extinction itself adds further complications and makes using these ratios cumbersome. For instance, calculating $R_I^{\rm obs} \equiv A_I/(A_B - A_V)$ involves three terms, each varying individually with epoch, total extinction and extinction law.

To make things simpler, we have chosen to work in the more natural space of A_X rather than using color excesses to parameterize the extinction. This is convenient because we fit the light curves in each passband directly, rather than fitting color curves, an approach that does not require light curves to have multiple color measurements at each epoch. Secondly, the extinction laws themselves are better characterized in ratios of extinctions, e.g., A_B/A_V, rather than in ratios of extinctions to color excesses.[6]

The first part of this framework is to separate out the time dependence of the extinction. For each passband X, we define the quantity,

$$\vec{\zeta_X} \equiv \frac{\vec{A_X}}{A_X^0}, \tag{1}$$

where we denote quantities that are functions of SN phase with vector arrows (i.e., $\vec{\zeta_X} = \vec{\zeta_X}(t)$), and A_X^0 is defined as the extinction in passband X at maximum light in B. Thus, $\vec{\zeta_X}(t = 0) \equiv 1$ by definition (all times are defined relative to maximum light in B). In Figure 4 we show our calculation of $\vec{\zeta_X}$ in *UBVRI* . The useful result is that $\vec{\zeta_X}$ captures all of the time dependence in the extinction *and* is insensitive to both the total extinction $E(B-V)_{\rm true}$ and the extinction law R_V. This point is also illustrated in Figure 4, where the dark gray bands show the variation in $\vec{\zeta_X}$ over

[5]We adopt the notation that without a superscript "true" or "obs", R_V corresponds to the R_V of CCM89, i.e., derived from photoelectric measurements of Galactic stars.

[6]This point is made explicitly by CCM89 who note that "There are some relationships which emerge more clearly when $A(\lambda)/A(V)$ is considered than when normalization by $E(B-V)$ is used."

the very wide range of 3 magnitudes of $E(B-V)_{\rm true}$ and the light gray bands show the variation of a wide range of R_V from 1.7 to 5.7 (including the full variation in $E(B-V)_{\rm true}$). While the figure shows some differences in $\vec{\zeta_X}$ at levels greater than a few percent (for instance, in I at early times), these are only realized for extreme values of both R_V and $E(B-V)_{\rm true}$. We can then confidently fix $\vec{\zeta_X}$ as shown by the heavy solid lines in the figure, independent of the reddening law and total extinction.

With the time dependence separated, we can relate the extinction in any passband at any epoch to the maximum light extinction A_X^0 in that passband. The maximum light extinctions in the different passbands are interrelated and we can define the relations between these (currently, five) parameters as a function of the total extinction and the reddening law. CCM89 show that the ratio A_X/A_V is a simple linear function of $(1/R_V)$. We have calculated this relationship at maximum light explicitly using our sample of spectra near that epoch, and fit for the coefficients α_X and β_X, defined by

$$\frac{A_X^0}{A_V^0} \quad = \quad \alpha_X + \frac{\beta_X}{R_V}. \tag{2}$$

The results are presented graphically in Figure 5, and listed in Table 2 (which also shows explicitly the relations for an $R_V = 3.1$ extinction law). Furthermore, the figure illustrates that A_X^0/A_V^0 is a very weak function of $E(B-V)_{\rm true}$ (in most cases the three open circles are indistinguishable), and we are justified in ignoring the dependence on the total extinction.

In the framework developed, then, we parameterize the extinction by two numbers: A_V^0, corresponding to the extinction in the V passband at maximum light, and R_V, describing the shape of the extinction law. The fixed coefficients α_X and β_X provide the maximum light extinctions in other passbands, and the vectors $\vec{\zeta_X}$ contain the time variation. While the parameterization in terms of $R_X^{\rm true}$ and $R_X^{\rm obs}$ is still useful for certain tasks (see below), we switch to this new framework in the MLCS2k2 fits.

Table 2. Maximum Light Extinction Coefficients

	$A_X^0/A_V^0 = \alpha_X + \beta_X/R_V$		
Passband (X)	α_X	β_X	$\alpha_X + \beta_X/3.1$
U	0.964	1.716	1.518
B	1.016	0.919	1.313
V	1.000	0.000	1.000
R	0.935	−0.300	0.839
I	0.767	−0.534	0.595

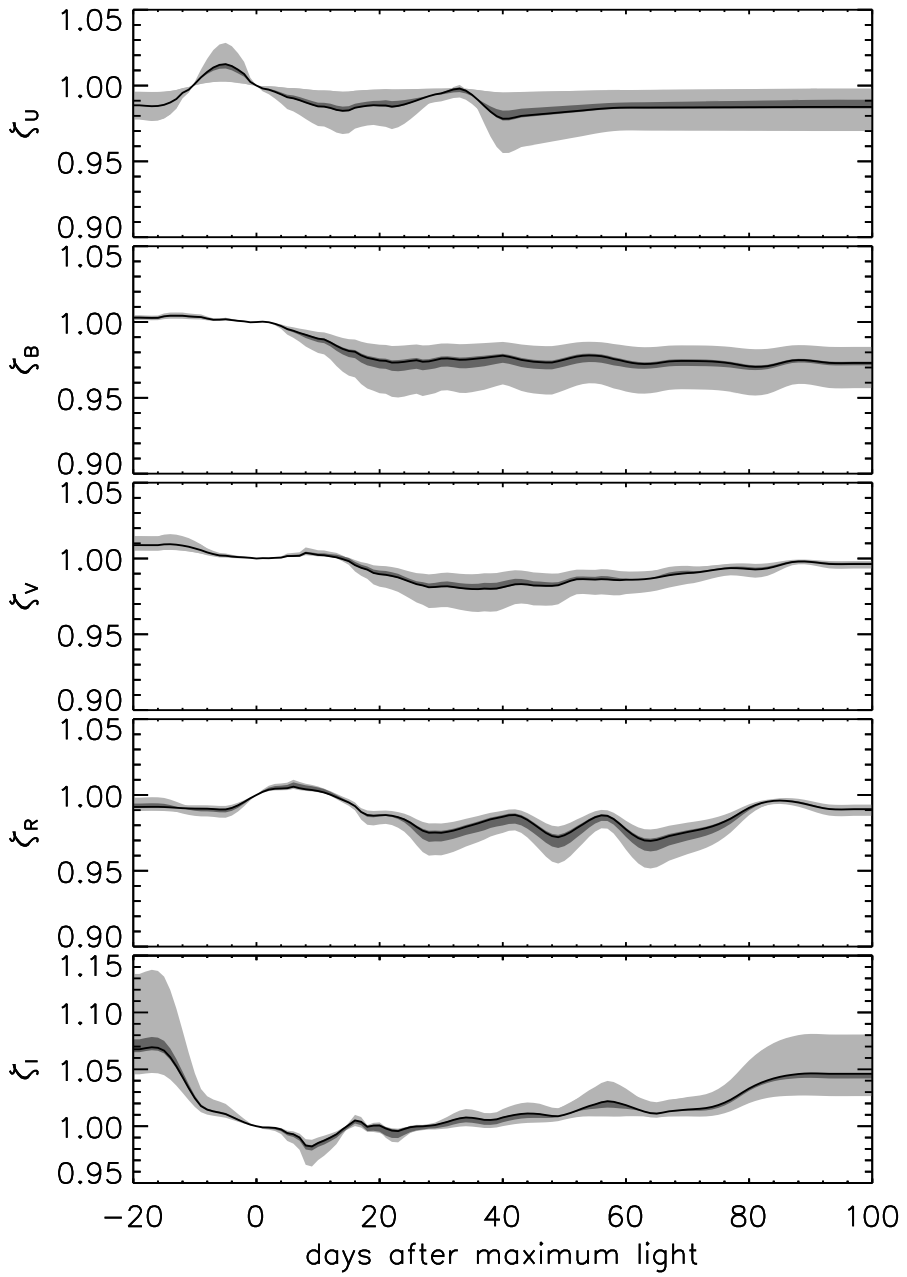

Fig. 4.— Calculation of $\vec{\zeta_X} \equiv \vec{A_X}/A_X^0$ in *UBVRI* . The dark solid line shows the result for $R_V = 3.1$ and $E(B-V)_{\rm true}$ approaching zero. The dark gray shaded area shows the range of variation in $\vec{\zeta_X}$ over 3 magnitudes in $E(B-V)_{\rm true}$, while the light gray shaded area indicates the variation in $\vec{\zeta_X}$ over that reddening range and over the range $1.7 \leq R_V \leq 5.7$.

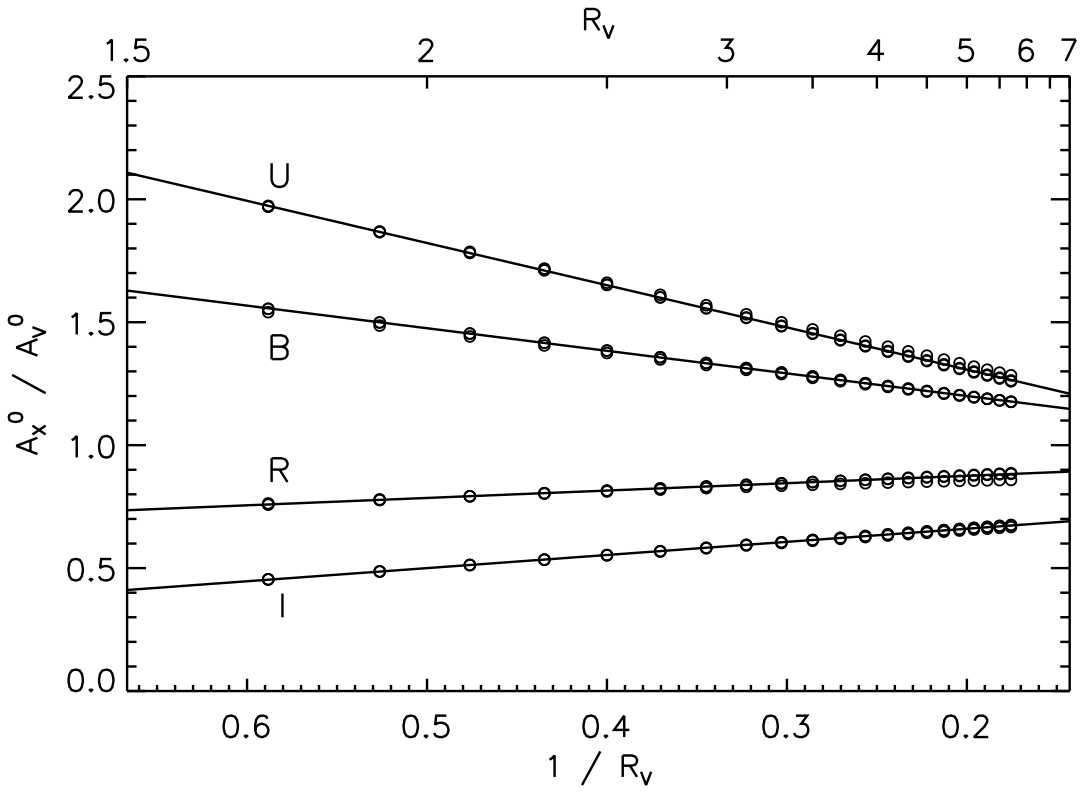

Fig. 5.— Variation of A^0_X/A^0_V as a function of R_V^{-1}. The sold lines indicate the best linear fit. The open circles show the calculated points; for each passband and R_V there are three open circles, with $E(B-V)_{\rm true} \simeq -0.5$, 0.0, and +2.5 mag, showing the small differences in the relations as a function of the total extinction.

2.3. Separating Reddening and Intrinsic Color

To define the training set that yields our desired template light curves, we need an estimate of the extinction in the host galaxy of each object. Various approaches are possible, e.g., assuming that SN Ia in early-type host galaxies or the bluest SN Ia define an extinction-free sample. Knowing the "zeropoint" of the extinction (i.e., the true, unreddened color of a SN Ia) is not strictly necessary if we are interested only in relative distances (or in tying the SN Ia distances to another set, such as the Cepheid scale), but it becomes essential if we want to use the positivity of the extinction (dust cannot brighten a source or make it appear bluer) as a constraint on our derived distances. We employ the observational results of Lira (1995), who noticed that the late time ($t \gtrsim +30$ days) $B-V$ color evolution of SN Ia was remarkably similar, regardless of light curve shape near maximum light. SN Ia undergoing this transition to the nebular phase also show very similar spectra (e.g., see Filippenko 1997). Phillips et al. (1999) used this "Lira Law," $(B-V)_0 = 0.725 - 0.0118(t_V - 60)$, giving the intrinsic color in terms of the number of days past V maximum light, to measure extinctions and to constrain the $B-V$ and $V-I$ maximum light colors of SN Ia (as a function of Δm_{15}). The Lira Law as quoted was derived from a fit of late-time photometry of four objects (SN 1992A, 1992bc, 1992bo and 1994D), estimated to be free of host-galaxy extinction. Phillips et al. (1999) estimate that the intrinsic dispersion about the relation is 0.05 mag.

We have attempted to check the Lira relation with another approach. Rather than trying to choose an extinction-free subsample of the data, we use all the data we can. Beginning with the sample of 133 SN Ia described above, we have corrected the photometry for Galactic extinction, using the reddening maps of Schlegel et al. (1998) and our calculation of $R_X^{\rm true}$ above, with the assumption that the Galactic component is described by an $R_V = 3.1$ extinction law. We have also applied the K-correction (see §2.1) and corrected for time dilation to bring the data to the SN rest frame. We have then constructed $B-V$ color curves for the sample, and attempted to measure the late-time color evolution. We find that the Lira late-time $B-V$ slope of -0.0118 mag day^{-1} does an excellent job of fitting the bulk of the observations.[7] We thus fix this slope and fit a straight line to all the $B-V$ observations between 32 and 92 days past B maximum light to determine the intercept, BV_{35} (which we reference to a fiducial epoch of $t = +35$ days) and its observational uncertainty $\sigma_{BV_{35}}$. Of the 133 objects listed in Table 1, 28 have no useful late-time color information, while an additional 23 have only poor data unsuitable for a good measurement, due either to too few late time points or points with large uncertainties. The BV_{35} measurements for the remaining 82 objects are listed in Table 3 and presented in a histogram in Figure 6.

We assume that this distribution is a result of three independent factors: first, observational uncertainty, second, an intrinsic $B-V$ color with an unknown scatter, and third, reddening by dust

[7]Using the 31 color curves of highest quality, we find a mean slope of -0.0123 mag day^{-1} with a standard deviation of 0.0011 mag day^{-1}.

Table 3. SN Ia Late-Time Colors

SN Ia	BV_{35} mag	$\sigma_{BV_{35}}$ mag	SN Ia	BV_{35} mag	$\sigma_{BV_{35}}$ mag
1972E	1.092	0.028	1997bp	1.305	0.073
1980N	1.139	0.027	1997bq	1.216	0.026
1981B	1.105	0.042	1997br	1.362	0.030
1986G	1.682	0.029	1997cw	1.521	0.042
1989B	1.438	0.040	1998V	1.123	0.031
1990O	1.145	0.044	1998ab	1.215	0.029
1990T	1.174	0.027	1998aq	1.099	0.026
1990Y	1.326	0.033	1998bp	1.127	0.029
1991S	1.177	0.042	1998bu	1.384	0.026
1991T	1.223	0.028	1998de	1.195	0.044
1991ag	1.121	0.029	1998dh	1.214	0.032
1991bg	1.040	0.031	1998dk	1.284	0.041
1992A	1.036	0.029	1998dm	1.461	0.031
1992J	1.148	0.048	1998es	1.166	0.042
1992K	1.045	0.034	1999aa	1.075	0.027
1992P	1.152	0.031	1999ac	1.142	0.029
1992al	1.091	0.026	1999aw	0.943	0.049
1992bc	0.981	0.028	1999by	1.067	0.027
1992bg	1.095	0.046	1999da	1.308	0.074
1992bl	1.006	0.046	1999dq	1.267	0.037
1992bo	1.036	0.072	1999ee	1.415	0.026
1993H	1.041	0.041	1999ek	1.262	0.052
1993L	1.283	0.045	1999gd	1.490	0.078
1993O	1.071	0.029	1999gh	1.100	0.026
1993ae	1.022	0.029	1999gp	1.166	0.035
1993ag	1.156	0.050	2000B	1.130	0.044
1994D	0.970	0.034	2000bh	1.176	0.026
1994M	1.233	0.029	2000bk	1.205	0.027
1994Q	1.154	0.039	2000ca	1.040	0.029
1994ae	1.055	0.027	2000cf	1.167	0.026
1995D	1.153	0.026	2000cx	0.827	0.025
1995E	1.857	0.089	2000dk	1.007	0.082
1995ac	1.117	0.037	2000fa	1.159	0.047
1995ak	1.331	0.033	2001V	1.144	0.026
1995al	1.225	0.032	2001bt	1.314	0.035
1995bd	1.274	0.033	2001cn	1.272	0.032
1996C	1.107	0.049	2001cz	1.221	0.032
1996X	1.083	0.035	2001el	1.358	0.027
1996bl	1.161	0.047	2002bo	1.450	0.027
1997E	1.111	0.031	2002er	1.233	0.030
1997Y	1.148	0.031	2003du	1.050	0.026

Note. — Determined from a linear fit to SN rest-frame $B-V$ color measurements between 32 and 92 days past B maximum light, with $(B-V)(t) = BV_{35} - 0.0118(t - 35)$. See text for details.

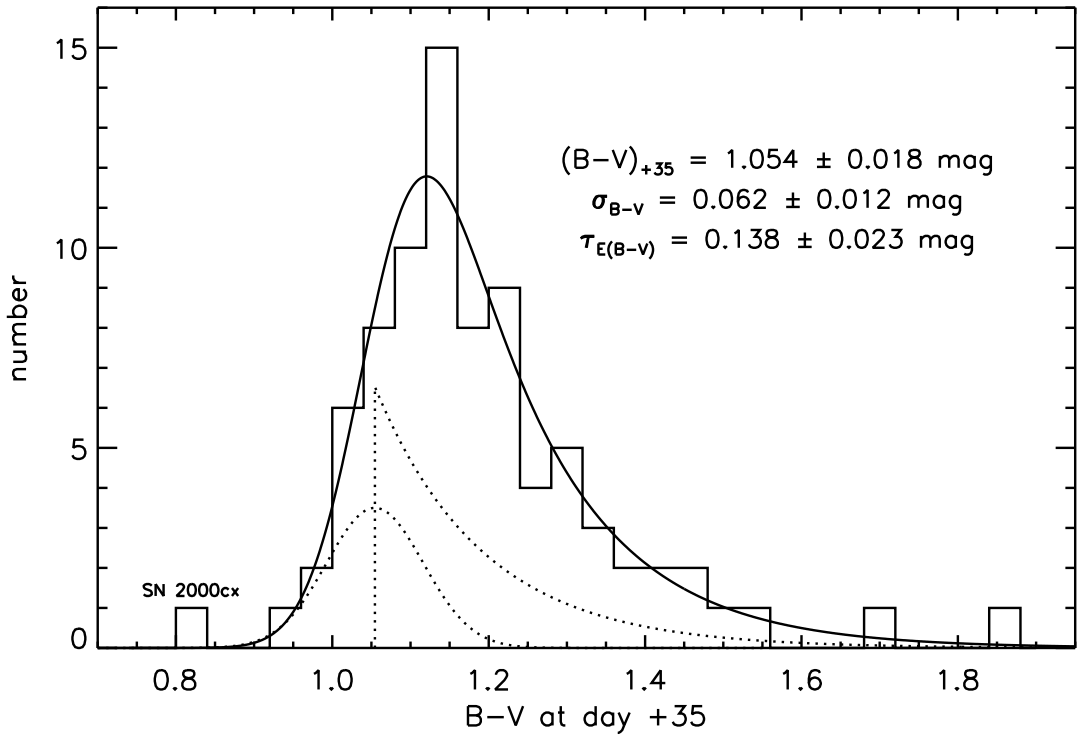

Fig. 6.— Histogram of 82 SN Ia with well-measured late-time $B-V$ color evolution. The data were corrected for Galactic extinction and the K-correction, and referenced to +35 days after B maximum, adopting a late-time color evolution slope of -0.0118 mag day^{-1}. The maximum-likelihood fit model is shown as the solid curve; it is the convolution of the dotted curves shown (at an arbitrary scale for clarity). SN 2000cx, a clear outlier, was not included in the fit.

in the host galaxy. We then model the distribution of the intrinsic component as a Gaussian with mean $(B-V)_{+35}$ and standard deviation σ_{B-V} (which subsumes the observational errors), and the distribution of the reddening as an exponential with scale length $\tau_{E(B-V)}$, such that the probability density of the reddening peaks at zero, and falls to $1/e$ of the peak at $\tau_{E(B-V)}$. The probability distribution function of the sum of these two components is just the convolution of the individual distributions, and we perform a maximum-likelihood analysis using each point to determine the best-fit model parameters. The results are also shown in Figure 6, with the convolution overplotted on the histogram and the components inset. The maximum-likelihood model parameters are $(B-V)_{+35} = 1.054 \pm 0.018$ mag, $\sigma_{B-V} = 0.062 \pm 0.012$ mag, and $\tau_{E(B-V)} = 0.138 \pm 0.023$ mag, where the uncertainties were determined by bootstrap resampling of the data set.

There are a couple of cautionary points about this result. First, we have excluded from the fit the very peculiar SN 2000cx (Li et al. 2001), which is a clear outlier in the histogram and whose light curve (but not peak luminosity) is significantly unlike other SN Ia (Li et al. 2001; Jha et al. 2006). In addition, because the SN Ia we study were discovered in a variety of supernova searches, they do not comprise a complete or well-defined sample, and thus may be biased with respect to the true distribution of SN Ia late-time color. In particular, there may be a significant population of heavily obscured SN Ia that are not present in the sample, leading to an underestimate of $\tau_{E(B-V)}$, assuming an exponential distribution is valid at all (Hatano, Branch, & Deaton 1998). While our derived value for $\tau_{E(B-V)}$ is valid for the sample we study and whose distances we derive in this paper, other supernova surveys with flux or volume limited samples, or searches in infrared, may find differing numbers heavily extinguished SN Ia and different estimates of $\tau_{E(B-V)}$.[8]

Fortunately, we are chiefly interested in $(B-V)_{+35}$ and σ_{B-V}, and it is unlikely our estimates of these are significantly biased. Our results with this maximum likelihood method are in good accord with the Lira relation (which predicts $(B-V)_{+35} \simeq 1.044$) and its estimated dispersion. Our approach has the advantage of using all normal SN Ia to determine the intrinsic color zeropoint, rather than just the bluest objects. As Figure 6 shows, in addition to having low reddening, the bluest objects are also intrinsically bluer than the mean unreddened color. Part of the "intrinsic" color scatter, σ_{B-V} is due to observational uncertainty in the color measurement. Based on our color measurements, with an average uncertainty of 0.037 mag, we can remove this component and estimate the true intrinsic color scatter $\sigma_{(B-V)\mathrm{int}} = 0.049$ mag.[9]

[8]If, for example, we truncate the observed distribution to eliminate the reddest objects with $BV_{35} \geq 1.5$ mag, the derived scale length is $\tau = 0.104 \pm 0.021$ mag.

[9]Nobili et al. (2003) suggest that the distribution of $B-V$ observations of unextinguished SN Ia near 35 days past maximum can be explained entirely by measurement errors, with no intrinsic component to the dispersion. However, here we have combined late-time data from 32 to 92 days into one measurement using the Lira law, and this combination reduces the observational uncertainty. Even with a conservative estimate of a positive correlation among the late-time data for a given SN, our results require an intrinsic late-time color dispersion with a significance $\gtrsim 3$-σ.

Our model then establishes independent distributions for both the intrinsic color of SN Ia and the reddening. Intrinsically, SN Ia at 35 days past maximum (and even later times, if corrected by the Lira slope to the reference +35 day epoch) have a $B-V$ color distribution which can be described by a Gaussian with a mean of 1.054 mag and standard deviation of 0.049 mag. In our sample, the distribution of host-galaxy reddening by dust $E(B-V)$ is well described by an exponential with a scale length of 0.138 mag. The observed color is the sum of the intrinsic color and the reddening.

A straightforward application of Bayes's theorem yields the prescription to turn the model around: determining estimates of the reddening (and intrinsic color) from a measurement of the observed color. For notational simplicity, we define $E \equiv E(B-V)$ as the host-galaxy reddening, L as the intrinsic late-time $B-V$ color, and O as the observed late-time $B-V$ color, with $O = E + L$. Bayes's theorem says that the conditional probability $p(E \mid O) \propto p(O \mid E)p(E)$, where $p(E)$ is just the reddening distribution derived above, $p(E) \propto \exp(-E/0.138)$, for $E \geq 0$. The other term, the probability of measuring an observed color *given* the reddening, $p(O \mid E)$, is simply equivalent to $p(L = O - E)$, the probability that the *intrinsic* color (which has a Gaussian distribution, as above) is that which added to E gives the observed color, O.

The conclusion is that for a SN Ia that has a measured late-time $B-V$ color BV_{35} with an observational uncertainty $\sigma_{BV_{35}}$ (with all quantities measured in magnitudes), the probability distribution of the host-galaxy reddening $E(B-V)$, again called E for notational simplicity, is given by

$$p(E \mid BV_{35}, \sigma_{BV_{35}}) \;\propto\; \begin{cases} \exp\left(-\frac{(BV_{35}-E-1.054)^2}{2\left(\sigma^2_{BV_{35}}+0.049^2\right)}\right)\exp\left(-\frac{E}{0.138}\right) & \text{if } E \geq 0, \\ 0 & \text{if } E < 0. \end{cases} \tag{3}$$

This is a generalization of the Bayesian filter of Riess, Press, & Kirshner (1996a), where our model now includes the uncertainty caused by the intrinsic scatter in SN Ia late-time color in addition to the observational uncertainty. We use equation 3 with the data in Table 3 to get the initial host-galaxy reddening estimates required in training MLCS2k2.

The intrinsic scatter in the late-time colors (0.049 mag) dominates the uncertainty in the mean unreddened color from the maximum likelihood fit (0.018 mag), and thus we strongly urge that "negative" extinction be disallowed in any model. The idea of negative extinctions (because of a color zeropoint that is estimated redward of the true color zeropoint) is a convenient fiction, but only if the intrinsic color scatter is smaller than the zeropoint uncertainty. Here we have the opposite case; blue SN Ia (with $BV_{35} = 1.0$ mag, for example) are blue because of the intrinsic color variation, not because they are the only "truly" unextinguished objects. Thus, "correcting" them with a negative extinction is a mistake. As long as there is no systematic error in the mean unreddened color approaching the level of the intrinsic scatter, the mean of equation 3, $\int_0^\infty p(E \mid BV_{35}, \sigma_{BV_{35}})EdE$, provides an *unbiased* estimate of the host-galaxy reddening.

3. Model

We are now in a position to define our light curve model. For each passband, X, we fit the observed light curves (corrected for Galactic extinction, K-correction, and time dilation), $\vec{m_X}$ as follows (arrowed quantities span the SN rest-frame phase):

$$\vec{m_X}(t - t_0) = \vec{M_X^0} + \mu_0 + \vec{\zeta_X}\,(\alpha_X + \beta_X/R_V)\,A_V^0 + \vec{P_X}\Delta + \vec{Q_X}\Delta^2, \tag{4}$$

where t_0 is the epoch of maximum light in B, $\vec{M_X^0}$ are the absolute magnitudes of the fiducial SN Ia, μ_0 is the true distance modulus, R_V and A_V^0 are the host-galaxy extinction parameters (§2.2), Δ is the luminosity/light-curve shape parameter, and $\vec{P_X}$ and $\vec{Q_X}$ are vectors describing the change in light curve shape as a (quadratic) function of Δ. There are five "free" parameters in the model: t_0, μ_0, Δ, A_V^0, and R_V. As in previous versions of MLCS, we solve for the optimal vectors $\vec{M_X^0}$, $\vec{P_X}$, and $\vec{Q_X}$ using a training set for which we estimate initial values of the free parameters based on relative distances from the Hubble Law.

Given a training set and solution for the optimal vectors, we construct an empirical model covariance matrix S that incorporates the variance and covariance in the residuals of the training set data from the model (minus the variance and covariance in the training set data itself). Following Riess et al. (1998a), the diagonal elements of the S matrix are derived from the variance about the model, while the off-diagonal elements are estimated from two-point correlations (in the same passband at different epochs, in different passbands at the same epoch and in different passbands at different epochs).

Armed with the template vectors and the model covariance matrix, we can apply the model. Along with the light curve observations $\vec{m_X}$, conscientious observers provide a covariance matrix of "noise", N, albeit typically only a diagonal one consisting of the variance of each data point (even though SN light curve data can be highly correlated, for instance in the fact that all the light curve points are usually referenced to the same few field comparison stars). We correct these data for Galactic extinction, and incorporate the uncertainty estimate of Schlegel et al. (1998), whereby $\sigma\,(E\,(B-V)_{\rm true}) \simeq 0.16 \times E(B-V)_{\rm true}$, updating both the diagonal and off-diagonal elements of N (the uncertainties in the Galactic extinction correction are highly correlated, but generally small). We also apply the K-correction (§2.1), and incorporate the K-correction uncertainty in the diagonal elements of N (unfortunately we do not have enough data to estimate the K-correction correlations) and correct for time dilation.

We find the best-fit model parameters via χ^2 minimization, with

$$\chi^2 = \vec{r}^{\,T} C^{-1} \vec{r}, \tag{5}$$

where $\vec{r}$ is the vector of residuals (in all bands) for a given set of model parameters, and $C = S + N$. We use a downhill simplex method (amoeba; Press et al. 1992) to perform the minimization

(though linear algebra suffices in solving for μ_0 and A_V^0, if the other model parameters are fixed) and determine their best-fit parameters. Because the S matrix is empirically determined from the training set, application of the model to objects in the training set will necessarily have a minimum reduced χ^2_ν ($\equiv \chi^2$ per degree of freedom) close to unity, but in applying the model to other objects, the minimum χ^2_ν still yields useful goodness-of-fit information (indicating how similar the light curves of the new object are to those in the training set, given the nature of the model).

We have also incorporated the ability to add priors on any of the model parameters directly into the fit. The previous versions of MLCS, for instance, used a Bayesian filter requiring the extinction to be non-negative, but this was enforced after the best fits were determined. The advantage of that approach was convenience and expediency, but at the expense of ignoring correlations among the parameters. Those versions of MLCS used μ_V, the distance modulus uncorrected for extinction, as the basic distance model parameter rather than $\mu_0 = \mu_V - A_V$, in order to minimize this undesirable correlation, thus making the Bayesian filter simple and effective. However, there are situations in which one might like to include other prior information into the fit. For example, a sparsely-sampled light curve may not allow for a good determination of the time of maximum light, but we may have other information about the time of maximum from spectroscopy (Riess et al. 1997a). In the extreme limit of the "snapshot" method, (Riess et al. 1998b), spectroscopy could be used to determine prior constraints on both t_0 and Δ. Alternately, we may have observations in additional, non-modeled passbands (such as in the near-infrared), which impose prior constraints on A_V^0 or R_V. Incorporating priors, $\hat{p}$, into the fit is straightforward, we simply adjust the χ^2 to

$$\chi^2 \;=\; \vec{r}^{\,T} C^{-1} \vec{r} - 2 \ln \hat{p}(t_0, \mu_0, \Delta, A_V^0, R_V), \tag{6}$$

taking care to reinterpret this "χ^2" in the proper way when estimating the goodness of the model fit (which depends only on the first term, as opposed to the parameter uncertainties). This procedure allows the parameters to be "naturally" filtered during the fit.

4. Training

The training set is the most critical part of the analysis; it requires objects with accurate estimates of the model parameters, in order to construct the template vectors and covariance matrix. As in Riess et al. (1998a), we use the Hubble law to determine precise relative distances, thus useful objects in the training set need to have recession velocities that are dominated by cosmological expansion, not peculiar motions. The objects also need to have well-measured light curves at maximum light so that t_0 and $V_{\max}$ (to be used in determining Δ, as below) can be reliably determined. Finally, we require accurate host-galaxy extinction estimates for the training set objects. This estimate comes from well-sampled B and V light curves at the epochs past +35 days when the intrinsic color is not a strong function of luminosity, as described in §2.3. Ideally, we would also

like estimates of the host-galaxy extinction law R_V for each SN, but these are not easily determined *a priori*, and values based on the SN light curves themselves would require knowledge of the intrinsic colors we are trying to determine! To avoid this conundrum, then, we restrict the initial training sample to objects not very significantly reddened (as determined from the $B-V$ color at ∼35 days past maximum), so that variation in R_V does not have a large effect, allowing us to fix R_V = 3.1 for the initial training set.

Our initial training set consists of 37 SN Ia, with $cz \geq 2500$ km s^{-1} (measured in the CMB frame) and well-sampled light curves beginning earlier than 10 days past maximum light: SN 1990O, 1990af, 1992P, 1992ae, 1992al, 1992bc, 1992bg, 1992bl, 1992bo, 1992bp, 1992br, 1993H, 1993O, 1993ag, 1994M, 1995ac, 1996C, 1996bl, 1997E, 1997Y, 1997bq, 1998V, 1998ab, 1998bp, 1998de, 1998es, 1999aa, 1999ac, 1999da, 1999gp, 2000ca, 2000cf, 2000dk, 2000fa, 2001V, 2001cz, and 2002er. For each SN, we initially calculate Δ as the difference between V magnitude at maximum light (corrected for host-galaxy extinction) and the Hubble line given the host-galaxy redshift. We assign an uncertainty in Δ from the quadrature sum of the uncertainty in the direct fit of $V_{\rm max}$, the extinction uncertainty and a distance uncertainty based on a peculiar velocity uncertainty of $\sigma = 300$ km s^{-1}. These initial guesses of Δ span a range of over two magnitudes, and the sample includes a wide range of over- and under-luminous objects.

From the initial guesses of the model parameters and uncertainties, we derive the best fit vectors, $\vec{M^0_X}$, $\vec{P_X}$, and $\vec{Q_X}$, as well as the model covariance matrix S, all of which are sampled daily over the range $-10 \leq t \leq +90$ days past B maximum, where the data are constraining. With these vectors, we can apply this initial model to our larger sample of supernovae; deriving new estimates of Δ and A^0_V while constraining the distance moduli to their Hubble Law estimates (within the uncertainties listed above). Iterating this procedure leads to convergence on a consistent set of model parameters, template vectors and a model covariance matrix.[10]

In Figure 7, we present the one-parameter family of unreddened template light curves in *UBVRI* over a wide range of luminosity, based on the final template vectors derived in the training process. The characteristic result that intrinsically brighter SN Ia (low Δ) have broader light curves is clearly established in all passbands. We note that while Δ is originally estimated by the relative V-band magnitude difference at maximum light, during the iterative training the meaning of Δ

[10]In principle, this procedure could artificially decrease the scatter in our distance measurements, if the contribution of individual SN Ia to the templates "circularly" affected their fits when the model is applied. In practice, however, the templates are derived from a large enough number of objects that this effect is negligible. We have further tested this by applying the model derived only from the initial training set to the remaining objects, as well as by partitioning the full sample and iteratively training the model on one half of the data, and then applying it to the other half. In all cases the scatter in the Hubble diagram of the objects not used in the training set is significantly decreased, typically from ∼0.5 mag to ≲0.2 mag. We thus choose to retain the largest training set sample we can to most robustly determine the templates and, importantly, their associated model uncertainty.

changes. It should be viewed simply as a unitless fit parameter that describes the family of light curves, and can differ significantly from its original value for a given supernova. In particular, it should not be subtracted directly from $V_{\rm max}$ to obtain a corrected peak magnitude, though this has been a convenient usage in the past.[11] The fiducial MLCS2k2 $\Delta = 0$ model light curve has $\Delta m_{15}(B)$= 1.07 (read directly off the B-band template) and stretch parameter, $s_B = 0.96$ (fit as described by Jha et al. 2006). The intrinsic absolute V magnitude at the time of B maximum light is given by

$$M_V(t = 0) = -19.504 + 0.736\Delta + 0.182\Delta^2 + 5\log\left(\frac{H_0}{65\ {\rm km\ s^{-1}\ Mpc^{-1}}}\right) \quad {\rm mag.} \qquad (7)$$

The MLCS2k2 relations also allow us to determine the intrinsic colors of SN Ia with varying luminosity at any epoch. In Figure 8, we show a sample of the color relations in $U-B$, $B-V$, and $V-I$, at maximum light and 35 days after maximum. Our fiducial $\Delta = 0$ SN Ia has $U-B = -0.47$ mag, $B-V = -0.07$ mag, $V-R = 0.00$ mag, and $V-I = -0.29$ mag, at the time of B maximum light. The intrinsic dispersion in these colors is captured in the model covariance matrix. Because the intrinsic colors are determined by the model at any epoch, all of the observations can be used to constrain the extinction and Δ, weighted by the observational and model uncertainties. This is a more flexible approach than just using late-time or maximum-light relations to determine the extinction (e.g., Phillips et al. 1999), or using colors at one specific epoch to determine the intrinsic luminosity and extinction (e.g., at $t = +12$ days, as suggested by Wang et al. 2005).

5. Application

We have applied the model to our full sample of 133 SN Ia, employing priors, $\hat{p}(t_0, \mu_0, \Delta, A_V^0, R_V)$, via equation 6. Of course, in applying the model to a SN Ia light curve we impose no prior constraints on the distance modulus, μ_0. We require t_0 to be within ± 3 days of the input estimate used to derive the time-dependent Galactic extinction and K-corrections; in cases where the fit t_0 is outside this range or otherwise inconsistent with the input value, we start the fit over using the updated estimate for t_0. We use a uniform prior on Δ over the range $-0.3 \leq \Delta \leq 1.6$, with a Gaussian rolloff (with $\sigma = 0.1$) on either side of that range; this restricts the fits to the range of Δ encompassed by the training set (roughly between -0.4 and 1.7) and for which the model is valid. We do not see objects in our sample "piling up" at these boundaries, but it will be important to check that

[11]The reason for this is the increased dispersion and shallower slope in SN Ia luminosity at the slowly-declining end of the distribution, which has become clear only with the growing samples of SN Ia now being used to calibrate the luminosity/light-curve-shape relationship. The iterative training for MLCS2k2 associates objects with similar light curve shapes, which leads the model vectors away from their starting point at $\vec{P_V}(t = 0) = 1$ and $\vec{Q_V}(t = 0) = 0$ to convergence at $\vec{P_V}(t = 0) = 0.736$ and $\vec{Q_V}(t = 0) = 0.182$.

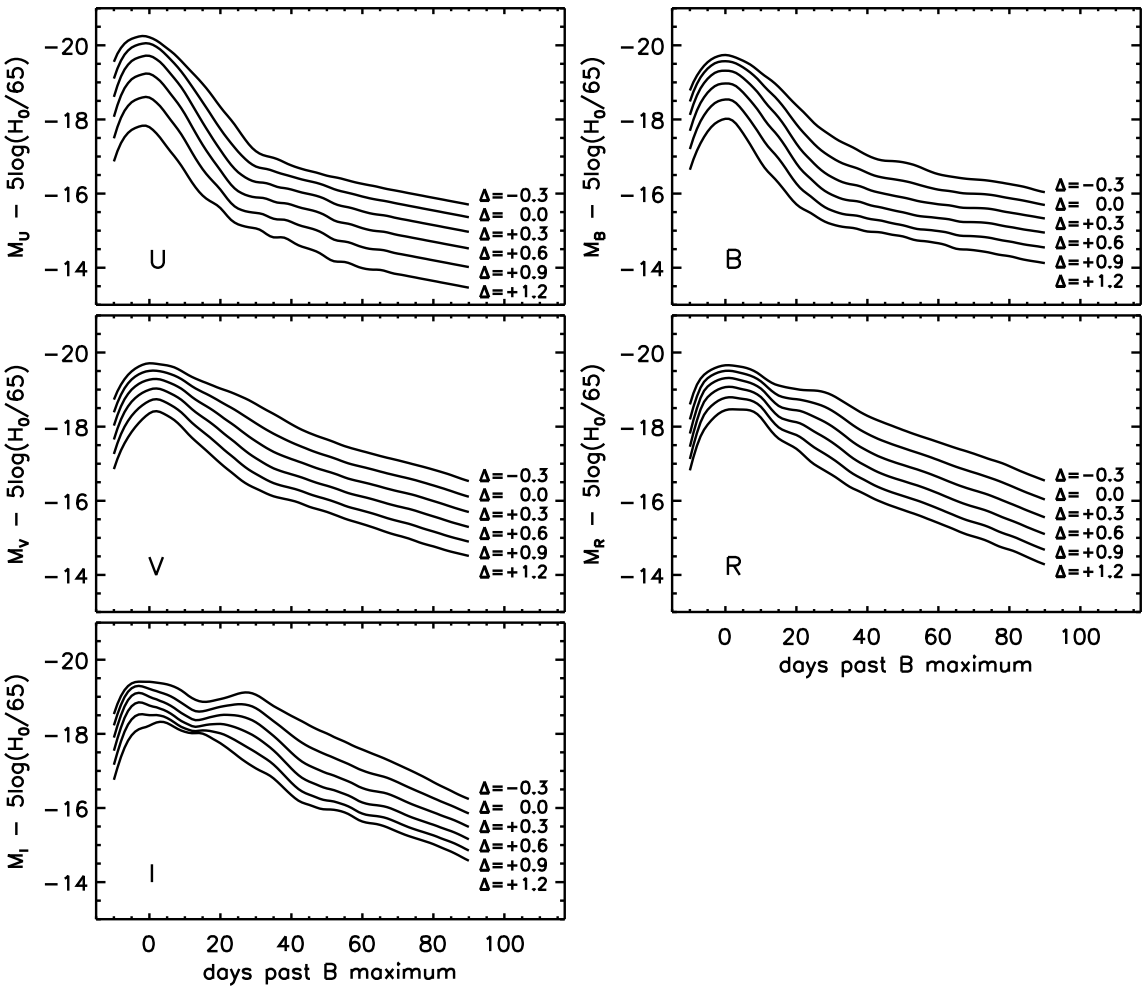

Fig. 7.— MLCS2k2 intrinsic *UBVRI* light curve templates, $\vec{M_X} = \vec{M_X^0} + \vec{P_X}\Delta + \vec{Q_X}\Delta^2$, shown over a range of luminosity and light-curve shape from $\Delta = -0.3$ (brighter) to $\Delta = +1.2$ (fainter).

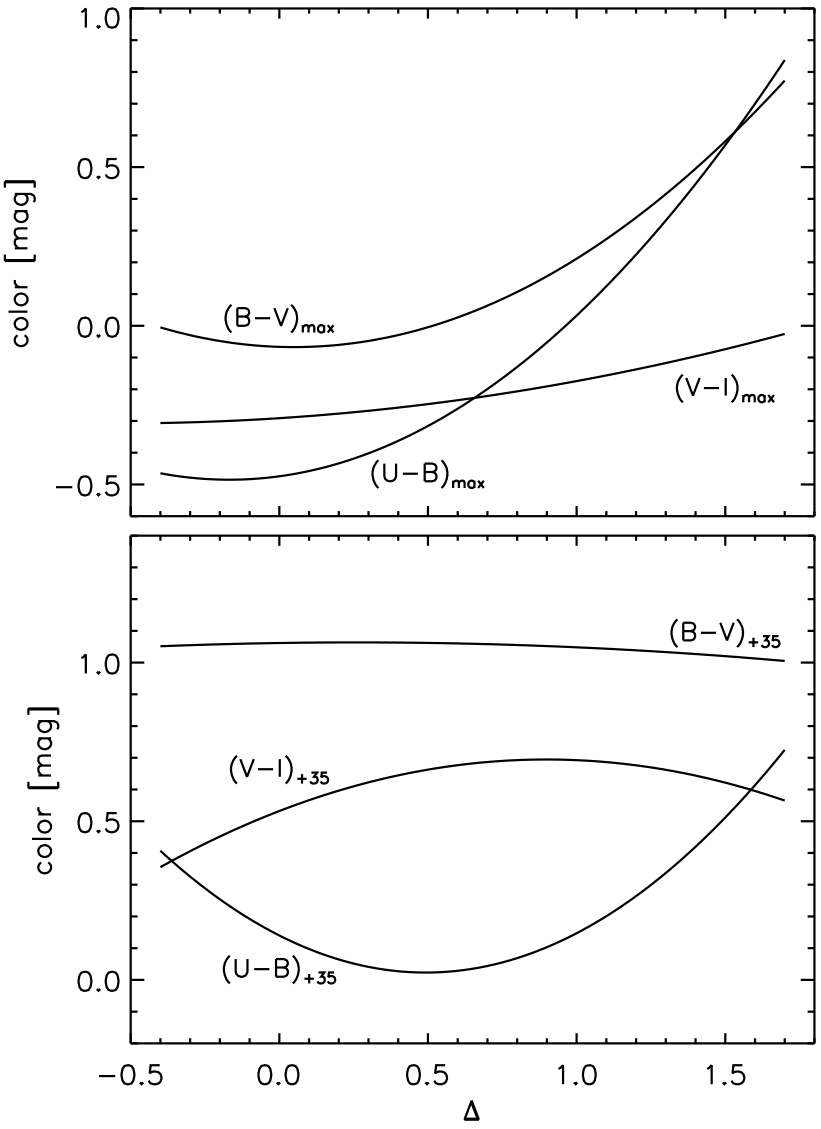

Fig. 8.— MLCS2k2 maximum light (top panel) and late time (+35 days, bottom panel) intrinsic $U-B$, $B-V$, and $V-I$ colors as a function of decreasing intrinsic luminosity (increasing Δ).

application of MLCS2k2 to a new object does not require a fit that extrapolates beyond the training set.

Additionally, we constrain the maximum light host-galaxy extinction parameter A_V^0 to be non-negative, as well as incorporate the results of our determination of the SN Ia intrinsic color and reddening distributions (§2.3). There we determined that the host-galaxy reddening distribution was well described by an exponential with a scale length of $\tau_{E(B-V)} = 0.138$ mag. Because our MLCS2k2 model parameter is A_V^0, the maximum light extinction in V, we need to convert the results based on the late-time $B-V$ color, multiplying by $R_V^{\rm obs}$ (to change from $E(B-V)$ to A_V) and dividing by ζ_V. With average late-time values of these quantities, we derive our final prior on the maximum light host-galaxy extinction, $\hat{p}(A_V^0) \propto \exp(-A_V^0/0.457 \text{ mag})$ for $A_V^0 \geq 0$. Our results show little sensitivity to the exact value for the exponential scale in the denominator.

Finally, we use a prior constraint on R_V estimated from its distribution over multiple lines of sight to stars in the Galaxy (CCM89). For $\hat{p}(R_V)$, we adopt a functional form that is Gaussian in R_V^{-1} with a mean $\langle R_V \rangle = 3.1$ and standard deviation $(\langle R_V^2 \rangle - \langle R_V \rangle^2)^{1/2} = 0.4$. The choice of a prior on R_V has a significant effect on the best-fit parameters of heavily extinguished SN Ia, and we discuss this issue more fully below (§6.4).

To fit the MLCS2k2 model, we first calculate χ^2 (equation 6) over a four-dimensional grid of $(t_0, \mu_0, \Delta, A_V^0)$, with a fixed $R_V = 3.1$. Because variation in the reddening law has only a very small effect on the measured distance if the extinction is low, we expand this to a five-dimensional grid (including R_V as a fit parameter) just for those objects which show $A_V^0 > 0.5$ mag in the initial fit. Though mapping χ^2 over a large grid is computationally expensive, it allows us to fully explore our non-linear model, and makes evident, for example, objects which could be well fit in separate regions of parameter space or otherwise have a complicated χ^2 surface (which can occur especially for SN Ia with sparse photometry).

In Figure 9 we show example light curve fits for SN 2000fa and SN 1999gh (Jha et al. 2006), whose light curves are typical in the nearby SN Ia sample. SN 2000fa has a slightly broader light curve than average and is moderately extinguished by dust in its host galaxy, while SN 1999gh is a fast-declining, subluminous SN Ia with little host extinction. The shaded regions in the figure show the model uncertainty (more precisely, the square root of the diagonal elements of S) which generally dominates the uncertainty in the data.

From the likelihood grid we calculate $p(t_0, \mu_0, \Delta, A_V^0, R_V) = \exp(-\chi^2/2)$, the posterior probability density function (pdf). We marginalize this distribution to determine the pdfs of the parameters of interest. Though the full surface is difficult to visualize or present, we show all of the two-dimensional marginalizations of the probability densities for SN 2000fa and SN 1999gh in Figure 10, clearly illustrating bivariate correlations among the model parameters. Finally, in Figure 11 we show the one-dimensional pdfs for each of the model parameters. Our best estimate

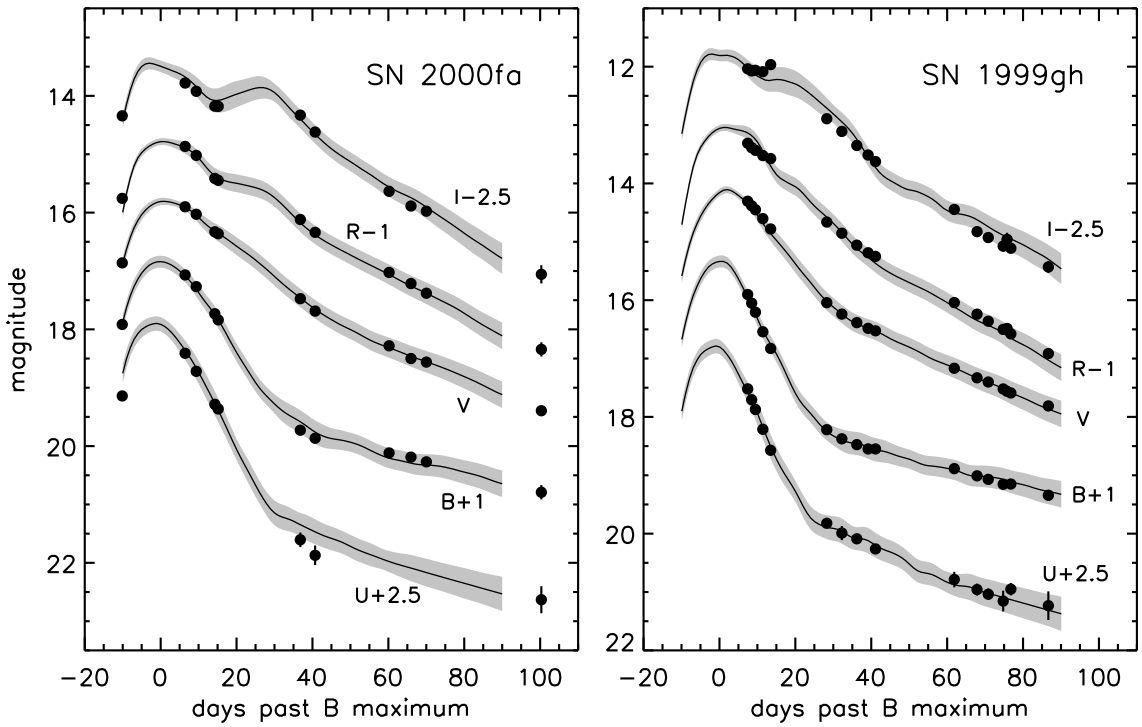

Fig. 9.— MLCS2k2 fits of SN 2000fa and SN 1999gh. The SN rest-frame *UBVRI* photometry (filled circles) is shown with the best-fit model light curves (solid lines), as well as the model uncertainty (shaded regions) derived from the diagonal elements of the model covariance matrix. The supernovae are well fit, even with gaps in the light curves and a lack of observations at maximum light.

of each parameter is given by the *mean* of these distributions (not the mode/peak), and their standard deviations give an estimate of the uncertainty. Note that in some cases these distributions are asymmetric or otherwise non-Gaussian (for example, $p(A_V^0)$ for SN 1999gh), so the mean and standard deviation do not always provide a complete description. In typical cases, however, the distribution of μ_0, the parameter of primary interest, can be well approximated by a Gaussian. While derivative calculations based on these parameters (fitting the Hubble diagram, for example) should formally employ the full pdf, we have found that after combination of just a few objects, the formally correct (but computationally intensive) method yields results indistinguishable from those based on the means and standard deviations.

We present the full results of the MLCS2k2 fits to our SN Ia sample in Table 4. The tabulated values correspond to the means and standard deviations of the posterior pdf for each parameter taken *individually*, i.e. marginalizing over all the other parameters. As such the model derived from setting each parameter to its mean value does not correspond exactly to the true best fit (at which the pdf is maximized), though the difference is typically small. Since we are generally interested in the individual parameter distributions (and the distance modulus in particular), it is more useful to present the fit results in this form.

Two objects, SN 2000cx and SN 2002cx, cannot be fit by MLCS2k2. Li et al. (2001, 2003) discuss the peculiarity of these objects, whose light curves are distinct from the vast majority of SN Ia. In addition, SN 1998D and SN 1999cw have poor fits, with very broad or multi-peaked pdfs. Both of these objects have a paucity of data (no more than three photometric points in any filter), and more importantly, the first observations for each object occurred well after maximum light (+32 and +24 days, respectively; see Table 1). This allows for a wide range of models to fit the data well, and the uncertain results are not very informative, but we present them for completeness.

Finally, analysis of the distance modulus residuals (see §6.1 and 6.2) leads us to conclude that the μ_0 (and m_V^0) uncertainties listed in Table 4 are slightly underestimated. This is likely due to our less-than-perfect knowledge of the model covariance matrix S. In particular, our analysis shows that the objects with the smallest distance uncertainties are the ones that show the strongest evidence for unmodeled variance, suggesting there is a systematic floor to the distance uncertainty (as opposed to a multiplicative factor to adjust all the uncertainties). We thus recommend that the μ_0 and m_V^0 uncertainties in Table 4 be increased by adding $\sigma_{\rm add} = 0.08$ mag in quadrature to yield a final estimate of $\sigma(\mu_0)$ and $\sigma(m_V^0)$, and we adopt this augmented uncertainty for all subsequent results. [12]

[12]Note that this number shows only the deficiency of our implementation; in a perfect version of a model like MLCS2k2, the average distance uncertainties would match the scatter in the residuals without augmentation. This is because the intrinsic variation of SN Ia around the model is encapsulated into the model covariance matrix, just not perfectly in our case. Other distance fitters that do not include any model uncertainty often add the standard deviation of the residuals in quadrature to individual distance errors; this would not be correct for MLCS2k2.

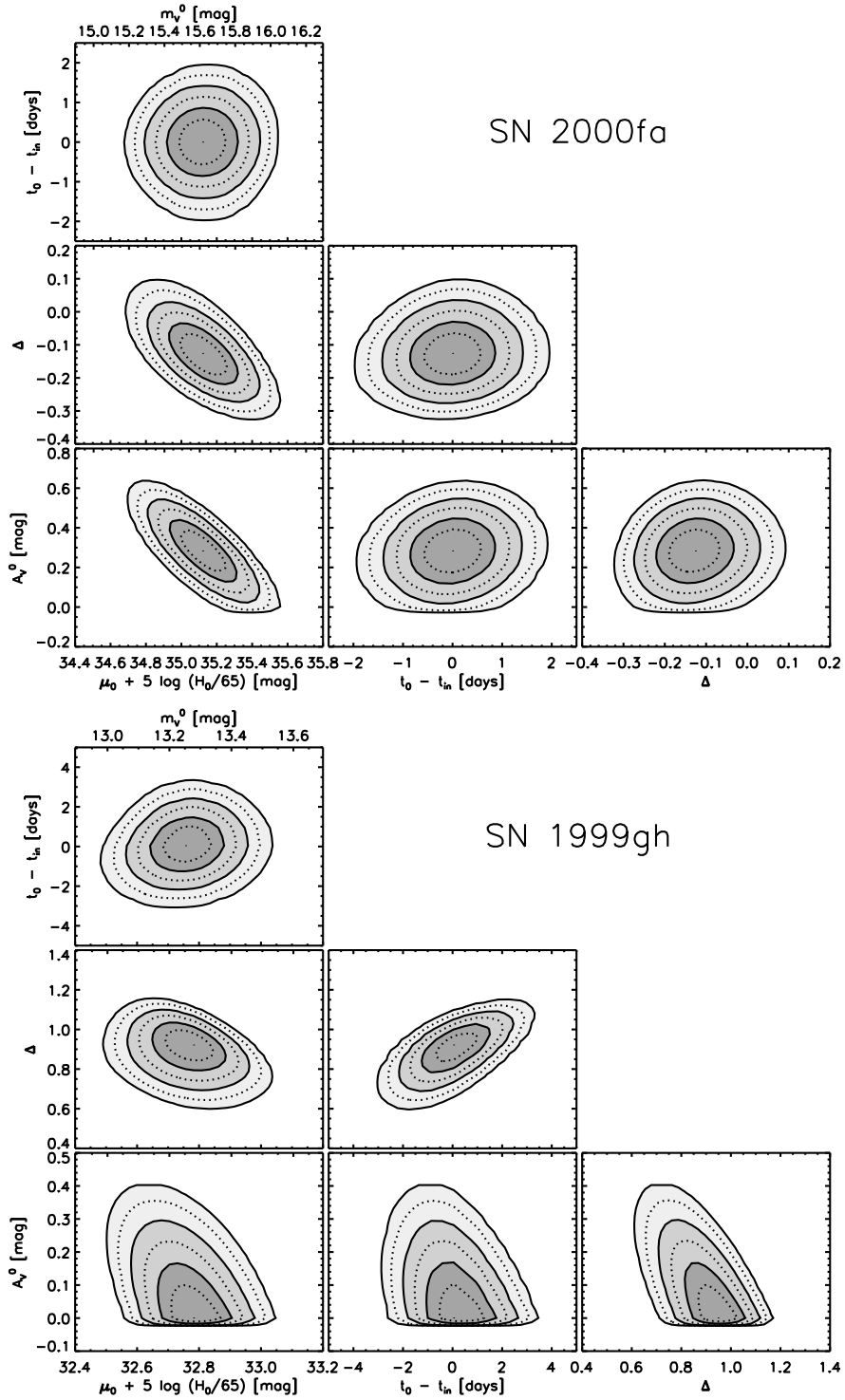

Fig. 10.— Two-dimensional MLCS2k2 probability densities for the fits to SN 2000fa and SN 1999gh. Each panel shows the four-dimensional probability density marginalized over the two remaining parameters. The solid lines and shaded regions indicate 1, 2, and 3-σ confidence regions (more precisely, 68.3%, 95.4%, and 99.7% enclosed probability regions), while the dotted lines show $\frac{1}{2}$-σ contours.

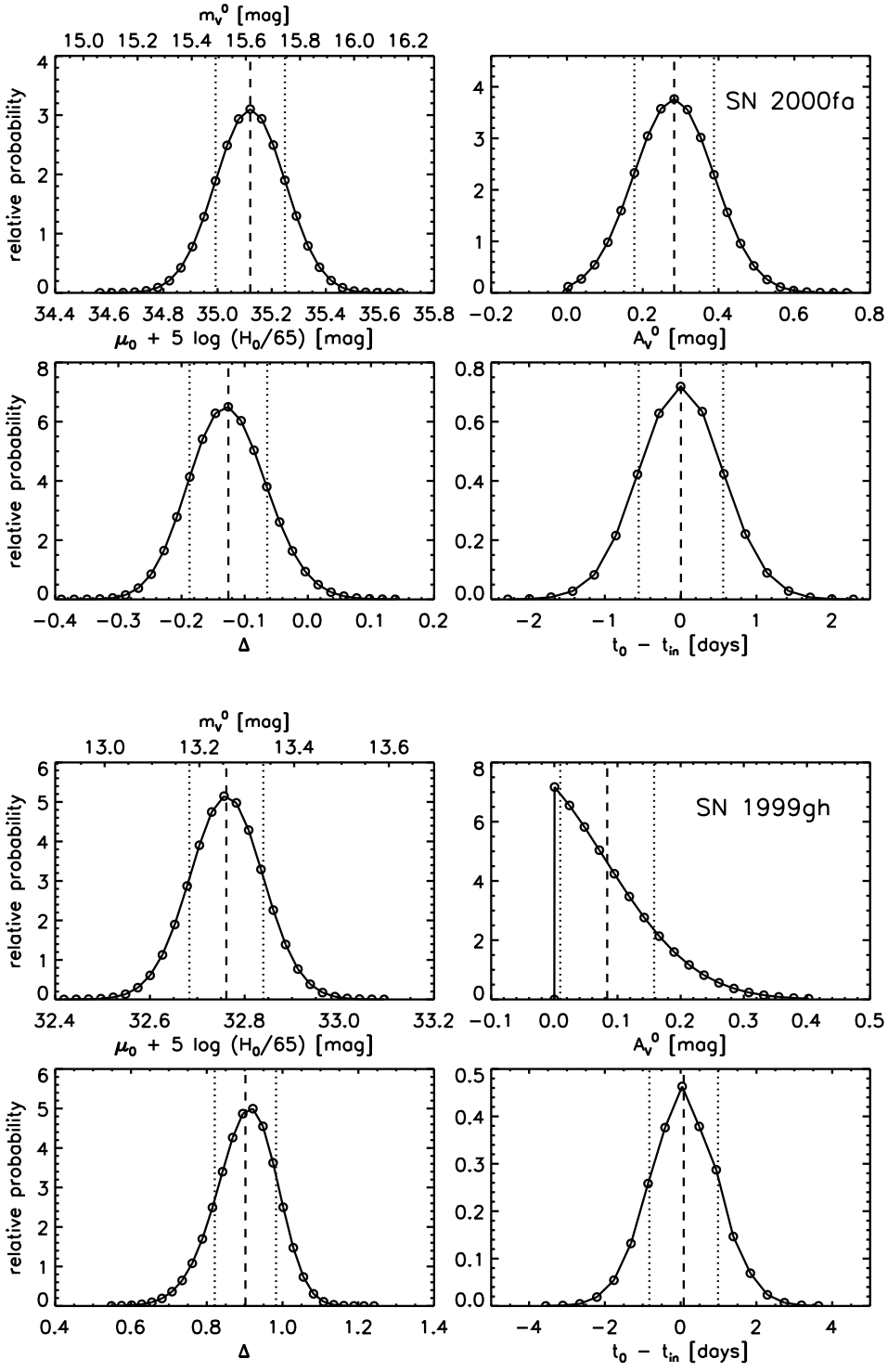

Fig. 11.— MLCS2k2 probability densities for the fits to SN 2000fa and SN 1999gh. Each panel shows the probability distribution for each free parameter, marginalizing over the three remaining parameters. The empty circles show the grid points at which the fits were calculated. The distribution mean is denoted by the dashed line, while the dotted lines show one standard deviation about the mean.

Table 4. MLCS2k2 Light Curve Fits

SN Ia	$t_0 - 2400000$ HJD	$\mu_0 + 5 \log h_{65}$ mag	Δ	A_V^0 mag	R_V	m_V^0 mag	Notes
1972E	41446.64 ± 0.96	27.829 ± 0.110	−0.145 ± 0.062	0.068 ± 0.059	3.1	8.324 ± 0.110	
1980N	44585.60 ± 0.63	31.602 ± 0.099	+0.032 ± 0.060	0.282 ± 0.082	3.1	12.098 ± 0.099	
1981B	44670.95 ± 0.73	31.104 ± 0.140	−0.081 ± 0.060	0.364 ± 0.121	3.1	11.599 ± 0.140	
1981D	44680.21 ± 0.53	31.009 ± 0.228	+0.257 ± 0.204	0.631 ± 0.270	3.07 ± 0.37	11.505 ± 0.228	
1986G	46561.36 ± 0.24	27.460 ± 0.203	+1.054 ± 0.065	2.227 ± 0.224	2.87 ± 0.27	7.956 ± 0.203	
1989B	47564.32 ± 0.59	30.040 ± 0.144	+0.035 ± 0.087	1.330 ± 0.144	2.86 ± 0.29	10.536 ± 0.144	
1990N	48081.90 ± 0.17	32.153 ± 0.090	−0.242 ± 0.046	0.174 ± 0.084	3.1	12.648 ± 0.090	
1990O	48076.12 ± 1.02	35.814 ± 0.095	−0.150 ± 0.066	0.071 ± 0.063	3.1	16.310 ± 0.095	HF
1990T	48083.06 ± 1.16	36.555 ± 0.169	−0.111 ± 0.095	0.200 ± 0.120	3.1	17.050 ± 0.169	HF
1990Y	48115.94 ± 1.28	36.221 ± 0.248	+0.036 ± 0.161	0.497 ± 0.150	3.03 ± 0.36	16.717 ± 0.248	HF
1990af	48195.86 ± 0.44	36.714 ± 0.160	+0.519 ± 0.113	0.144 ± 0.134	3.1	17.209 ± 0.160	HF
1991M	48334.98 ± 1.41	33.516 ± 0.179	+0.191 ± 0.112	0.269 ± 0.174	3.1	14.012 ± 0.179	
1991S	48348.17 ± 1.18	37.274 ± 0.131	−0.147 ± 0.074	0.129 ± 0.101	3.1	17.770 ± 0.131	HF
1991T	48374.03 ± 0.14	30.776 ± 0.080	−0.220 ± 0.031	0.340 ± 0.070	3.1	11.271 ± 0.080	
1991U	48356.18 ± 1.38	35.612 ± 0.167	−0.096 ± 0.086	0.379 ± 0.187	3.1	16.108 ± 0.167	HF
1991ag	48414.23 ± 1.45	34.007 ± 0.097	−0.134 ± 0.061	0.060 ± 0.056	3.1	14.503 ± 0.097	HF
1991bg	48603.12 ± 0.31	31.418 ± 0.101	+1.404 ± 0.047	0.611 ± 0.123	3.21 ± 0.41	11.913 ± 0.101	
1992A	48640.63 ± 0.19	31.654 ± 0.067	+0.447 ± 0.054	0.038 ± 0.032	3.1	12.150 ± 0.067	
1992G	48669.96 ± 1.06	32.584 ± 0.141	−0.198 ± 0.047	0.499 ± 0.136	3.07 ± 0.37	13.079 ± 0.141	
1992J	48671.64 ± 1.60	36.453 ± 0.265	+0.445 ± 0.236	0.259 ± 0.185	3.1	16.949 ± 0.265	HF
1992K	48674.37 ± 1.76	33.207 ± 0.153	+1.378 ± 0.116	0.223 ± 0.144	3.1	13.702 ± 0.153	HF
1992P	48719.20 ± 0.86	35.585 ± 0.124	−0.142 ± 0.082	0.136 ± 0.092	3.1	16.081 ± 0.124	HF
1992ae	48803.18 ± 1.34	37.731 ± 0.167	+0.051 ± 0.102	0.163 ± 0.141	3.1	18.227 ± 0.167	HF
1992ag	48806.95 ± 0.81	35.247 ± 0.151	+0.027 ± 0.077	0.424 ± 0.134	3.1	15.743 ± 0.151	HF
1992al	48837.86 ± 0.49	34.125 ± 0.065	−0.144 ± 0.035	0.045 ± 0.038	3.1	14.621 ± 0.065	HF
1992aq	48833.33 ± 1.18	38.651 ± 0.117	+0.193 ± 0.116	0.065 ± 0.053	3.1	19.147 ± 0.117	HF
1992au	48830.62 ± 1.55	37.379 ± 0.216	+0.292 ± 0.196	0.115 ± 0.097	3.1	17.875 ± 0.216	HF
1992bc	48912.06 ± 0.17	34.859 ± 0.042	−0.236 ± 0.030	0.017 ± 0.014	3.1	15.354 ± 0.042	HF
1992bg	48915.39 ± 1.23	36.126 ± 0.130	+0.008 ± 0.076	0.130 ± 0.091	3.1	16.622 ± 0.130	HF
1992bh	48920.43 ± 0.97	36.899 ± 0.133	−0.051 ± 0.085	0.204 ± 0.114	3.1	17.395 ± 0.133	HF
1992bk	48938.95 ± 1.59	37.184 ± 0.170	+0.414 ± 0.157	0.097 ± 0.082	3.1	17.679 ± 0.170	HF
1992bl	48946.33 ± 1.14	36.497 ± 0.123	+0.353 ± 0.117	0.061 ± 0.060	3.1	16.993 ± 0.123	HF
1992bo	48986.26 ± 0.16	34.742 ± 0.091	+0.595 ± 0.072	0.051 ± 0.049	3.1	15.237 ± 0.091	HF
1992bp	48980.41 ± 0.74	37.793 ± 0.106	+0.095 ± 0.092	0.060 ± 0.056	3.1	18.289 ± 0.106	HF
1992br	48984.63 ± 1.34	37.977 ± 0.185	+0.888 ± 0.173	0.125 ± 0.115	3.1	18.472 ± 0.185	HF
1992bs	48985.05 ± 1.30	37.636 ± 0.161	−0.031 ± 0.089	0.172 ± 0.137	3.1	18.132 ± 0.161	HF
1993B	49003.99 ± 1.35	37.779 ± 0.148	−0.115 ± 0.076	0.198 ± 0.119	3.1	18.274 ± 0.148	HF
1993H	49068.92 ± 0.46	35.109 ± 0.095	+0.904 ± 0.076	0.139 ± 0.086	3.1	15.605 ± 0.095	HF
1993L	49095.40 ± 1.51	31.986 ± 0.305	+0.041 ± 0.198	0.722 ± 0.172	3.04 ± 0.36	12.482 ± 0.305	
1993O	49134.40 ± 0.43	37.140 ± 0.095	+0.025 ± 0.070	0.077 ± 0.059	3.1	17.636 ± 0.095	HF
1993ac	49269.70 ± 1.19	36.881 ± 0.189	−0.054 ± 0.108	0.377 ± 0.191	3.1	17.377 ± 0.189	HF
1993ae	49288.58 ± 1.19	34.468 ± 0.187	+0.401 ± 0.157	0.055 ± 0.055	3.1	14.963 ± 0.187	HF
1993ag	49316.67 ± 0.68	37.041 ± 0.131	+0.119 ± 0.089	0.166 ± 0.097	3.1	17.537 ± 0.131	HF
1993ah	49302.52 ± 1.33	35.640 ± 0.200	+0.147 ± 0.164	0.136 ± 0.121	3.1	16.135 ± 0.200	HF
1994D	49432.47 ± 0.10	31.187 ± 0.067	+0.142 ± 0.035	0.109 ± 0.047	3.1	11.682 ± 0.067	

Table 4—Continued

SN Ia	$t_0 - 2400000$ HJD	$\mu_0 + 5 \log h_{65}$ mag	Δ	A_V^0 mag	R_V	m_V^0 mag	Notes
1994M	49473.61 ± 0.90	35.244 ± 0.121	+0.261 ± 0.079	0.226 ± 0.115	3.1	15.739 ± 0.121	HF
1994Q	49496.72 ± 1.09	35.759 ± 0.141	−0.140 ± 0.075	0.192 ± 0.121	3.1	16.255 ± 0.141	HF
1994S	49518.28 ± 0.50	34.356 ± 0.077	−0.084 ± 0.074	0.054 ± 0.045	3.1	14.852 ± 0.077	HF
1994T	49514.54 ± 0.52	36.012 ± 0.112	+0.731 ± 0.103	0.093 ± 0.075	3.1	16.507 ± 0.112	HF
1994ae	49684.65 ± 0.15	32.563 ± 0.065	−0.191 ± 0.036	0.070 ± 0.047	3.1	13.058 ± 0.065	
1995D	49768.60 ± 0.44	32.813 ± 0.074	−0.186 ± 0.041	0.081 ± 0.060	3.1	13.308 ± 0.074	
1995E	49774.67 ± 0.54	33.198 ± 0.178	+0.006 ± 0.057	2.241 ± 0.176	2.85 ± 0.28	13.694 ± 0.178	
1995ac	49992.99 ± 0.40	36.511 ± 0.108	−0.231 ± 0.047	0.252 ± 0.107	3.1	17.007 ± 0.108	HF
1995ak	50021.16 ± 0.93	34.741 ± 0.138	+0.122 ± 0.065	0.613 ± 0.131	3.12 ± 0.39	15.237 ± 0.138	HF
1995al	50028.96 ± 0.44	32.714 ± 0.081	−0.282 ± 0.035	0.177 ± 0.065	3.1	13.209 ± 0.081	
1995bd	50086.31 ± 0.24	34.006 ± 0.125	−0.239 ± 0.051	0.523 ± 0.241	3.01 ± 0.35	14.502 ± 0.125	HF
1996C	50128.42 ± 0.90	35.947 ± 0.104	−0.104 ± 0.055	0.136 ± 0.091	3.1	16.443 ± 0.104	HF
1996X	50190.85 ± 0.33	32.432 ± 0.065	+0.095 ± 0.048	0.061 ± 0.044	3.1	12.927 ± 0.065	
1996Z	50215.24 ± 1.46	32.760 ± 0.238	+0.112 ± 0.210	0.609 ± 0.316	3.05 ± 0.36	13.256 ± 0.238	HF
1996ab	50224.69 ± 1.07	38.934 ± 0.146	+0.164 ± 0.127	0.098 ± 0.091	3.1	19.430 ± 0.146	HF
1996ai	50255.21 ± 0.81	31.151 ± 0.187	−0.098 ± 0.068	3.662 ± 0.185	2.09 ± 0.12	11.647 ± 0.187	
1996bk	50368.46 ± 1.02	32.195 ± 0.142	+1.011 ± 0.124	0.711 ± 0.184	3.10 ± 0.38	12.691 ± 0.142	
1996bl	50376.32 ± 0.58	36.096 ± 0.113	−0.116 ± 0.064	0.208 ± 0.115	3.1	16.592 ± 0.113	HF
1996bo	50386.93 ± 0.30	34.043 ± 0.138	+0.057 ± 0.070	0.938 ± 0.138	3.02 ± 0.35	14.538 ± 0.138	HF
1996bv	50403.72 ± 1.27	34.213 ± 0.157	−0.206 ± 0.065	0.547 ± 0.159	3.07 ± 0.37	14.709 ± 0.157	HF
1997E	50467.58 ± 0.41	34.105 ± 0.091	+0.341 ± 0.084	0.213 ± 0.104	3.1	14.600 ± 0.091	HF
1997Y	50486.88 ± 1.37	34.563 ± 0.104	+0.060 ± 0.078	0.196 ± 0.087	3.1	15.058 ± 0.104	HF
1997bp	50548.94 ± 0.52	32.895 ± 0.092	−0.180 ± 0.049	0.537 ± 0.086	2.88 ± 0.31	13.391 ± 0.092	HF
1997bq	50557.99 ± 0.18	33.458 ± 0.109	−0.095 ± 0.063	0.513 ± 0.095	3.03 ± 0.35	13.953 ± 0.109	HF
1997br	50559.26 ± 0.23	32.248 ± 0.104	−0.303 ± 0.031	0.804 ± 0.112	3.03 ± 0.35	12.743 ± 0.104	
1997cn	50586.64 ± 0.77	34.532 ± 0.070	+1.381 ± 0.046	0.071 ± 0.059	3.1	15.027 ± 0.070	HF
1997cw	50630.75 ± 0.98	34.075 ± 0.151	−0.179 ± 0.064	1.092 ± 0.145	2.97 ± 0.33	14.570 ± 0.151	HF
1997dg	50720.05 ± 0.84	36.149 ± 0.114	−0.006 ± 0.076	0.201 ± 0.102	3.1	16.645 ± 0.114	HF
1997do	50766.21 ± 0.45	33.601 ± 0.118	−0.146 ± 0.080	0.312 ± 0.102	3.1	14.097 ± 0.118	HF
1997dt	50785.60 ± 0.31	32.723 ± 0.191	−0.126 ± 0.070	1.849 ± 0.198	3.03 ± 0.34	13.219 ± 0.191	
1998D	50841.07 ± 2.02	34.089 ± 0.627	+0.571 ± 0.482	0.346 ± 0.186	3.1	14.585 ± 0.627	poor fit
1998V	50891.27 ± 0.84	34.395 ± 0.102	−0.055 ± 0.064	0.209 ± 0.115	3.1	14.891 ± 0.102	HF
1998ab	50914.43 ± 0.25	35.213 ± 0.100	−0.118 ± 0.051	0.394 ± 0.082	3.1	15.709 ± 0.100	HF
1998aq	50930.80 ± 0.13	31.974 ± 0.046	−0.063 ± 0.036	0.024 ± 0.019	3.1	12.470 ± 0.046	
1998bp	50936.39 ± 0.33	33.304 ± 0.075	+1.114 ± 0.057	0.188 ± 0.100	3.1	13.800 ± 0.075	HF
1998bu	50952.40 ± 0.23	30.283 ± 0.117	−0.015 ± 0.038	1.055 ± 0.114	3.13 ± 0.36	10.778 ± 0.117	
1998co	50987.76 ± 1.32	34.431 ± 0.126	+0.464 ± 0.196	0.301 ± 0.183	3.1	14.926 ± 0.126	HF
1998de	51026.69 ± 0.17	34.400 ± 0.082	+1.448 ± 0.036	0.398 ± 0.101	3.1	14.896 ± 0.082	HF
1998dh	51029.83 ± 0.22	32.846 ± 0.087	−0.051 ± 0.042	0.471 ± 0.061	2.76 ± 0.27	13.342 ± 0.087	
1998dk	51056.58 ± 1.48	33.802 ± 0.219	−0.127 ± 0.134	0.508 ± 0.152	3.10 ± 0.38	14.297 ± 0.219	HF
1998dm	51062.03 ± 1.16	33.067 ± 0.178	−0.192 ± 0.073	1.045 ± 0.160	3.08 ± 0.37	13.563 ± 0.178	
1998dx	51071.32 ± 0.80	36.917 ± 0.099	+0.190 ± 0.099	0.086 ± 0.065	3.1	17.413 ± 0.099	HF
1998ec	51088.41 ± 1.07	35.082 ± 0.161	−0.169 ± 0.077	0.569 ± 0.125	3.01 ± 0.35	15.578 ± 0.161	HF
1998ef	51113.99 ± 0.22	34.142 ± 0.105	+0.269 ± 0.083	0.046 ± 0.044	3.1	14.638 ± 0.105	HF
1998eg	51110.69 ± 1.23	35.353 ± 0.120	+0.014 ± 0.118	0.224 ± 0.118	3.1	15.849 ± 0.120	HF
1998es	51141.89 ± 0.15	33.263 ± 0.078	−0.287 ± 0.030	0.227 ± 0.073	3.1	13.758 ± 0.078	HF

6. Discussion

6.1. Hubble Flow Sample

Constructing a Hubble diagram of nearby SN Ia (Hubble 1929; Kirshner 2004) requires a Hubble flow sample, for which the measured recession velocities are dominated by the cosmological redshift (as opposed to peculiar motions). We consider objects with $cz \geq 2500$ km s^{-1} in the CMB rest-frame to be in the Hubble flow, yielding 101 objects out of our original 133. Additionally, we require good distances for these SN Ia, eliminating SN 2002cx which could not be fit by MLCS2k2. Similarly, we further cull the Hubble Flow sample to exclude objects whose first observation occurs more than 20 days past maximum light ($t_1 > 20$ d; see Table 1), eliminating two SN Ia (SN 1998D and SN 1999cw). Excessive host-galaxy extinction also leads to uncertain distances and we exclude objects with mean $A_V^0 > 2.0$ mag (another two objects: SN 1995E and SN 1999cl). We explore the consequences of this relatively permissive extinction cut below in §6.4.

We constructed a Hubble diagram of the 96 SN Ia that passed these cuts, and noticed a significant outlier: SN 1999ej in NGC 495 (Friedman, King, & Li 1999; $cz_{\rm CMB} = 3831$ km s^{-1}) gave a residual of ∼0.6 mag relative to the tight locus defined by the other objects. Spectroscopy of SN 1999ej showed it to be a normal SN Ia (Jha et al. 1999b) and the photometric data (Jha et al. 2006), though not plentiful with only 4 fit points each in *UBVRI* , nonetheless provide a good MLCS2k2 distance with no indication of peculiarity. The solution to this puzzle is that NGC 495 is in a particularly dense region of the group/poor cluster Zw 0107+3212 (whose brightest cluster galaxy is the nearby NGC 507). The cluster has a mean redshift $c\bar{z}_{\rm CMB} \simeq 4690$ km s^{-1} and estimated velocity dispersion σ ranging from 440–590 km s^{-1} (Ramella et al. 2002; Miller et al. 2002). Using this cluster mean redshift instead for SN 1999ej makes it fully consistent with the rest of the sample, suggesting the observed recession velocity of NGC 495 is strongly affected by its environment, but we have chosen simply to exclude SN 1999ej from the Hubble flow sample. From a NED search, we did not find any independent evidence for large peculiar velocities among the other Hubble flow objects.

Our final Hubble flow sample is the largest compiled to date for SN Ia in the nearby Universe with homogeneous distances. It consists of 95 SN Ia (denoted HF in Table 4), including 35 out of 44 of the objects presented by Jha et al. (2006), and more than doubles the MLCS Hubble flow sample of Jha et al. (1999a).

The Hubble diagram for this sample is shown in Figure 12, where we have fit for only one free parameter, the intercept.[13] This intercept is scale-dependent, but can be expressed several different

[13]We have adopted an $\Omega_{\rm M} = 0.3$, $\Omega_\Lambda = 0.7$ cosmology, which is significant for the more distant objects, and assumed a peculiar velocity uncertainty of ±300 km s^{-1}, important for the nearby objects. Including in quadrature the error floor (see §5) of $\sigma_{\rm add} = 0.08$ mag yields a reduced χ^2 of 1.06 for 94 degrees of freedom. This combination of

Table 4—Continued

SN Ia	$t_0 - 2400000$ HJD	$\mu_0 + 5 \log h_{65}$ mag	Δ	A_V^0 mag	R_V	m_V^0 mag	Notes
1999X	51203.48 ± 1.04	35.546 ± 0.132	−0.181 ± 0.075	0.139 ± 0.095	3.1	16.041 ± 0.132	HF
1999aa	51231.97 ± 0.15	34.468 ± 0.042	−0.271 ± 0.028	0.020 ± 0.018	3.1	14.963 ± 0.042	HF
1999ac	51250.60 ± 0.17	33.334 ± 0.081	−0.086 ± 0.039	0.308 ± 0.072	3.1	13.830 ± 0.081	HF
1999aw	51253.96 ± 0.29	36.551 ± 0.043	−0.369 ± 0.032	0.019 ± 0.018	3.1	17.047 ± 0.043	HF
1999by	51309.50 ± 0.14	31.158 ± 0.073	+1.348 ± 0.030	0.170 ± 0.083	3.1	11.653 ± 0.073	
1999cc	51315.62 ± 0.46	35.859 ± 0.092	+0.337 ± 0.097	0.148 ± 0.088	3.1	16.355 ± 0.092	HF
1999cl	51342.28 ± 0.26	30.604 ± 0.163	+0.031 ± 0.087	2.666 ± 0.160	2.22 ± 0.15	11.099 ± 0.163	
1999cp	51363.22 ± 0.26	33.520 ± 0.098	−0.103 ± 0.102	0.072 ± 0.062	3.1	14.015 ± 0.098	HF
1999cw	51352.49 ± 1.47	33.363 ± 0.141	−0.306 ± 0.067	0.161 ± 0.073	3.1	13.859 ± 0.141	poor fit
1999da	51370.57 ± 0.17	33.905 ± 0.101	+1.451 ± 0.038	0.233 ± 0.115	3.1	14.400 ± 0.101	HF
1999dk	51413.92 ± 0.78	34.273 ± 0.098	−0.233 ± 0.047	0.201 ± 0.094	3.1	14.769 ± 0.098	HF
1999dq	51435.70 ± 0.15	33.668 ± 0.067	−0.338 ± 0.024	0.369 ± 0.077	3.1	14.163 ± 0.067	HF
1999ee	51469.29 ± 0.14	33.472 ± 0.088	−0.208 ± 0.030	0.797 ± 0.085	2.76 ± 0.27	13.968 ± 0.088	HF
1999ef	51457.78 ± 1.27	36.657 ± 0.111	−0.057 ± 0.077	0.051 ± 0.044	3.1	17.153 ± 0.111	HF
1999ej	51482.37 ± 0.85	34.459 ± 0.123	+0.302 ± 0.088	0.166 ± 0.099	3.1	14.954 ± 0.123	
1999ek	51481.65 ± 0.50	34.360 ± 0.111	+0.050 ± 0.067	0.475 ± 0.251	3.1	14.856 ± 0.111	HF
1999gd	51518.40 ± 1.14	34.606 ± 0.167	+0.024 ± 0.073	1.381 ± 0.156	2.99 ± 0.33	15.101 ± 0.167	HF
1999gh	51513.53 ± 0.91	32.761 ± 0.078	+0.902 ± 0.081	0.084 ± 0.074	3.1	13.257 ± 0.078	HF
1999gp	51550.30 ± 0.17	35.622 ± 0.061	−0.323 ± 0.030	0.076 ± 0.051	3.1	16.118 ± 0.061	HF
2000B	51562.85 ± 1.30	34.628 ± 0.216	+0.253 ± 0.190	0.286 ± 0.136	3.1	15.123 ± 0.216	HF
2000E	51576.80 ± 0.35	31.721 ± 0.107	−0.277 ± 0.039	0.609 ± 0.189	3.01 ± 0.35	12.216 ± 0.107	
2000bh	51636.31 ± 1.47	35.309 ± 0.131	−0.026 ± 0.067	0.138 ± 0.093	3.1	15.805 ± 0.131	HF
2000bk	51646.02 ± 1.08	35.390 ± 0.156	+0.613 ± 0.129	0.290 ± 0.148	3.1	15.885 ± 0.156	HF
2000ca	51666.12 ± 0.46	35.250 ± 0.060	−0.125 ± 0.048	0.030 ± 0.024	3.1	15.746 ± 0.060	HF
2000ce	51667.45 ± 1.01	34.376 ± 0.179	−0.149 ± 0.060	1.761 ± 0.179	2.91 ± 0.30	14.872 ± 0.179	HF
2000cf	51672.33 ± 0.83	36.382 ± 0.104	−0.006 ± 0.065	0.194 ± 0.097	3.1	16.878 ± 0.104	HF
2000cn	51707.83 ± 0.16	35.153 ± 0.086	+0.716 ± 0.076	0.171 ± 0.109	3.1	15.648 ± 0.086	HF
2000cx	···	···	···	···	···	···	bad fit
2000dk	51812.47 ± 0.28	34.408 ± 0.077	+0.578 ± 0.067	0.033 ± 0.032	3.1	14.904 ± 0.077	HF
2000fa	51892.25 ± 0.57	35.121 ± 0.128	−0.126 ± 0.061	0.283 ± 0.105	3.1	15.616 ± 0.128	HF
2001V	51973.28 ± 0.16	34.187 ± 0.065	−0.280 ± 0.032	0.092 ± 0.052	3.1	14.683 ± 0.065	HF
2001ay	52023.96 ± 0.78	35.926 ± 0.102	−0.405 ± 0.045	0.374 ± 0.098	3.1	16.422 ± 0.102	HF
2001ba	52034.18 ± 0.54	35.889 ± 0.075	−0.093 ± 0.056	0.041 ± 0.037	3.1	16.385 ± 0.075	HF
2001bt	52063.91 ± 0.21	33.952 ± 0.114	+0.071 ± 0.052	0.616 ± 0.111	3.00 ± 0.35	14.447 ± 0.114	HF
2001cn	52071.10 ± 0.74	34.130 ± 0.106	+0.007 ± 0.052	0.447 ± 0.100	3.1	14.625 ± 0.106	HF
2001cz	52103.89 ± 0.31	34.294 ± 0.111	−0.078 ± 0.054	0.254 ± 0.116	3.1	14.790 ± 0.111	HF
2001el	52182.55 ± 0.20	31.544 ± 0.077	−0.193 ± 0.032	0.696 ± 0.059	2.40 ± 0.19	12.040 ± 0.077	
2002bf	52337.87 ± 0.50	35.480 ± 0.134	−0.111 ± 0.065	0.254 ± 0.131	3.1	15.975 ± 0.134	HF
2002bo	52356.89 ± 0.14	31.945 ± 0.105	−0.048 ± 0.041	1.212 ± 0.099	2.57 ± 0.22	12.441 ± 0.105	
2002cx	···	···	···	···	···	···	bad fit
2002er	52524.84 ± 0.15	33.034 ± 0.085	+0.170 ± 0.057	0.470 ± 0.112	3.1	13.530 ± 0.085	HF
2003du	52765.62 ± 0.50	33.189 ± 0.049	−0.247 ± 0.028	0.037 ± 0.026	3.1	13.685 ± 0.049	

Note. — Values listed are means and standard deviations for each of the parameters, as determined from their one-dimensional probability distributions marginalized over the other parameters. We use the standard notation $h_{65} \equiv H_0/(65 \text{ km s}^{-1} \text{ Mpc}^{-1})$. The extinction parameters A_V^0 and R_V correspond to host-galaxy extinction only; Galactic reddening is listed in Table 1. The corrected apparent peak magnitude m_V^0 differs from the distance modulus μ_0 by an additive constant, $m_V^0 \equiv \mu_0 + M_V^0$.

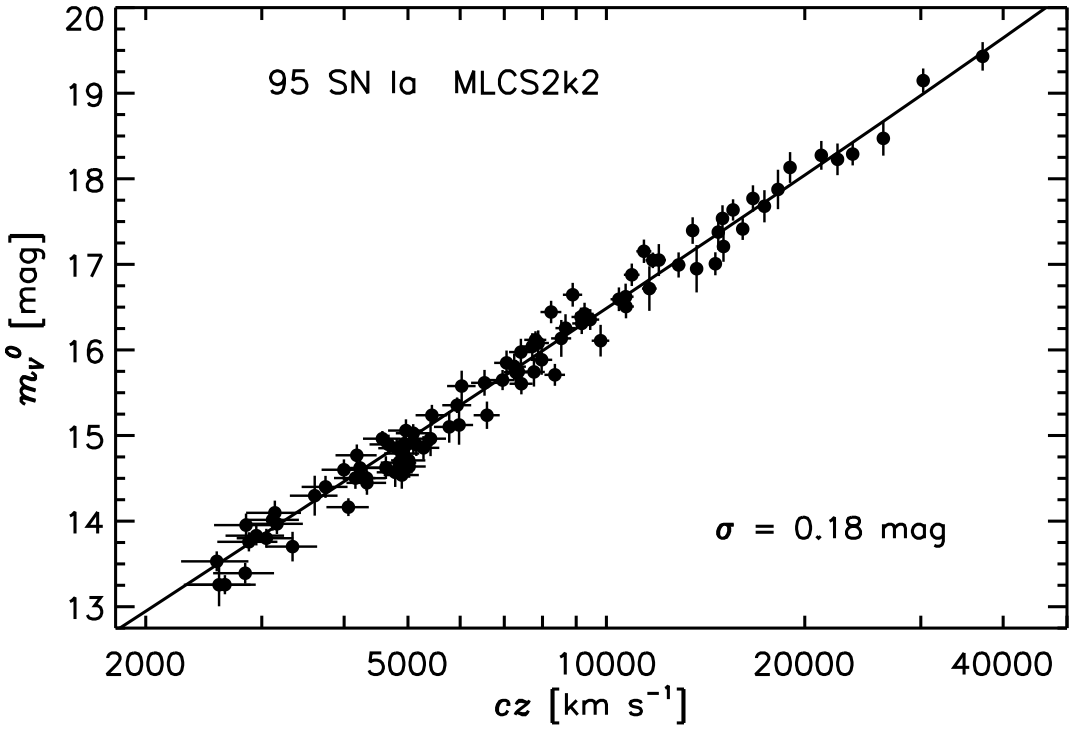

Fig. 12.— Apparent magnitude-redshift relation for our Hubble flow sample of 95 SN Ia, using MLCS2k2 to correct for host-galaxy extinction and intrinsic luminosity differences, and redshifts in the CMB frame. The shape of the solid-line is fixed by the inverse-square law and (for high *cz*) the adopted $\Omega_M = 0.3$, $\Omega_\Lambda = 0.7$ cosmology; the intercept is the only free parameter and it is determined to ±0.018 mag.

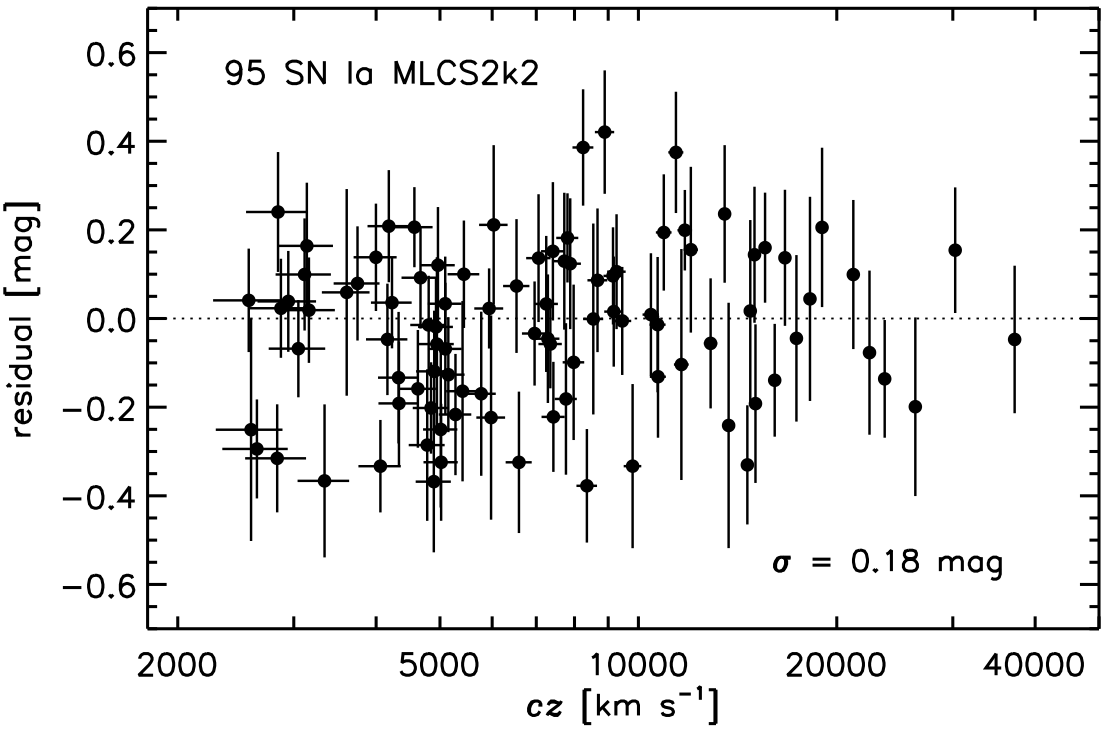

Fig. 13.— Magnitude residuals of the Hubble flow sample after MLCS2k2 correction, relative to the best-fit Hubble line shown in Figure 12.

ways. One relates it to the absolute magnitude of the fiducial SN Ia, and provides the derivation for the zeropoint in equation 7 (which in turn defines the relation between μ_0 and m_V^0):

$$M_V^0 - 5\log H_0 = m_V^0 - 25 - 5\log\left(c\,(1+z)\int_0^z \left[\Omega_{\rm M}\,(1+z')^3 + \Omega_\Lambda\right]^{-1/2} dz'\right), \tag{8}$$

valid for a flat, $\Omega_{\rm M} + \Omega_\Lambda = 1$ Universe. The weighted fit to the full Hubble flow sample gives $M_V^0 - 5\log h_{65} = -19.504 \pm 0.018$ mag (statistical uncertainty only). Alternately we can follow the notation of Jha et al. (1999a) and calculate the "intercept of the ridge line," a_V, defined as[14]

$$a_V = \log\left(c\,(1+z)\int_0^z \left[\Omega_{\rm M}\,(1+z')^3 + \Omega_\Lambda\right]^{-1/2} dz'\right) - 0.2m_V^0, \tag{9}$$

again assuming an $\Omega_{\rm M} + \Omega_\Lambda = 1$ Universe. The full Hubble flow sample gives a best-fit value and formal uncertainty of $a_V = 0.7139 \pm 0.0037$. Unfortunately we cannot directly compare these intermediate results with the values given by Jha et al. (1999a), because MLCS2k2 uses new template vectors with new magnitude and Δ zeropoints, which uniformly shifts all distances, a_V, and M_V^0.

The scatter about the Hubble line in Figures 12 and 13 is $\sigma = 0.18$ mag (~8% in distance). Part of the scatter in the Hubble diagram comes from our inexact knowledge of cosmological redshifts because of galactic peculiar velocities. Our estimate of the peculiar velocity uncertainty of $\pm$ 300 km s^{-1} corresponds to an uncertainty of 0.26 mag for the nearest objects in the Hubble flow sample ($cz \simeq 2500$ km s^{-1}), which drops to under 0.02 mag for the most distant object ($cz = 37239$ km s^{-1}). The mean peculiar velocity uncertainty for the full sample is 0.11 mag[15], and subtracting this in quadrature from the overall dispersion implies that the *intrinsic* dispersion in SN Ia distances is at most 0.14 mag ($\lesssim$ 7% in distance) for samples similar to the one presented here.

Our Hubble flow sample is the largest ever fit self-consistently with one technique, and comprises data from diverse sources. In addition, we have attempted to limit the number of objects rejected from the sample. We believe the measured dispersion is more reflective of the true dispersion among SN Ia as they are currently being observed. Further restricting samples to the best objects (e.g., those with low reddening or close to fiducial luminosity/light-curve shape) clearly

---

the peculiar velocity uncertainty and $\sigma_{\rm add}$ results in a good fit across the whole Hubble flow sample as well as selected subsamples.

[14]In Jha et al. (1999a) the intercept of the ridge line was given as $a_V = \log cz - 0.2m_V^0$. Here we explicitly show the dependence on cosmological parameters.

[15]Because of the inverse dependence on the redshift, this is not the same as the peculiar velocity uncertainty at the mean redshift, $c\bar{z}_{\rm CMB} = 8796$ km s^{-1}, where $\pm$300 km s^{-1} corresponds to $\pm$0.07 mag.

provides an avenue to reducing the dispersion, but it is important that these restrictions be carefully defined to avoid biasing applications of these samples to measuring cosmological parameters such as H_0, Ω_Λ, or w. For example, Guy et al. (2005) show that the quoted dispersion of 0.08 mag and 0.07 mag for the color-selected samples presented by Wang et al. (2003) and Wang et al. (2005), respectively, increase to 0.15 mag and 0.18 mag, when less stringent color cuts are applied. Comparison of MLCS2k2 to other SN Ia distance-fitting techniques based on the scatter in respective Hubble diagrams requires supernova samples that are comparable (and ideally identical) in size and scope.

We display the distribution of the Hubble flow residuals versus the measured Δ and A_V^0 in Figure 14. No obvious trends are present, though the scatter of the points decreases with increasing Δ, meaning the lower luminosity SN Ia have a tighter correlation around the luminosity/light-curve shape relationship. If we arbitrarily divide the sample into three bins, with slow decliners ($\Delta < -0.15$), normal SN Ia ($-0.15 \leq \Delta \leq 0.3$), and fast decliners ($\Delta > 0.3$), the residual dispersions are $\sigma = 0.21$ mag ($N = 17$ objects), 0.18 mag ($N = 57$), and 0.14 mag ($N = 21$), respectively.

In Figure 15 we show correlations in the MLCS2k2 fit parameters (Δ and A_V^0), as well as the residuals in the Hubble flow sample, with host-galaxy morphological type and projected separation. These confirm well-known trends for SN Ia (e.g., Hamuy et al. 2000, and references therein): slow-declining (low Δ, high luminosity) SN Ia and heavily extinguished SN Ia are not generally found in early-type galaxies or in the outskirts of their hosts. Note there are some exceptions, such as SN 1990Y, 1991bg, and 1993ac, all fit with mean $A_V^0 \geq 0.3$ mag in elliptical hosts (though in the case of the very subluminous SN 1991bg, there is a significant correlation between Δ and A_V^0). The lower panels of Figure 15 show the residuals after MLCS2k2 calibration of the Hubble flow sample; note the large reduction in the vertical scale, showing the efficacy of corrections for intrinsic luminosity differences and extinction. The Hubble flow SN Ia do not show any trend in their residuals with respect to host galaxy morphology or projected galactocentric distance, though perhaps the residual scatter is decreased at large separations. There is also a hint that SN Ia in elliptical hosts have slightly negative residuals after MLCS2k2 correction (meaning they are corrected to be too bright/too nearby); however the weighted average residual is only -0.06 ± 0.06 mag, consistent with zero. Grouping together E and E/S0 hosts (which show a similar paucity of slowly-declining SN Ia in the upper left panel) yields a weighted mean residual of -0.02 ± 0.04 mag. The observed scatter in the residuals of the early-type hosts is less than the overall sample, with $\sigma = 0.11$ mag for elliptical hosts only, and $\sigma = 0.13$ mag for E, E/S0, and S0 hosts; a large fraction of this scatter may be from peculiar velocities, which should contribute $\sim$0.09 mag to the dispersion for these galaxies.

Gallagher et al. (2005) have approached these issues in more detail, with integrated spectra of the host galaxies of many of these SN Ia, allowing them to correlate SN properties (before and after MLCS2k2 correction) with additional parameters such as host metallicity, star formation rate,

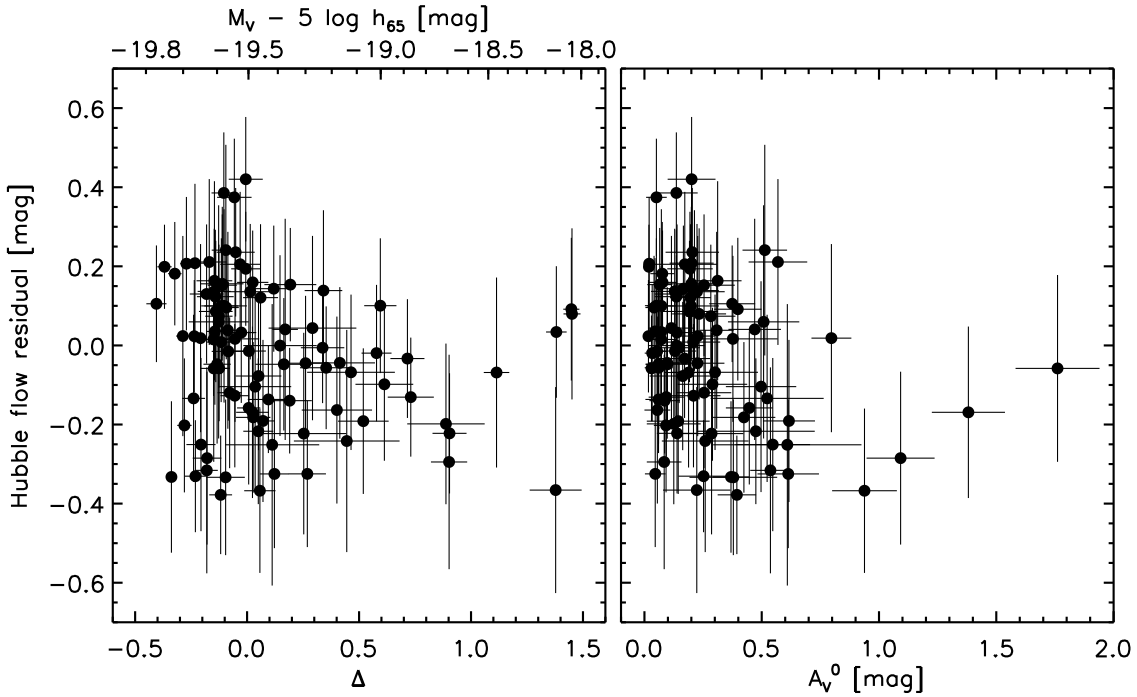

Fig. 14.— MLCS2k2 Hubble flow sample residuals versus mean values of the light-curve shape parameter Δ and host-galaxy extinction A_V^0. The conversion from Δ to the peak V absolute magnitude, given on the top axis of the left panel, is based on equation 7.

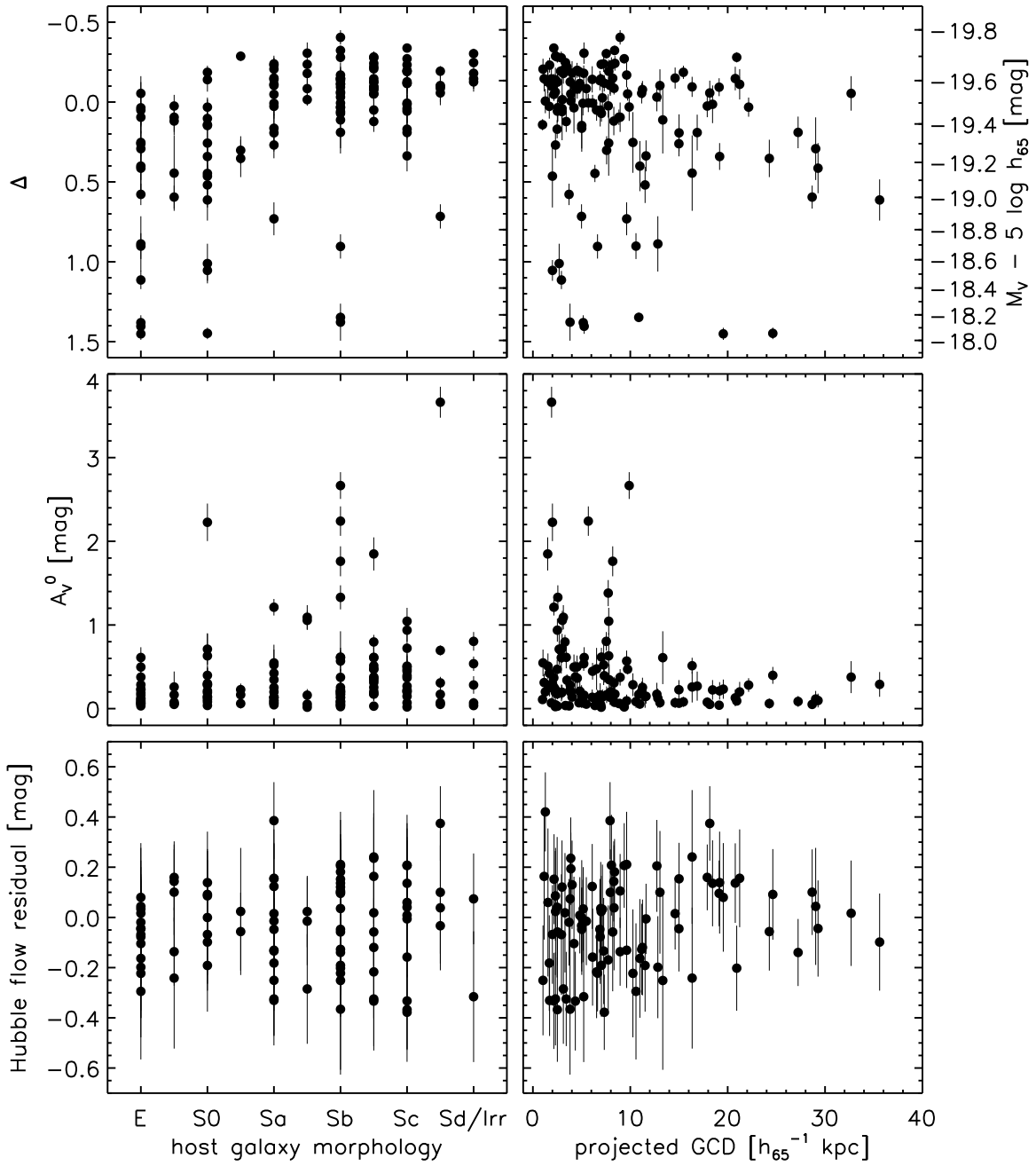

Fig. 15.— Correlations with host-galaxy morphology and projected galactocentric distance (GCD). The top panels show mean values of the light-curve shape parameter Δ for the full sample, and the middle panels show the distribution of host-galaxy extinction A_V^0. The bottom panels show the residuals relative to the best fit Hubble line for the Hubble flow sample only (after MLCS2k2 correction for luminosity differences and extinction). Projected GCDs are calculated using the angular offsets presented in Table 1, with angular diameter distances ($\Omega_M = 0.3$, $\Omega_\Lambda = 0.7$) calculated from the redshift for objects with $cz_{CMB} \geq 2500$ km s^{-1} and from the MLCS2k2 supernova distances for objects with lower recession velocities.

and star formation history. Their results suggest no clear correlations with the MLCS2k2 Hubble flow residuals, though there is marginal evidence for a relation between the residuals and host metallicity.

6.2. A Hubble Bubble?

Zehavi et al. (1998) presented evidence for a large local void based on SN Ia distances which suggested a monopole in the peculiar velocity field. They found that the Hubble constant estimated from SN Ia within 70 h^{-1} Mpc was 6.5% ± 2.2% higher than H_0 measured from SN Ia outside this region, assuming a flat $\Omega_M = 1$ Universe. The significance of this void decreases in the current concordance cosmology ($\Omega_M = 0.3$, $\Omega_\Lambda = 0.7$) to 4.5% ± 2.1%, but it is still worthwhile to test whether the larger SN Ia sample and updated distances presented here provide evidence for or against a void.

Following Zehavi et al. (1998), it is convenient to work with the supernova distances in units of km s^{-1}, making them independent of the distance scale. The ambiguity in the zeropoint of the Hubble diagram disappears if we use the quantity $H_0 d_{SN}$, which can be calculated

$$H_0 d_{SN} = 65 \left[10^{0.2(\mu_{65}-25)}\right] \quad \text{km s}^{-1}, \tag{10}$$

where we define $\mu_{65} \equiv \mu_0 + 5 \log h_{65}$, tabulated in the third column of Table 4. These can be compared to scale-independent luminosity distances: for an object at a cosmological redshift z in a flat Universe,

$$H_0 d_L(z) = c\,(1+z) \int_0^z \left[\Omega_M\,(1+z')^3 + \Omega_\Lambda\right]^{-1/2} dz', \tag{11}$$

and the difference $u = H_0 d_L(z) - H_0 d_{SN}$ is the host galaxy peculiar velocity. The deviation from the Hubble law is given by $\delta H/H = u/H_0 d_{SN}$.

The top panel of Figure 16 shows $\delta H/H$ for the 95 SN Ia in the full Hubble flow sample, where we have used our standard assumptions: a peculiar velocity uncertainty of ±300 km s^{-1}, $\sigma_{add} = 0.08$ mag, and a $\Omega_M = 0.3$, $\Omega_\Lambda = 0.7$ cosmology. We then partition the full sample into two parts at each value of $H_0 d_{SN}$ (such that there are at least six objects in the smaller subset) and calculate the best-fit Hubble constants H_{inner} and H_{outer}, and their corresponding uncertainties (see equations 2 and 3 of Zehavi et al. 1998). We define the void amplitude, $\delta_H \equiv (H_{inner} - H_{outer})/H_{outer}$, and display this quantity, with its uncertainty, as a function of the partition radius in the middle panel of Figure 16. We normalize δ_H by its uncertainty in the lower panel to illustrate the void significance.

The full Hubble flow sample clearly shows a void signature; the most significant void is derived when the sample is partitioned at $H_0 d_{SN} \simeq 7400$ km s^{-1} (between SN 2000ca and SN

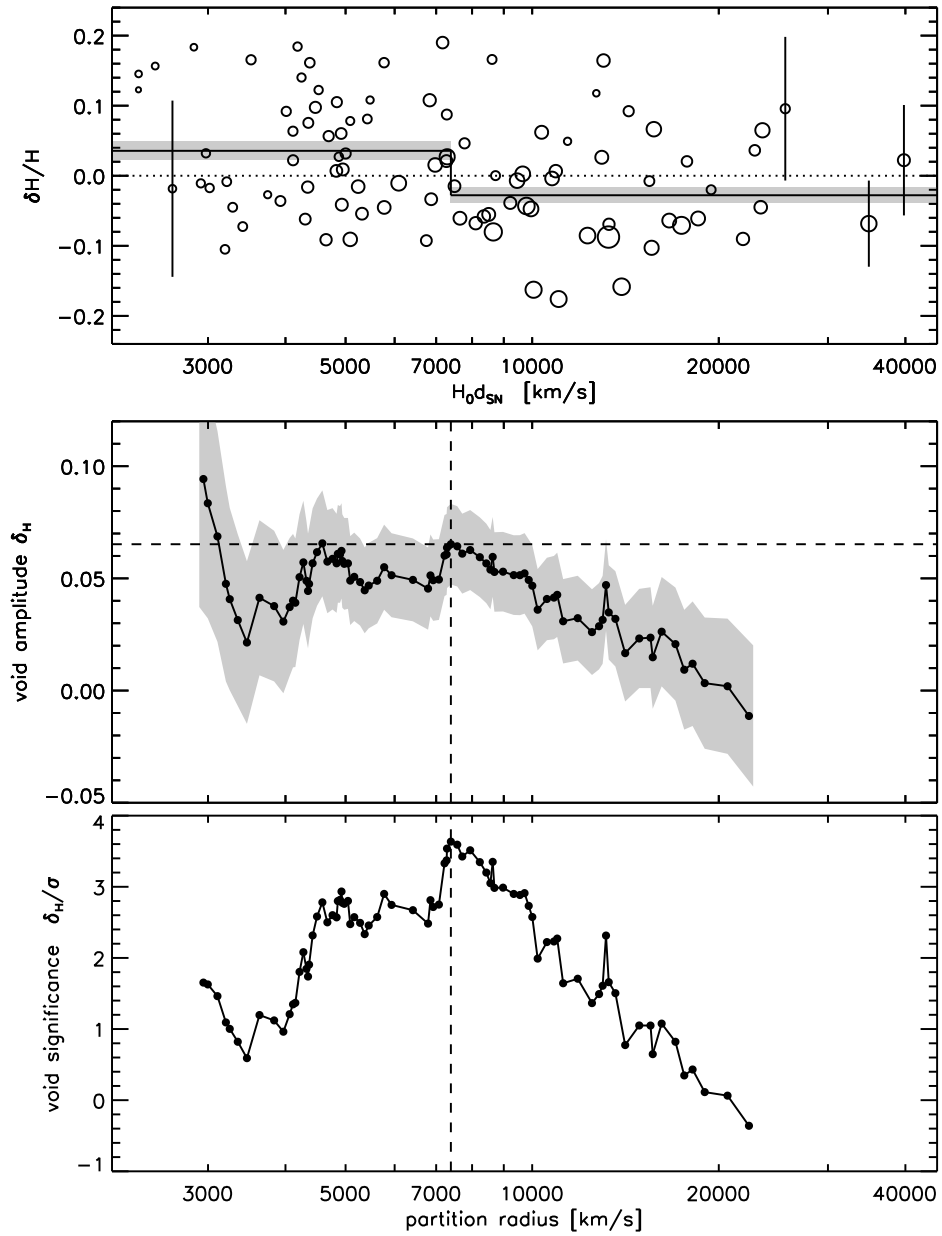

Fig. 16.— Indications of a local void. The top panel shows the deviation from the Hubble law for each object in the full Hubble flow sample. The radius of each circle is inversely proportional to the uncertainty, with several representative points showing the error bars explicitly to calibrate the symbol size. The solid line shows the best-fit Hubble constants in the two-zone model with the most significant void; the shaded regions give the 1-σ uncertainty on each of these values. The middle panel shows the void amplitude, $\delta_H \equiv H_{\rm inner}/H_{\rm outer} - 1$, as a function of the radius at which the sample is partitioned, with the shaded region illustrating the 1-σ uncertainty. The lower panel shows the significance of the void, i.e. the void amplitude divided by its uncertainty. The most significant void occurs when the sample is partitioned at $H_0 d_{\rm SN} \simeq 7400$ km s^{-1}, with $\delta_H = 6.5 \pm 1.8\%$.

2000bh at $H_0 d_{\rm SN} = 7293$ and 7494 km s^{-1}, respectively), with $\delta_H = 6.5 \pm 1.8\%$, similar in both location and amplitude to the Zehavi et al. (1998) result. We have performed a number of statistical tests to assess the significance of the result. We created 3×10^5 Monte Carlo realizations of the data set with Hubble law deviations drawn from a Gaussian distribution with a standard deviation equal to the uncertainty in each data point, and fit for the most significant void or overdensity at each partition radius. Only 0.2% of the time was there a void as significant as the one seen in the actual data (at any location). Because this result depends upon our assumed error distribution, we also created synthetic data sets with the Hubble law deviations randomly resampled from the deviations in the full data set (both with and without resampling of their errors). We have also performed a full bootstrap resampling analysis to determine the distribution of the void amplitude and significance around their best fit values. In all of these tests a void with the significance as in the actual data was seen at most 1.2% of the time, and typically much less often, depending on the details of the synthetic sample, suggesting the result is valid at the 2.5 to 3.5-σ level of confidence.

The result also seems robust to jackknife tests; eliminating any one, two, or even three points from the sample does not result in a very large change in the void characteristics. With the three largest outliers removed (without justification; these objects which are not peculiar in any way), the void amplitude only decreases to $5.2 \pm 1.8\%$. We have also confirmed that the result persists using the 51 SN Ia from 1997 onwards only, an independent sample from Zehavi et al. (1998). The newer data show an even stronger result, $\delta_H = 9.1 \pm 2.6\%$ (at the same location), but there are only a handful of recent SN Ia more distant than 10,000 km s^{-1} and the most robust results come from the full sample. Indications of this void can also be seen in other distance estimates to SN Ia (though with largely overlapping samples), including the "gold" sample of Riess et al. (2004), which used a slightly earlier implementation of MLCS2k2 (Jha 2002), and Δm_{15} distances presented by Prieto, Rest, & Suntzeff (2006), suggesting it is not an artifact limited to our particular analysis.

The significance of the void at 7400 km s^{-1} is high partly because it is near the middle of the sample, such that $H_{\rm inner}$ and $H_{\rm outer}$ (and thus, their ratio) are most precisely measured. The data suggest that void of similar amplitude may be present if the sample is partitioned near $H_0 d_{\rm SN} \simeq 4800$ km s^{-1}. Indeed, if we attempt to fit a three-zone model, the data support a model with $\delta_H \simeq 8\%$ closer than 4600 km s^{-1}, and $\delta_H \simeq 5\%$ for 4600 km s^{-1} $\lesssim H_0 d_{\rm SN} \lesssim$ 7400 km s^{-1}, both relative to the outer region beyond 7400 km s^{-1}. However, another three-zone scenario with nearly the same likelihood has $\delta_H \simeq 5\%$ nearer than 7400 km s^{-1}, and an *overdense* region with $\delta_H \simeq -2\%$ at 7400 km s^{-1} $\lesssim H_0 d_{\rm SN} \lesssim$ 14000 km s^{-1} relative to the more distant Hubble flow, which is similar to the three-zone infall region model seen by Zehavi et al. (1998). Because there are fewer points in each region, the uncertainties in these numbers are increased to $\sim$2.5%. Moreover, the data do not favor a three zone model over a two zone model (a χ^2 decrease of less than 1 per new model parameter), unlike the situation for a two zone model over a one zone model (a χ^2 decrease of more than 7 per new parameter).

While it seems likely this void signature is present in the SN data, is it really present in the Universe? The void boundary does occur at a distance comparable to large mass concentrations in the local Universe, including the Great Wall and the Southern Wall (Geller 1997 and references therein). A void with $\delta_H = 6.5\%$ on this scale would imply an underdensity $\delta\rho/\rho \simeq 20$ to 40% for $\Omega_M = 0.3$, depending on our location within the void (Lahav et al. 1991; Turner, Cen, & Ostriker 1992). Such a large-scale density contrast, while not ruled out, is relatively unlikely in current ΛCDM models; the fraction of mass residing in such a void ranges from 10^{-4} to a few percent, depending on the exact size and underdensity (Furlanetto & Piran 2006). Furthermore, tests of the Hubble bubble using other distance measures have not corroborated the SN Ia result. Using Tully-Fisher distances to galaxy clusters, Giovanelli et al. (1999) find $\delta_H = 1.0 \pm 2.2\%$ at 7000 km s^{-1}, while Hudson et al. (2004) derive $\delta_H = 2.3 \pm 1.9\%$ via Fundamental Plane cluster distances, both consistent with no void. Each method is subject to various systematic effects that could lead to spurious results. For the SN, these include K-corrections (but which are unlikely to cause a ∼0.1 mag error at $z \simeq 0.03$), the effect of higher-order multipoles on the monopole signature (but the sky distribution of the Hubble flow objects generally shows the void in all directions), or a possible photometric offset between the Calán/Tololo sample (accounting for most of the more distant objects) and more recent samples such as CfA I and II (making up most of the more nearby objects; Prieto, Rest, & Suntzeff 2006). More data (throughout the nearby redshift range, $z \lesssim 0.15$) and a more thorough analysis are needed to definitively resolve this open issue.

Regardless of whether the Hubble bubble is due to a real local void in the Universe or an artifact of SN Ia distances, the feature is present in the Hubble flow SN sample, and this has important implications for using SN Ia as tools for precision cosmology.[16] The Hubble flow sample is critical to both measurements of H_0 (a differential measurement between the Hubble flow objects and nearby Cepheid-calibrated SN Ia) and Ω_Λ or w (a differential measurement between the Hubble flow objects and high-redshift SN Ia), and both applications are affected by this result. The effect on H_0 is readily apparent; our derived H_0 will be 6.5% higher using a Hubble flow sample with $H_0 d_{SN} \lesssim 7400$ km s^{-1} compared to a Hubble flow sample with $H_0 d_{SN} \gtrsim 7400$ km s^{-1}. This is mitigated if we use the full Hubble flow sample, but that still yields a small but not insignificant effect: the full sample H_0 is larger by 3% compared to just the subsample beyond 7400 km s^{-1} (which gives an intercept of the ridge line, $a_V = 0.7015 \pm 0.0049$).

For high-redshift applications, the void signature can be much more important. Whereas the choice of using the full Hubble flow sample or one just with objects beyond the void region (with $z \gtrsim 0.025$) does not significantly affect the conclusion from SN Ia that we live in an accelerating

[16]This is not to say the reason for the discrepancy is not important. If the SN Ia are revealing a true void, one would presumably proceed to measure the global Hubble constant and other cosmological parameters simply using a Hubble flow sample beyond the void region (with $z \gtrsim 0.025$; Riess et al. 2004). However, if the indications for a void are due to an unknown systematic error, the effects on the cosmological utility of SN Ia could be much more severe.

Universe (Riess et al. 2004), such a choice has a large effect in current efforts to measure the equation of state of the dark energy. In Figure 17 we show constraints on w from a simulation in which the current Hubble flow sample is used in conjunction with an artificial data set of 200 SN Ia with $0.3 \leq z \leq 0.8$, as expected from the ongoing ESSENCE survey (Miknaitis et al. 2007). The results show a ∼20% difference in the derived value of w using the full Hubble flow sample compared to one only including objects with $H_0 d_{\rm SN} \geq 8000$ km s^{-1} — twice the target statistical uncertainty of the survey. For future surveys with thousands of high redshift SN Ia, this single systematic uncertainty in the Hubble flow sample could easily dwarf all other sources of uncertainty combined. Clearly, then, precision cosmology with SN Ia will require an investment in *nearby* SN Ia (both in data and analysis) comparable to the immense efforts ongoing and envisioned at high redshift.

6.3. The Local Group Motion

The precision of SN Ia distances makes them well suited to measure peculiar velocities of nearby galaxies (e.g., Riess, Press, & Kirshner 1995b). Many new SN Ia are being discovered at redshifts conducive to studying the local flow field ($z \lesssim 0.03$). In Figure 18, we show a clear detection of the motion of the Local Group relative to the frame defined by nearby SN Ia. We plot the host galaxy peculiar velocities (in the Local Group frame, $u_{\rm LG} = H_0 d_{\rm L}(z_{\rm LG}) - H_0 d_{\rm SN}$) of 69 SN Ia with 1500 km s^{-1} $\leq H_0 d_{\rm SN} \leq$ 7500 km s^{-1} in Galactic coordinates (excluding the cluster member SN 1999ej and SN 2000cx which could not be fit by MLCS2k2). The distance range was chosen to exclude Virgo cluster galaxies at the lower end, and be within the void signature discussed above at the upper end (so that monopole deviations are minimized, in addition to excluding objects with increasingly uncertain absolute peculiar velocities).

A dipole signature is clearly present in the data; a simple (naive) dipole fit to these SN data indicates the Local Group is moving at 541 ± 75 km s^{-1} towards $(l, b) = (258^\circ \pm 18^\circ, +51^\circ \pm 12^\circ)$. This is consistent with the position and amplitude of the CMB dipole, 635 km s^{-1} towards (269°, +28°), at approximately the 2-σ confidence level. In addition, the paucity of SN Ia discovered at low Galactic latitude skews the best fit dipole away from the Galactic plane, suggesting that the SN Ia peculiar velocities are providing evidence for convergence of the local flow field to the CMB dipole at roughly the depths probed by these objects.

The full MLCS2k2 sample is quite amenable to more sophisticated analysis of the flow field (Riess et al. 1997b), such as recently performed by Radburn-Smith, Lucey, & Hudson (2004), who constrained $\beta \equiv \Omega_{\rm M}^{0.6}/b = 0.55 \pm 0.06$ comparing the nearby SN sample of Tonry et al. (2003) with the IRAS PSCz galaxy survey (Saunders et al. 2000). The ever-increasing nearby SN sample should also allow for merging and extension of elaborate local flow models, for example, such as provided by surface-brightness fluctuation distances (Tonry et al. 2000). For maximum utility, we strongly encourage nearby SN discovery efforts in the southern hemisphere (which would help fill

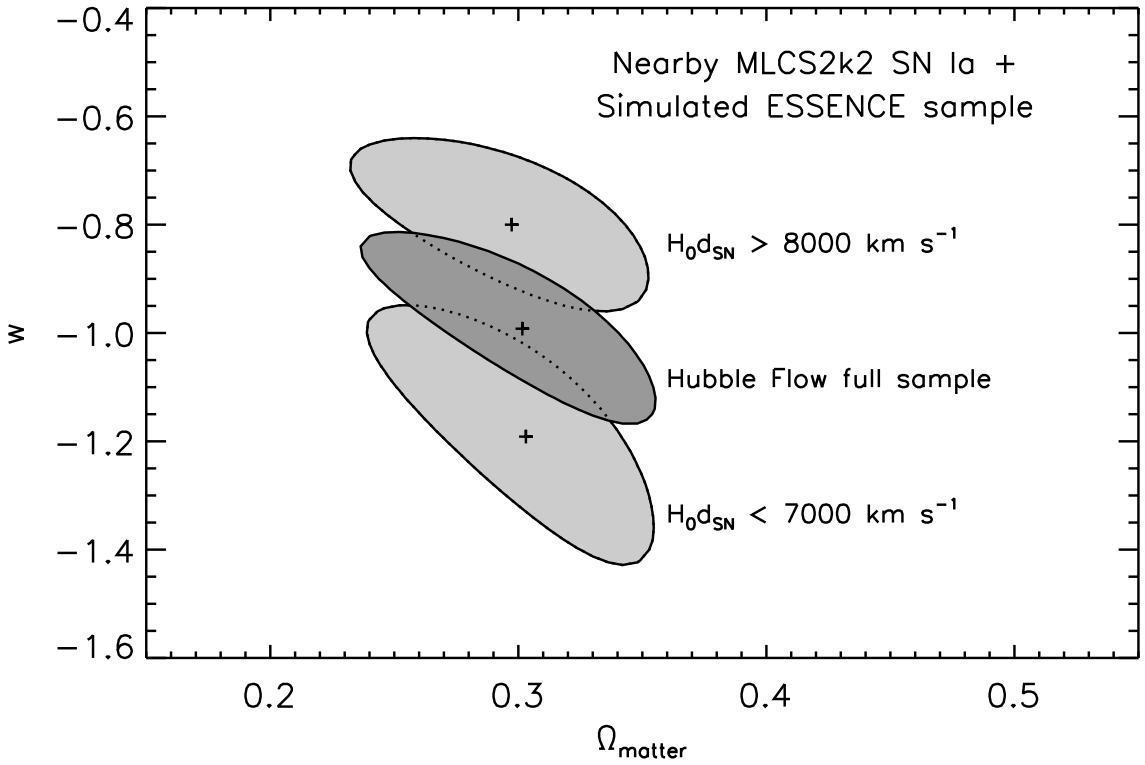

Fig. 17.— Effect of a local void on constraints of the dark energy equation of state, using a simulated sample of 200 SN Ia with $0.3 \leq z \leq 0.8$ as expected from the ESSENCE survey (Miknaitis et al. 2007). We perform a cosmological fit using the same simulated high-redshift sample plus three nearby samples: (1) the full MLCS2k2 Hubble flow sample with 95 SN Ia, (2) the nearby Hubble flow objects with $H_0 d_{\rm SN} < 7000$ km s^{-1} (48 SN Ia) and (3) the distant Hubble flow objects with $H_0 d_{\rm SN} > 8000$ km s^{-1} (40 SN Ia). The figure shows 68.3% (1-σ) confidence regions (shaded), and the mean values of $\Omega_{\rm M}$ and w (crosses). The input cosmology for the simulated objects is $\Omega_{\rm M} = 0.3$, $\Omega_\Lambda = 0.7$ ($w = -1$), with the distance scale set by the full Hubble flow sample. In the cosmological fit, we assume a flat Universe and a prior on $\Omega_{\rm M} = 0.30 \pm 0.04$. The different low-redshift samples have a strong effect on the estimation of w, with $w = -0.99 \pm 0.12$ for the full Hubble flow sample, $w = -1.19 \pm 0.17$ for the nearby Hubble flow sample and $w = -0.80 \pm 0.11$ for the distant Hubble flow sample.

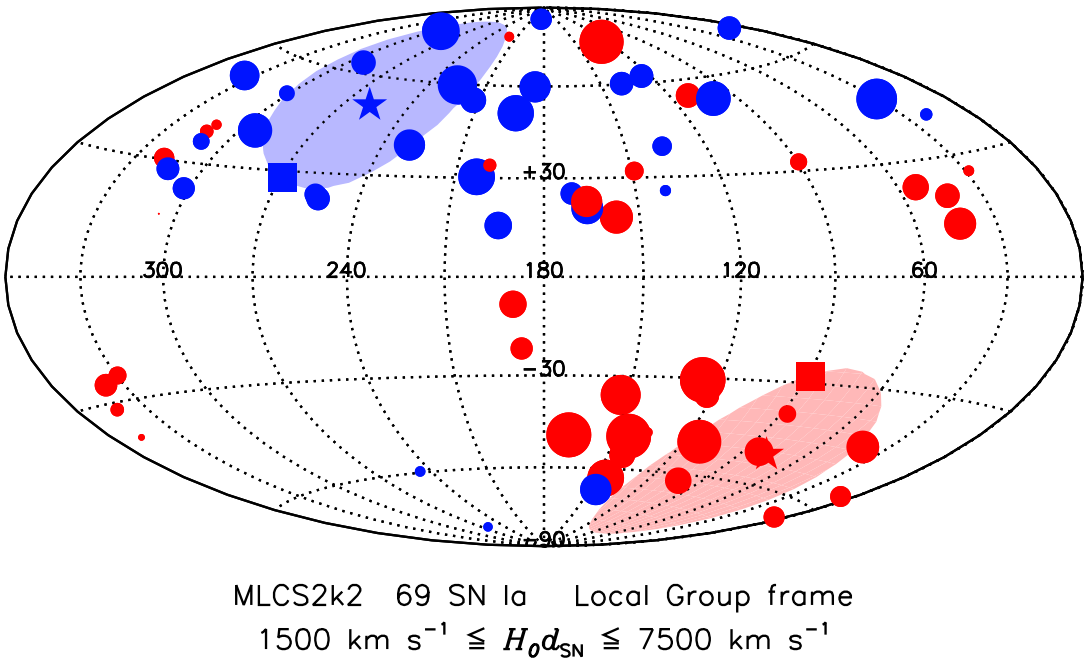

Fig. 18.— Peculiar velocities of 69 SN Ia with 1500 km s^{-1} $\leq H_0 d_{\rm SN} \leq$ 7500 km s^{-1} in the rest-frame of the Local Group, plotted in Galactic coordinates (with central meridian $\ell = 180°$). The blue circles indicate SN Ia in galaxies with negative peculiar velocities (i.e., approaching us relative to the cosmic expansion). The red circles indicate positive peculiar velocities, objects from which we are moving away. The area of the symbols is proportional to the amplitude of the peculiar velocity. The squares mark the location of the CMB dipole (Fixsen et al. 1996) and are drawn to scale relative to the circles, with the Local Group moving towards (269°, +28°) at 635 km s^{-1}. The stars show the position and amplitude of the best-fit simple dipole model to the SN data, with the shaded area indicating locations within the formal 2-σ confidence region.

the empty region in the lower right quadrant of Figure 18).

6.4. Extragalactic Extinction Laws

Extinguished SN Ia, though less than ideal distance indicators, nevertheless provide one of the few ways to constrain the extinction law along individual lines of sight through distant galaxies (see also e.g., Muñoz et al. 2004, but note McGough et al. 2005). The traditional method of using SN Ia to determine the extinction and reddening properties of extragalactic dust (typically parameterized by R_V) has been to plot the magnitude residuals (assuming a relative distance, such as from the Hubble law) in a given passband and epoch (for example, in B or V at maximum light) versus the SN color at some epoch (for instance, $B-V$ also at maximum light). Because SN Ia are not perfect standard candles, this simple method fails: the magnitude residuals and the intrinsic colors are both functions of intrinsic luminosity. In the calibrated candle framework, the light-curve shape provides the intrinsic luminosity (through a parameterization such as Δm_{15}). However, SN Ia with different light curve shapes have varying luminosities *and* colors, so determination of R_V depends critically on disentangling the intrinsic variation from the contributions of dust.[17]

By choosing objects in early-type host galaxies, or those that are not located in spiral arms, and using the observations at times when the intrinsic colors are nearly independent of luminosity (e.g., the Lira law for the late-time evolution of $B-V$; §2.3), it is possible to derive and correct for the relation between intrinsic luminosity and color and construct a sample of magnitude residuals and color excesses which are dominated by the effect of host-galaxy dust. From this procedure Phillips et al. (1999) found $R_V = 2.6 \pm 0.4$, lower than but roughly consistent with the canonical $R_V = 3.1$ for Galactic dust. Similarly, Altavilla et al. (2004) find $R_V = 2.5$ and Reindl et al. (2005) give $R_V = 2.65 \pm 0.15$, using generally similar (though different in detail) methods of separating the intrinsic and dust effects on luminosity and color. Using a previous incarnation of MLCS (albeit one with too strong a dependence of intrinsic color on light curve shape) Riess et al. (1996b) found $R_V = 2.55 \pm 0.30$.

Here we present a different method of determining R_V, individually for each SN Ia, using MLCS2k2. This alternative is discussed by Riess et al. (1996b), and does not require an independent estimate of the SN Ia distance. Rather, we include R_V directly as an MLCS2k2 fit parameter, and make use of the relations between the extinction in different passbands (see Figure 5 and Table 2). With only two observed passbands, such as B and V (and thus, only one observed color), the

[17]Tripp & Branch (1999) constructed a two parameter model for SN Ia distances based on fitting SN Ia peak magnitudes as a linear function of Δm_{15} and peak $B-V$ that explicitly forgoes any attempt at the difficult problem of separating these two causes for faint, red SN Ia. This model is particularly sensitive to the makeup of the sample, and requires care in its application. The same applies to the model of Parodi et al. (2000).

three parameters μ_0, A_V^0, and R_V are degenerate, so we require observations in at least three passbands to constrain R_V directly.[18] Because the distance modulus shifts magnitudes in all passbands uniformly, this approach is effectively the same as constraining R_V from multiple color excesses (e.g., $E(V-I)/E(B-V)$; Riess et al. 1996b).

An advantage of this method is that we do not require independent distances; therefore, extinguished SN Ia with recession velocities too small to give reliable Hubble flow distances can still be used to constrain R_V. In addition, because MLCS2k2 explicitly utilizes a model covariance matrix, the constraints on R_V properly account for correlated uncertainties in the data and the model, as well as the effect of the intrinsic dispersion in the luminosities and colors. Furthermore, MLCS2k2 requires the data in all passbands (for one SN) be fit by a consistent R_V, and required constraints such as $R_B = R_V + 1$ are automatically enforced (not necessarily the case in the alternate method where residuals in B and V are independently regressed against the color excess; Phillips et al. 1999; Reindl et al. 2005).

The main disadvantage to this approach is a lack of sensitivity. The intrinsic variation in SN Ia colors, observational uncertainties, and the subtle relative color differences (in the optical bands) with changes in the extinction law combine to make the constraints on R_V relatively weak for individual SN Ia. Unfortunately, the U band, which has the most sensitivity to varying R_V, also has the most intrinsic dispersion (and this is clearly not related to R_V; Jha et al. 2006). In the upper panel of Figure 19, we plot a histogram of the mean values of R_V for the sufficiently extinguished SN Ia tabulated in Table 4, and show the relation between R_V and A_V^0 for these objects in the lower panel.

On first inspection, the data show a clustering near $R_V \simeq 3.1$, with a handful of objects with smaller values and hardly any with significantly larger values. However, because of the lack of sensitivity to R_V even for these moderately extinguished objects, the results turn out to be quite dependent on the choice of prior, $\hat{p}(R_V)$. As described in §5, we have used a prior on R_V based on its distribution along Galactic lines of sight from CCM89 which is a Gaussian in R_V^{-1} and is shown as the solid curve in the upper panel of Figure 19. When data are increasingly informative, the posterior pdf is decreasingly sensitive to the choice of prior, but in this case the data only weakly constrain R_V and the prior matters. Using the extreme case of a uniform prior for $R_V \geq 1.6$ (implying we are completely ignorant of the relative likelihood of these different kinds of dust distributions) yields the dotted blue histogram and points in Figure 19. Even this is not completely satisfactory, because three objects favor R_V at the (arbitrary) lower limit of the prior, which be-

[18] Another approach that would work for Hubble flow SN Ia with only two observed passbands in the MLCS2k2 framework would be to use the Hubble law to put a prior on μ_0, and then fit for A_V^0 and R_V. This would essentially be the same as using magnitude residuals with respect to the Hubble line as discussed above. However, almost all of the nearby SN Ia presented here have observations in three or more filters, and so we can use the direct method.

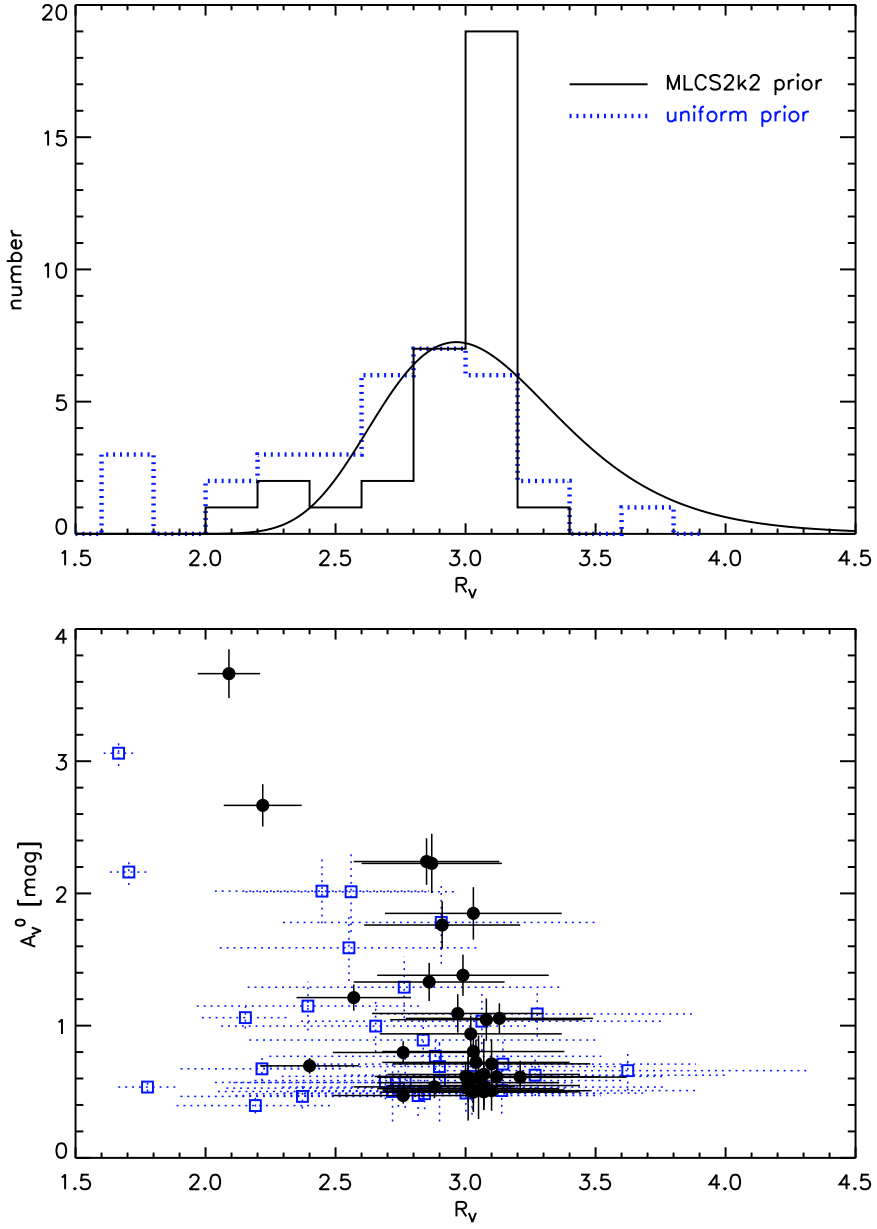

Fig. 19.— Distribution of the host galaxy extinction law parameter, R_V, and its correlation with the host galaxy extinction A_V^0. The solid curve in the upper panel shows the adopted MLCS2k2 prior, $\hat{p}(R_V)$, which is a Gaussian in R_V^{-1}, and has a mean $R_V = 3.1$ with a standard deviation of 0.4. The solid histogram shows the distribution of the mean R_V for 33 extinguished SN Ia, using MLCS2k2 and $\hat{p}(R_V)$, listed in Table 4. The dotted histogram (blue in the electronic edition) shows the distribution if a uniform prior for $R_V \geq 1.6$ is adopted instead. The filled circles in lower panel show the mean R_V and A_V^0 using the MLCS2k2 prior for these 33 objects, while the empty squares with dotted error bars (blue in the electronic version) correspond to results based on the uniform prior.

comes increasingly unlikely (and perhaps unphysical; Draine 2003 and references therein): lower R_V corresponds to dust that reddens more and more for a given attenuation, favoring smaller and smaller grains.

Nevertheless, even with this significant dependence on the prior, some results regarding R_V are robust. The effect of the prior is less important for objects which have very high extinction ($A_V^0 \gtrsim 2$ mag). In particular, the two most heavily extinguished objects in the sample, SN 1996ai and SN 1999cl, both firmly require $R_V < 3.1$. In addition, the posterior pdf has important differences from the prior pdf (which is displayed normalized to the same total area). There is a distinct deficit of SN Ia which yield R_V significantly greater than 3.1, whereas many such sight lines exist in the Milky Way (particularly in dense clouds, with $R_V \simeq 4$ to 5). The SN Ia R_V distribution may be more similar to lines of sight in the Magellanic Clouds (Gordon & Clayton 1998; Misselt, Clayton, & Gordon 1999) which typically have lower R_V, and it might be worthwhile to investigate priors on R_V derived from more sophisticated models and larger samples of stars, including LMC and SMC lines of sight (Reichart 2001). An important possibility to consider is that the dust around heavily extinguished SN Ia may be local to the SN environment; SN 1995E, for example, with $A_V^0 = 2.24 \pm 0.18$ mag, occurred in a relatively face-on host galaxy, suggesting our line of sight to the SN does not have a large path length in the galaxy disk. If "local" dust plays a significant role, the R_V distribution could be quite different for moderately and heavily extinguished SN Ia, and such an effect may be difficult to discern using the method which correlates residuals with color because the most reddened objects have the largest lever arm.

Constraints on R_V could also be strengthened if we included photometry in other passbands. Observations further in the UV would be increasingly sensitive to variations in R_V, but they are difficult to obtain (requiring space-based data for nearby extinguished SN Ia or very deep ground-based data for distant extinguished SN Ia for which the desired wavelengths redshift past the atmospheric cutoff), and the intrinsic SN Ia magnitudes and dispersions are unexplored at these wavelengths. On the other hand, near-infrared data will be extremely valuable in providing a long wavelength baseline to constrain both the extinction and the extinction law (e.g., Krisciunas et al. 2006 and references therein). We are currently developing a method to incorporate infrared photometry into MLCS2k2 by using observations in *JHK* to provide a joint prior constraint on R_V and A_V^0, that is then used to fit the optical data (Jha, Prieto, & Krisciunas, in preparation).

What are the effects of possible variations in R_V on our derived MLCS2k2 distances? The results from the extinguished objects with a uniform prior have a mean $\langle R_V \rangle = 2.7$ (with the default MLCS2k2 prior, the mean is 2.9). The majority of the Hubble flow sample has low extinction, where R_V variation has nearly negligible effects, and we had fixed $R_V \equiv 3.1$ for objects with $A_V^0 < 0.5$ mag. We have refit the full Hubble flow sample using a new prior with the same shape but $\langle R_V \rangle = 2.7$, as well as a fixed $R_V \equiv 2.7$ for objects with $A_V^0 < 0.5$ mag. On average, the distance moduli increase by 0.019 mag, with an average increase for the fixed R_V subsample of

0.014 mag (both corresponding to less than a 1% increase in distance). The effect of a smaller R_V on differential measurements (such as determining H_0 from the Hubble flow sample and a Cepheid calibrated sample) would be less, because all distances would be slightly increased. At present, we find no compelling evidence to favor a constant $R_V = 2.7$ over $R_V = 3.1$ *for low-extinction SN Ia samples* such as are typically used in cosmological applications. Allowing for R_V variations over this range could yield a plausible estimate of the systematic uncertainty, but more problematic for precision cosmology would be a systematic change in the R_V distribution with redshift,

We thank Alex Filippenko, Weidong Li, Kevin Krisciunas, and Nick Suntzeff for providing access to unpublished spectroscopy and photometry. We also thank Peter Challis, Peter Garnavich, Peter Nugent, Steve Furlanetto, and Tom Matheson for helpful discussions, as well as the anonymous referee for useful suggestions. SJ gratefully acknowledges support at UC Berkeley via a Miller Research Fellowship and NSF grant AST-0307894 to A. V. Filippenko, as well as the Panofsky Fellowship at KIPAC/SLAC, supported in part by the Department of Energy contract DE-AC02-76SF00515. Research on supernovae at Harvard University is supported by NSF Grant AST-0205808.

This research has made use of the NASA/IPAC Extragalactic Database (NED) which is operated by the Jet Propulsion Laboratory, California Institute of Technology, under contract with the National Aeronautics and Space Administration.

A. Extinction Priors

Measurements of the luminosity distances to type Ia supernovae need to account for the line-of-sight absorption by dust to yield a precise and accurate estimate. The most common approach is to measure the color excess resulting from selective absorption, and with the use of a reddening law, estimate the extinction. Unfortunately, uncertainty in the fiducial color frequently dominates the individual distance uncertainty, arising from the uncertainty (added in quadrature) of two true flux measurements and the intrinsic dispersion of SN Ia colors. Frequent and high precision monitoring of nearby SN Ia can remove the contribution of measurement uncertainty, revealing the intrinsic color dispersion to be approximately 0.05 mag for optical colors as shown in Figure 6. Multiplying this intrinsic uncertainty by a standard reddening law, $R_V = 3.1$, yields the observed SN Ia distance dispersion of 0.15-0.20 mag. However, failure to measure colors to better precision than the intrinsic dispersion may result in greatly degraded distance precision.

A significant improvement in the extinction estimate can be realized by the use of a Bayesian prior on the extinction parameter because a good deal is known about the likely values of extinction, *a priori*. The most basic and unassailable truths about extinction are that it cannot be

negative[19] and that increasing values are decreasingly likely due to the unlikely viewing angles required for large extinction, and for some surveys, magnitude limits. Models by Hatano, Branch, & Deaton (1998), Commins (2004), and Riello & Patat (2005) show that for late type galaxies, the likelihood distribution for extinguished lines of sight follows an exponential function with a maximum at zero extinction. In Figure 6 we use this function constrained by the a posteriori color distribution to determine a decay constant for the exponential of ∼0.5 mag in A_V. The use of such an extinction prior represents great potential improvement to this precision-limiting measure of SN Ia distances. This approach was first used by Riess, Press, and Kirshner (1996a) and later by Riess et al. (1998a) and Phillips et al. (1999) as well as in the present work. However, the well known danger of using a priori information is that it may be in error and thus propagate systematic errors into the final distance estimate. In addition, one must be careful to use an unbiased estimator of extinction from the posterior likelihood distribution to avoid additional systematic error. To weigh the advantages and disadvantages of using extinction priors for *realistic* measurements of SN Ia, we have undertaken a set of Monte Carlo simulations.

Our simulations model 10^4 SN Ia, each with a fixed intrinsic $B-V$ color drawn from a Gaussian distribution (with zero mean, and standard deviation $\sigma_{\rm int}$) and an extinction A_V drawn from an exponential distribution (with scale length τ). We then simulate $n_{\rm obs}$ measurements of the SN $B-V$ color, each with a Gaussian error $\sigma_{\rm meas}$, and subsequently "fit" for the extinction, determining its posterior probability distribution function with the application of a prior (either the true one describing the input extinction distribution, a more conservative prior, none at all, or an incorrect one). For each posterior pdf we extract both the mean and the mode, calculate the error between the posterior estimate and the input extinction, and analyze this error distribution over the whole simulated sample. These quantities may also be calculated analytically using Bayes's Theorem, but we prefer the numerical approach for ease of the incorporation of a variety of functional forms for the extinction prior.[20]

As an example, we show in Figure 20 the results for $n_{\rm obs} = 5$, $\sigma_{\rm meas} = 0.1$ mag, $\sigma_{\rm int}$ =0.05 mag, and $\tau = 0.5$ mag, parameters chosen to correspond to adequate but minimal color measurements, such as those used in Riess et al. (1998a) for the detection of cosmic acceleration, and we have fit the simulated sample with both the correct prior ($\hat{p}(A_V) \propto \exp(-A_V/\tau)$, with $\tau = 0.5$ mag) and no prior at all (allowing the fit A_V to be negative as well).

As shown, use of the mean of the individual extinction likelihoods results in an unbiased estimate of the extinction and an increased precision relative to the absence of an extinction prior.

[19]For the case of rare light echoes in the presence of excessive quantities of circumstellar dust, scattering can add some additional light to the observer's view, though the net effect is still positive extinction, albeit with a different ratio of selective to total absorption as discussed by Wang (2005).

[20]The simulation routine is available at http://astro.berkeley.edu/∼saurabh/mlcs2k2/

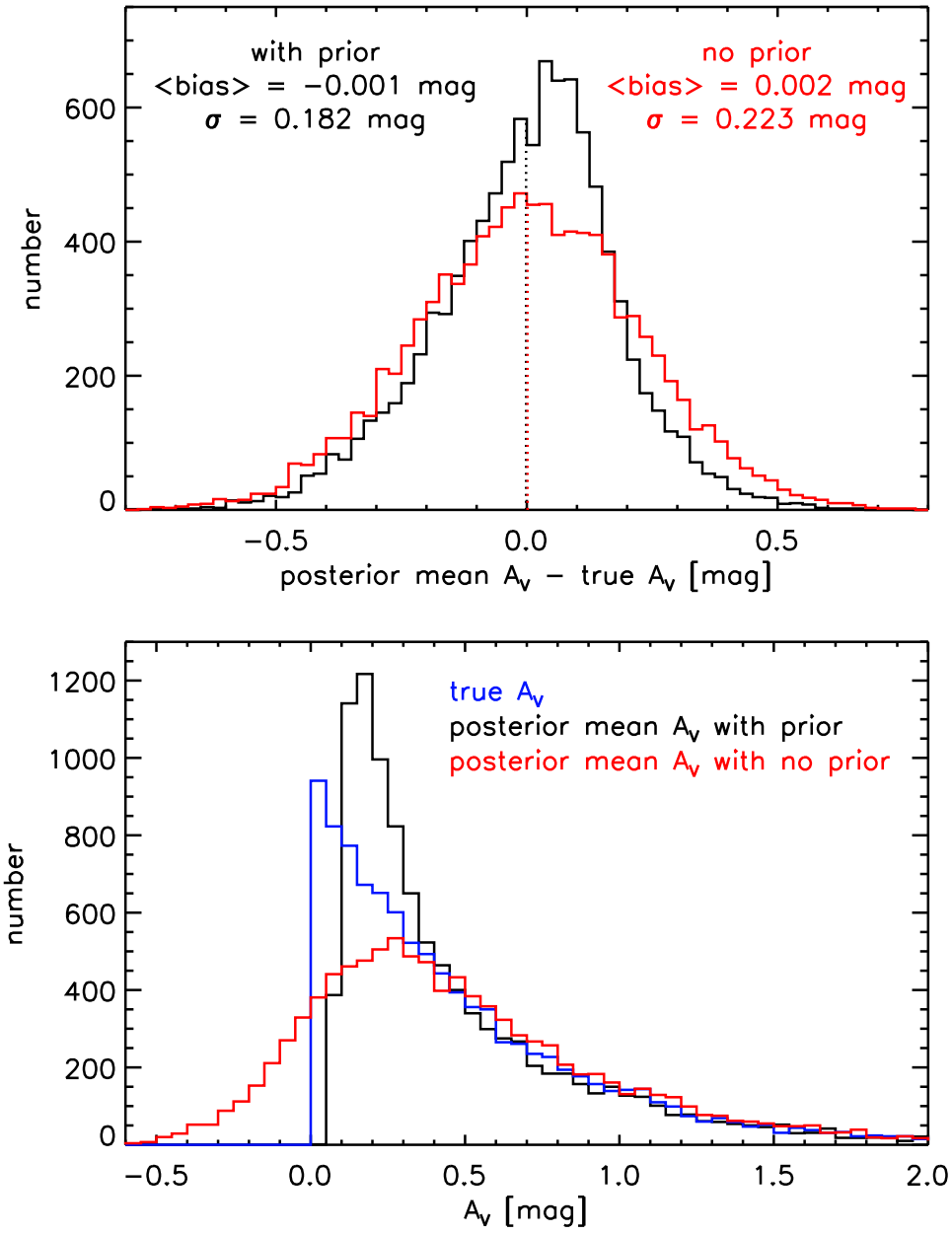

Fig. 20.— Distributions of the extinction bias (top panel) and input and posterior mean extinction (bottom panel) from a simulation of 10^4 SN Ia, with a Gaussian intrinsic $B-V$ color scatter of $\sigma_{\rm int} = 0.05$ mag, "observed" on 5 epochs with a precision of $\sigma_{\rm meas} = 0.1$ mag in each color measurement. The SN are drawn from an exponential A_V distribution with a scale length $\tau = 0.5$ mag (blue histogram), and then fit with a prior matching the extinction distribution (black), as well as without any prior (red). For each fit, the mean of the posterior extinction distribution (with and without a prior) is used as the extinction estimate, and these distributions are shown in the lower panel. The upper panel then shows the difference between the posterior mean extinction and the true extinction. Use of the correct extinction prior shows no mean bias (dotted lines), and improves the precision of the extinction measurement.

Because the weight of distance estimates for cosmological parameter estimation is proportional to the square of the uncertainty, the precision of 0.18 mag per SN Ia using the prior represents a 50% improvement over the use of no prior for this realistic case. For more poorly measured colors ($\sigma_{\rm meas}$ = 0.2 mag) or fewer independent measurements, the improvement approaches a factor of two, akin to doubling the cosmological sample.

Another way extinction priors yield benefits besides improved distance precision is by reining in errors in the knowledge of the intrinsic properties of SN Ia. The most relevant example is our estimate of the fiducial, unreddened color of an SN Ia, used to estimate the color excess and the net extinction. As an example we consider in Figure 21 the extinction bias resulting from a mis-estimate of the unreddened color (with the previous minimal but adequate color measurements). Without a prior the systematic extinction error is exactly the color error multiplied by the reddening law. With the prior, the extinction error becomes smaller because the valuable knowledge about the likely extinction weighs in, reducing the effect of the measurement inaccuracy. Taking a realistic example of an 0.03 mag mis-estimate in the unreddened color, the bias is reduced from 0.10 mag without a prior to 0.07 mag with the prior. However, the net bias for most cosmological measurements will be negligible if the color error (and extinction distribution) is independent of redshift. For cosmological measurements, this color error may be usefully thought of as a *color evolution*. Again, for such a color evolution, the net bias is reduced by one-third with the use of an extinction prior.

Nonetheless, a basic disadvantage of using priors is that biases may result from the use of an incorrect prior.[21] As an example we show in Figure 22 the extinction bias as a function of the exponential decay scale length assumed for the prior. Values differing from the input of τ = 0.5 mag result in an under- or over-estimate of the mean extinction. Using the results from Riello & Patat (2005) we can guess the approximate size of an error in τ by imagining it was determined from galaxy-based simulations and in so doing we have mis-estimated the relative importance of the bulge to the total luminosity in late-type galaxies. The dotted lines show that a 30% error in this ratio (and thus reducing or augmenting the scale length by a factor of 1.5) results in a $\sim$0.03 mag bias. In practice (i.e., for cosmological applications) a net bias would only result from unaccounted for differences in τ between high and low redshift such as may result from evolution or sample selection. Interestingly, we also find that the effect of taking a so-called “weak” prior,

[21]A bias can also occur when a moment other than the mean of the individual extinction likelihood function is used as discussed by Perlmutter et al. (1999). For example, in Riess et al. (1998a) the maximum likelihood (i.e., the mode of posterior distribution) was initially used, which results in an 0.06 mag bias as determined from our simulation. However, because the bias occurs for both low and high redshift SN Ia similarly, the net bias (i.e., in the difference) was much smaller. Modeling the low-redshift SN Ia as having twice as many observations each with twice the individual precision ($n_{\rm obs}$=10, $\sigma_{\rm meas}$ = 0.05 mag) shows that the net bias is 0.02 mag in the distance difference at low and high redshifts, much smaller than the 0.05 mag error in the mean of the high-redshift sample.

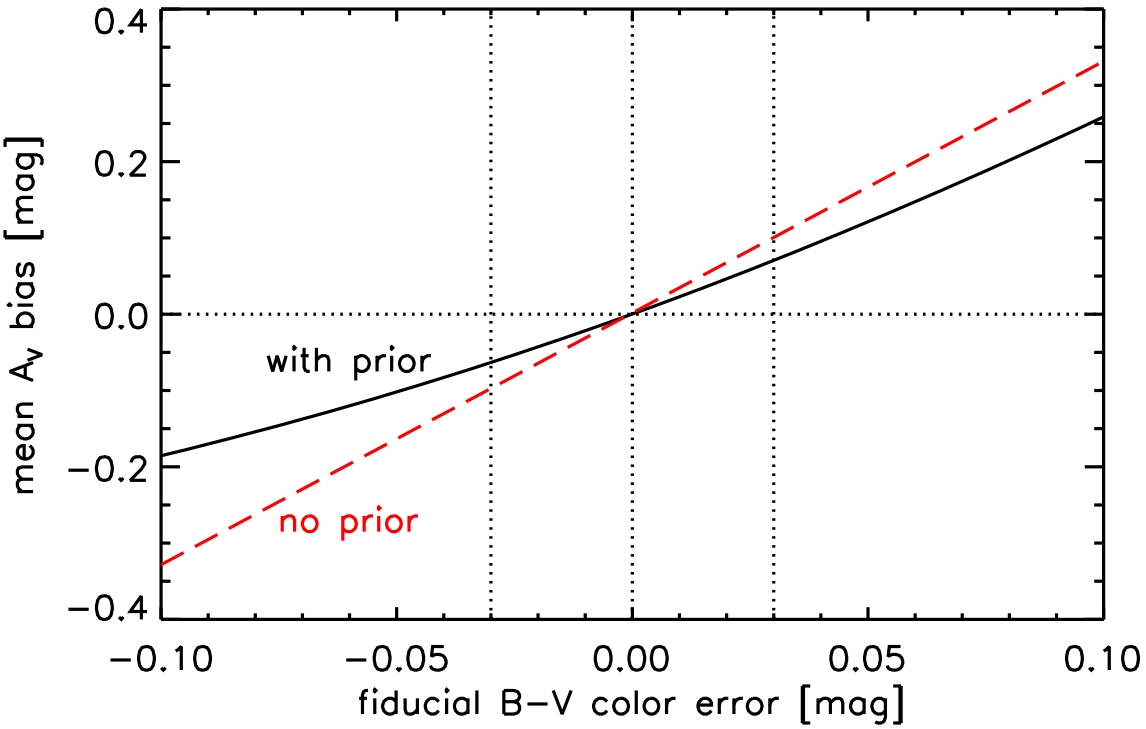

Fig. 21.— Mitigating effect of the extinction prior given an error or evolution in the mean intrinsic color. The use of the prior (solid) reduces the extinction bias by a factor of one-third relative to no prior (dashed, red in the electronic edition). The dotted lines show a plausible range of ±0.03 mag in the mean intrinsic color.

that $\hat{p}(A_V)$ is constant for $A_V \geq 0$, and zero for $A_V < 0$ is a worse choice, resulting in a bias of 0.07 mag. The reason is that the mean of such a prior is unnaturally large, biasing the extinction estimate in that direction. Likewise, assuming negligible extinction will result in an underestimate, equal to the mean of the true distribution (which, for an exponential, is the value of the scale length itself). The lesson is intuitively clear, when using a prior it is important to take the best estimate (and estimate a systematic error from the range of good guesses) as a seemingly ”conservative” or ”weak” version can be worse.

For a specific SN sample it is probably best to simulate the sources and sizes of uncertainty depending on the data quality before determining whether the use of an extinction prior offers more to gain than to lose. Our simulations reveal nothing that intuition does not: a good measurement is better than a bad prior, and a good prior will improve imperfect measurements.

REFERENCES

Altavilla, G., et al. 2004, MNRAS, 349, 1344

Benetti, S., et al. 2004, MNRAS, 348, 261

Bessell, M.S. 1990, PASP, 102, 1181

Buta, R.J., & Turner, A. 1983, PASP, 95, 72

Candia, P. et al. 2003, PASP, 115, 277

Cardelli, J.A., Clayton, G.C., & Mathis, J.S. 1989, ApJ, 345, 245 (CCM89)

Commins, E.D. 2004, New Astronomy Review, 48, 567

Draine, B.T. 2003, ARA&A, 41, 241

Filippenko, A.V., Richmond, M.W., Branch, D., Gaskell, C.M., Herbst, W., Ford, C.H., Treffers, R.R., Matheson, T., Ho, L.C., Dey, A., Sargent, W.L.W., Small, T.A., & van Breugel, W.J.M. 1992, AJ, 104, 1543

Filippenko, A.V. 1997, ARA&A, 35, 309

Fitzpatrick, E.L. 1999, PASP, 111, 63

Fixsen, D.J., Cheng, E.S., Gales, J.M., Mather, J.C., Shafer, R.A., Wright, E.L. 1996, ApJ, 473, 576

Ford, C.H., Herbst, W., Richmond, M.W., Baker, M.L., Filippenko, A.V., Treffers, R.R., Paik, Y., & Benson, P.J. 1993, AJ, 106, 1101

Freedman, W.L., et al. 2001, ApJ, 553, 47

Friedman, A., King, J.Y., & Li, W.D. 1999, IAU Circ. 7286

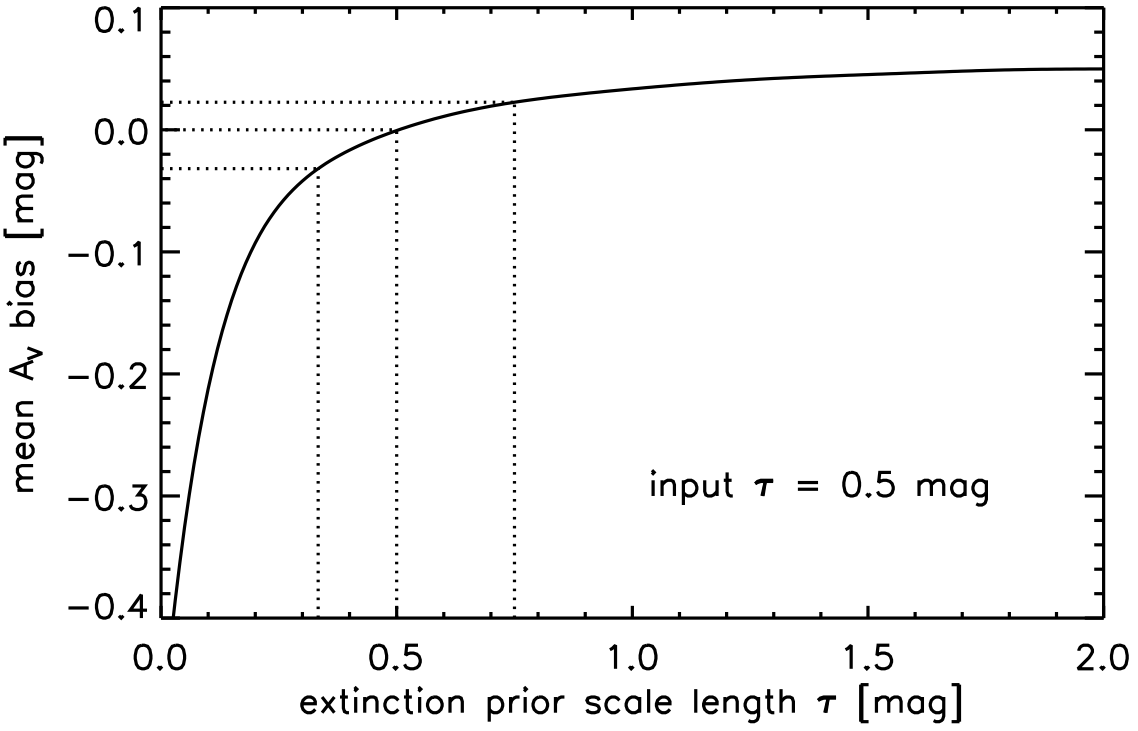

Fig. 22.— Effect of using an incorrect prior. The solid line shows the result of fitting the input distribution (created with $\tau = 0.5$ mag) with different priors, varying the prior scale length. The dotted lines highlight the results of using the correct prior ($\tau = 0.5$ mag, no bias) and priors with τ larger or smaller by a factor of 1.5. This plausible range of variation (particularly in comparing different SN samples) could lead to a bias of ∼0.03 mag.

Furlanetto, S., & Piran, T. 2006, MNRAS, 366, 467

Gallagher, J.S., Garnavich, P.M., Berlind, P., Challis, P., Jha, S., & Kirshner, R.P. 2005, ApJ, 634, 210

Garnavich, P.M., Bonanos, A.Z., Jha, S., Kirshner, R.P., Schlegel, E.M., Challis, P., Macri, L.M., Hatano, K., Branch, D., Bothun, G.D., & Freedman, W.L. 2004, ApJ, 613, 1120

Geller, M.J. 1997, Reviews in Modern Astronomy, 10, 159

Germany, L.M., Reiss, D.J., Schmidt, B.P., Stubbs, C.W., & Suntzeff, N.B. 2004, A&A, 415, 863

Giovanelli, R., Dale, D.A., Haynes, M.P., Hardy, E., & Campusano, L.E. 1999, ApJ, 525, 25

Goldhaber, G., et al. 2001, ApJ, 558, 359

Gordon, K.D. & Clayton, G.C. 1998, ApJ, 500, 816

Guy, J., Astier, P., Nobili, S., Regnault, N., & Pain, R. 2005, A&A, 443, 781

Hamuy, M., Phillips, M.M., Maza, J., Wischnjewsky, M., Uomoto, A., Landolt, A.U., & Khatwani, R. 1991, AJ, 102, 208

Hamuy, M., Phillips, M.M., Wells, L., & Maza, J. 1993, PASP, 105, 787

Hamuy, M., Phillips, M.M., Maza, J., Suntzeff, N.B., Schommer, R.A., & Avilés, R. 1995, AJ, 109, 1

Hamuy, M., Phillips, M.M., Suntzeff, N.B., Schommer, R.A., Maza, J., Smith, R.C., Lira, P., & Avilés, R. 1996a, 112, 2438

Hamuy, M., et al. 1996b, AJ, 112, 2408

Hamuy, M., Trager, S.C., Pinto, P.A., Phillips, M.M., Schommer, R.A., Ivanov, V., & Suntzeff, N.B. 2000, AJ, 120, 1479

Hatano, K., Branch, D., & Deaton, J. 1998, ApJ, 502, 177

Hudson, M.J., Smith, R.J., Lucey, J.R., & Branchini, E. 2004, MNRAS, 352, 61

Hubble, E.P. 1929, Proc. Natl. Acad. Sci., 15, 168

Jha, S., et al. 1999a, ApJS, 125, 73

Jha, S., Challis, P., Garnavich, P., Kirshner, R., & Calkins, M. 1999b, IAU Circ. 7298

Jha, S. 2002, Ph.D. Thesis, Harvard University

Jha, S., et al. 2006, AJ, 131, 527

Kim, A., Goobar, A., & Perlmutter, S. 1996, PASP, 108, 190

Kirshner, R.P. 2004, Proc. Natl. Acad. Sci., 101, 8

Knop, R.A., et al. 2003, ApJ, 598, 102

Krisciunas, K., Hastings, N.C., Loomis, K., McMillan, R., Rest, A., Riess, A.G., & Stubbs, C. 2000, ApJ, 539, 658

Krisciunas, K., Phillips, M.M., Stubs, C., Rest, A., Miknaitis, G., Riess, A.G., Suntzeff, N.B., Roth, M., Persson, S.E., & Freedman, W.L. 2001, AJ, 122, 1616

Krisciunas, K., Suntzeff, N.B., Candia, P., Arenas, J., Espinoza, J., Gonzalez, D., Gonzalez, S., Höflich, P.A., Landolt, A.U., Phillips, M.M., & Pizarro, S. 2003, AJ, 125, 166

Krisciunas, K., et al. 2004a, AJ, 127, 1664

Krisciunas, K., et al. 2004b, AJ, 128, 3034

Krisciunas, K., Prieto, J.L., Garnavich, P.M., Riley, J.-L.G., Rest, A., Stubbs, C., & McMillan, R. 2006, AJ, 131, 1639

Lahav, O., Lilje, P. B., Primack, J. R., & Rees, M. J. 1991, MNRAS, 251, 128

Leibundgut, B., Tammann, G.A., Cadonau, R., & Cerrito, D. 1991, A&AS, 89, 537

Leibundgut, B., et al. 1993, AJ, 105, 301

Leonard, D.C., Li, W., Filippenko, A.V., Foley, R.J., & Chornock, R. 2005, ApJ, 632, 450

Li, W., Qiu, Y.L., Qiao, Q.Y., Zhu, X.H., Hu, J.Y., Richmond, M.W., Filippenko, A.V., Treffers, R.R., Peng, C.Y., & Leonard, D.C. 1999, AJ, 117, 2709

Li, W., Filippenko, A.V., Gates, E., Chornock, R., Gal-Yam, A., Ofek, E.O., Leonard, D.C., Modjaz, M., Rich, R.M., Riess, A.G., & Treffers, R.R. 2001, PASP, 113, 1178

Li, W., et al. 2003, PASP, 115, 453

Lira, P. 1995, Master's Thesis, University of Chile

Lira, P., et al. 1998, AJ, 115, 234

McGough, C., Clayton, G.C., Gordon, K.D., & Wolff, M.J. 2005, ApJ, 624, 118

Meikle, W.P.S., et al. 1996, MNRAS, 281, 263

Miknaitis, G., et al. 2007, in preparation

Miller, N.A., Ledlow, M.J., Owen, F.N., & Hill, J.M. 2002, AJ, 123, 3018

Misselt, K.A., Clayton, G.C., & Gordon, K.D. 1999, ApJ, 515, 128

Modjaz, M., Li, W.D., Filippenko, A.V., King, J.Y., Leonard, D.C., Matheson, T., & Treffers, R.R. 2001, PASP, 113, 308

Muñoz, J.A., Falco, E.E., Kochanek, C.S., McLeod, B.A., & Mediavilla, E. 2004, ApJ, 605, 614

Nobili, S., Goobar, A., Knop, R., & Nugent, P. 2003, A&A, 404, 901

Nobili, S., et al. 2005, A&A, 437, 789

Nugent, P., Kim, A., & Perlmutter, S. 2002, PASP, 114, 803

O'Donnell, J.E. 1994, ApJ, 422, 158

Parodi, B.R., Saha, A., Sandage, A., Tammann, G.A. 2000, ApJ, 540, 634

Patat, F., Benetti, S., Cappellaro, E., Danziger, I.J., Della Valle, M., Mazzali, P.A., Turatto, M. 1996, MNRAS, 278, 111

Perlmutter, S., et al. 1997, ApJ, 483, 565

Perlmutter, S., et al. 1999, ApJ, 517, 565

Phillips, M.M., et al. 1987, PASP, 99, 592

Phillips, M.M. 1993, ApJ, 413, L105

Phillips, M.M., Lira, P., Suntzeff, N.B., Schommer, R.A., Hamuy, M., & Maza, J. 1999, AJ, 118, 1766

Pignata, G., et al. 2004, MNRAS, 355, 178

Press, W.H., Teukolsky, S.A., Vetterling, W.T., & Flannery, B.P. 1992, Numerical Recipes in C, 2nd ed., New York: Cambridge University Press

Prieto, J.L., Rest, A., & Suntzeff, N.B. 2006, ApJ, 647, 501

Radburn-Smith, D.J., Lucey, J.R., & Hudson, M.J. 2004, MNRAS, 355, 1378

Ramella, M., Geller, M.J., Pisani, A., & da Costa, L.N. 2002, AJ, 123, 2976

Reichart, D.E. 2001, ApJ, 553, 235

Reindl, B., Tammann, G.A., Sandage, A., & Saha, A. 2005, ApJ, 624, 532

Richmond, M.W., Treffers, R.R., Filippenko, A.V., van Dyk, S.D., Paik, Y., Peng, C., Marschall, L.A., Laaksonen, B.D., Macintosh, B., & McLean, I.S. 1995, AJ, 109, 2121

Riello, M., & Patat, F. 2005, MNRAS, 362, 671

Riess, A.G., Press, W.H., & Kirshner, R.P., 1995a, ApJ, 438, L17

Riess, A.G., Press, W.H., & Kirshner, R.P., 1995b, ApJ, 445, L91

Riess, A.G., Press, W.H., & Kirshner, R.P. 1996a, ApJ, 473, 88

Riess, A.G., Press, W.H., & Kirshner, R.P. 1996b, ApJ, 473, 588

Riess, A.G., et al. 1997a, AJ, 114, 722

Riess, A.G., Davis, M., Baker, J., & Kirshner, R.P. 1997b, ApJ, 488, L1

Riess, A.G., et al. 1998a, AJ, 116, 1009

Riess, A.G., Nugent, P., Filippenko, A.V., Kirshner, R.P., & Perlmutter, S. 1998b, ApJ, 504, 935

Riess, A.G., et al. 1999, AJ, 117, 707

Riess, A.G., et al. 2004, ApJ, 607, 665

Riess, A.G., Li, W., Stetson, P.B., Filippenko, A.V., Jha, S., Kirshner, R.P., Challis, P.M., Garnavich, P.M., & Chornock, R. 2005, ApJ, 627, 579

Salvo, M.E., Cappellaro, E., Mazzali, P.A., Benetti, S., Danziger, I.J., Patat, F., & Turatto, M. 2001, MNRAS, 321, 254

Sandage, A., Tammann, G.A., Saha, A., Reindl, B., Macchetto, F.D., & Panagia, N. 2006, ApJ, 653, 843

Saunders, W., et al. 2000, MNRAS, 317, 55

Schlegel, D. J., Finkbeiner, D. P., & Davis, M. 1998, ApJ, 500, 525

Strolger, L.-G., et al. 2002, AJ, 124, 2905

Stritzinger, M., et al. 2002, AJ, 124, 2100

Suntzeff, N.B., et al. 1999, AJ, 117, 1175

Szabó, Gy.M., Sárneczky, K., Vinkó, J., Csák, B., Mészáros, Sz., Székely, P., & Bebesi, Zs. 2003, A&A, 408, 915

Tonry, J.L., Blakeslee, J.P., Ajhar, E.A., & Dressler, A. 2000, ApJ, 530, 625

Tonry, J.L. et al. 2003, ApJ, 594, 1

Tripp, R., & Branch, D. 1999, ApJ, 525, 209

Tsvetkov, D.Yu. 1982, Sov. Astron. Lett. 8, 115

Turatto, M., Benetti, S., Cappellaro, E., Danziger, I.J., Della Valle, M., Gouiffes, C., Mazzali, P.A., & Patat, F. 1996, MNRAS, 283, 1

Turatto, M., Piemonte, A., Benetti, S., Cappellaro, E., Mazzali, P.A., Danziger, I.J., & Patat, F. 1998, AJ, 116, 2431

Turner, E. L., Cen, R., & Ostriker, J. P. 1992, AJ, 103, 1427

Valentini, G., et al. 2003, ApJ, 595, 779

Wang, L., Goldhaber, G., Aldering, G., & Perlmutter, S. 2003, ApJ, 590, 944

Wang, L. 2005, ApJ, 635, L33

Wang, X., Wang, L., Zhou, X., Lou, Y.-Q., & Li, Z. 2005, ApJ, 620, L87

Wells, L. A., et al. 1994, AJ, 108, 2233

Zehavi, I., Riess, A.G., Kirshner, R.P., & Dekel, A. 1998, ApJ, 503, 483

This preprint was prepared with the AAS LaTeX macros v5.2.